IONIC LIQUID ASSISTED SYNTHESIS AND CHARACTERISATION OF ZnO NANOPARTICLES

N. Srinivasa Rao,[a] Ch. Satya Vani[b] and M. V. B. Rao[a]*

Keywords: ZnO, Ionic liquids, XRD, TEM, FT-IR, UV-DRS and Particle Analyzer.

A green approach has been developed for the synthesis of nanocrystalline zinc oxide (ZnO) with the aid of room-temperature synthesized ionic liquids (RTIL's) as crystal growth modifiers by low-temperature precipitation technique. The role of RTIL's (propylammonium acetate (PAA), propylammonium formate (PAF), 3-hydroxy propylammonium acetate (3-HPAA), 3-hydroxy propylammonium formate (3HPAF) and their concentration effect on the particle size is studied in this protocol. The formed nanoparticles are characterized by XRD, TEM, FT-IR and UV-DRS. XRD spectra of nanoparticles exhibit typical diffraction peaks of hexagonal phase with wurtzite ZnO structure corresponding to JCPDS 36-1451. TEM results revealed that spherical nanoparticles obtained with an average particle size in the range of 5-20 nm. UV-Vis-DRS spectra of the ZnO nanoparticles shows blue shift compared to the bulk ZnO, attributed to quantum confinement effect.

* Corresponding Authors
[a] Department of Chemistry, Krishna University, Machilipatnam, AP, India
[b] Department of Chemistry, Indian Institute of Technology, Chennai, Tamilnadu

Introduction

ZnO nanoparticles have been extensively studied over the past few years because of their size-dependent electronic and optical properties.[1] Zinc oxide (ZnO) has attracted immense research interest worldwide during the present decade. Its wide band gap (3.37 eV)[2] and high exciton binding energy (60 meV)[3] makes it a potential material for applications in blue light emitting devices (LED),[4] dye-sensitized solar cell,[5] gas sensors,[6] ceramics,[7] field emission devices,[8] luminescent materials,[9] biomedical[10] and photocatalysis.[11]

In this regard, developing a low-cost process to control the morphology and optical properties is the main challenge to building ZnO nanostructure-based technologies. It is well-known that by reducing the size of materials, their properties can be modified drastically.[12-16] Considerable efforts have been devoted to controlling the morphology and size of ZnO nanostructures.[17-20]

Room-temperature ionic liquids (RTILs) have received considerable attention due to theirs beneficial chemical and physical properties.[21,22] There is significant progress in the applications of RTILs to synthetic-organic chemistry, catalysis, separation, electrochemistry, biopolymers and molecular self-assemblies.[23,24] RTIL's have recently received a great deal of attention as potential new green media for nanomaterial synthesis.[25-28] In continuation of our investigations into nanomaterial preparation by using natural gums [29], the selection of the RTIL's was justifiable by the fact that it can be obtained at a relatively low price and its synthesis method is simple.[30]

The aim of this work is to report the green synthesis of zinc oxide nanoparticles via pressure vial method in different RTIL's. Through this technique, spherical nanoparticles can be synthesized by a precise variation of the concentration of RTIL's. The pressure vial process has proved to be a useful technique for generating various nanostructured materials. Our study shows that the nanostructures are of good crystalline quality with low structural and electronic defects.

Experimental

All the reagents were of analytical grade and were used without further purification. Zinc acetate dihydrate and sodium hydroxide (NaOH) were obtained from SD Fine Chemicals, India.

All the solutions were prepared with deionized water. Zinc acetate dihydrate (1 mmol) was dissolved in 10 ml of distilled water and different concentrations of RTIL's (propylammonium acetate (PAA), propylammonium formate (PAF), 3-hydroxypropylammonium acetate (3 HPAA), 3-hydroxypropylammonium formate (3HPAF) (0.1 ml, 0.5 ml) was added and stirred for 10 minutes. After complete dissolution, 10 ml of NaOH (0.1 M) was slowly added dropwise to the above solution under magnetic stirring for 10 min. The precursor solution was transferred to a tightly fitted screw capped pressure vial, and the bottles were kept in an oil bath for 2 hrs by maintaining the temperature of 80°C.

The product was separated by centrifugation, washed thoroughly with deionized water followed by ethanol. The white precipitate dried in hot air oven at 60 °C for 2 hrs. The synthesized RTIL's are used for synthesizing ZnO nanoparticles which are listed below in Table 1.

Table 1. Synthesized Room Temperature Ionic Liquids (RTILs)

Name	Chemical formula	Acronym
3-Hydroxypropylam-monium formate	$C_4H_{11}NO_3$	3-HPAF
3-Hydroxypropylam-monium acetate	$C_5H_{13}NO_3$	3-HPAA
Propylammonium formate	$C_4H_{11}NO_2$	PAF
Propylammonium acetate	$C_5H_{13}NO_2$	PAA

Characterization

The structural properties of the obtained products were recorded using a Rigaku X-ray powder diffractometer (Cu radiation, λ = 0.1546 nm) running at 40 kV and 40 mA (Tokyo, Japan). TEM images were observed on TECNAI FE12 TEM instrument operating at 120 kV using SIS imaging software. The particles were dispersed in methanol, and a drop of it was placed on formvar-coated copper grid followed by air drying. UV-Vis-DRS spectra were recorded on a Perkin-Elmer Lambda 750 spectrophotometer. FT-IR spectra were recorded on Thermo Nicolet Nexus (Washington, USA) 670 spectrophotometer.

Results and discussion

Structural characterization of ZnO nanoparticles

Figure 1 shows the crystallinity and phase of the synthesized nanocrystalline ZnO with different RTIL's via pressure vial method. The sharp diffraction peaks manifest that the synthesized ZnO nanoparticles have high crystallinity. The nanoparticles of ZnO were synthesised with four different RTIL's (PAA, PAF, 3HPAA, 3HPAF) and the XRD patterns show similar peak positions (Figure 1 a-d). The prominent peaks labelled at angles of 31.6°, 34.2°, 36.1°, 47.3°, 56.3°, 62.7°, 66.2°, 67.5° and 68.8° belong to the (100), (002), (101), (102), (110), (103), (200), (112), and (201) planes respectively. All the diffraction peaks show a very good agreement with the reported values of the Joint Committee on Powder Diffraction Standards data (JCPDS 36-1451) and confirm the formation of hexagonal phase with the lattice constants of $a = b = 3.2498$ Å, and $c = 5.2066$ Å.[31,32]

The results indicate that the synthesised powders consist of pure phase and no other characteristic peaks of other material were detected. The average crystalline size of the ZnO particles is estimated by using Debye–Scherrer's Equation.[33]

$$D = \frac{0.94\lambda}{\beta \cos\theta}$$

where

D is the average crystalline size
λ is the X-ray wavelength of 1.54 Å,
θ is the Bragg diffraction angle, and
β is the FWHM.

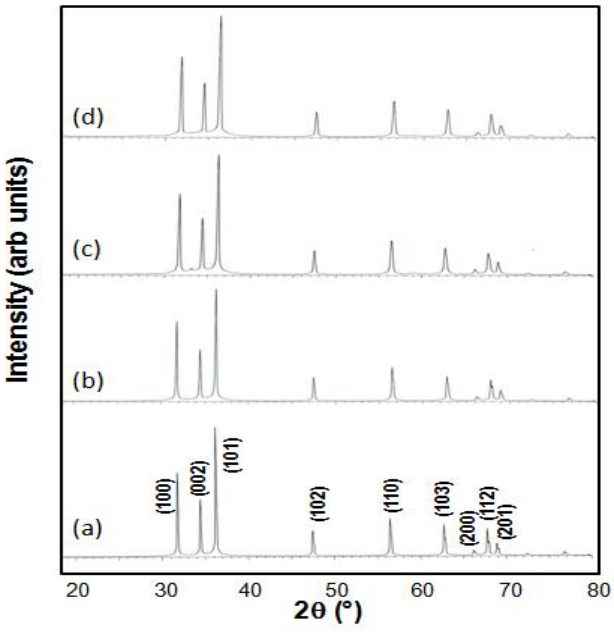

Figure 1. XRD patterns of ZnO nanoparticles synthesised in pressure vial with RTIL (a) PAA (b) PAF (c) 3 HPAA (d) 3 HPAF.

Size control of ZnO nanoparticles

To access the size of the as-synthesized samples, we performed TEM, and the images are presented in Figure 2. As they can be seen in Fig. 2a, ZnO particles synthesized without RTIL's are very large as well as in various shapes such as spheres (~ diameter = 40 nm and length in few microns) and cubes (~ in the range 30 - 210 nm). The influence of RTIL's on the formation of ZnO nanoparticles in pressure vial method was studied at two molar concentrations of IL's – 0.1ml and 0.5ml. At 0.1 ml RTIL's concentration, ZnO nanoparticles are not distinct, and they appear to be less in number. Increasing the concentration of RTILs to 0.5ml exhibited spherical ZnO nanoparticles of about 10-20 nm. It is likely that initially, Zn^{2+} ions form bonds with the high number of coordinating functional groups of the RTIL's, leading to nucleation and preferentially crystal growth. In the most cases, the van der Waals interactions between the surface molecules of the formed nanoparticles form the driving force for self-assembly, and then ZnO nanocrystals can be assembled to form large ZnO spheres. In the presence of RTIL's, in pressure vial method, the produced sphere-like structures consisting of ZnO nanoparticles (Fig. 2b, c), are of nearly uniform size distribution between 5–20 nm (Fig. 2a), that compares well in accordance with the size – 21.6 nm estimated with XRD studies.

Particle size distribution shown in Fig. 2b clearly indicate a remarkable reduction in the average size of ZnO nanoparticles from 130 nm to 10 nm in the presence of 0.1 ml RTIL's. A small increase in the average particle size was

observed when the reaction was carried out in 0.5ml RTIL's (pressure vial method) that can be assumed due to the re-agglomeration of the nanosized particles in the pressure medium of higher concentration. The higher surface area is attributed to the formation of smaller particles.

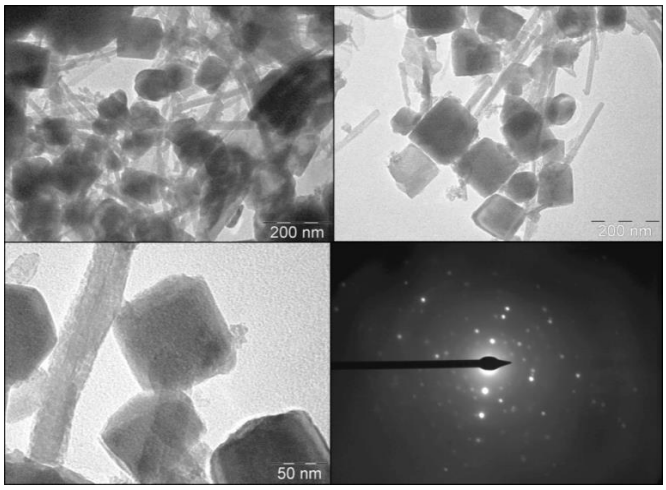

Figure 2a. ZnO particles synthesized without RTIL's

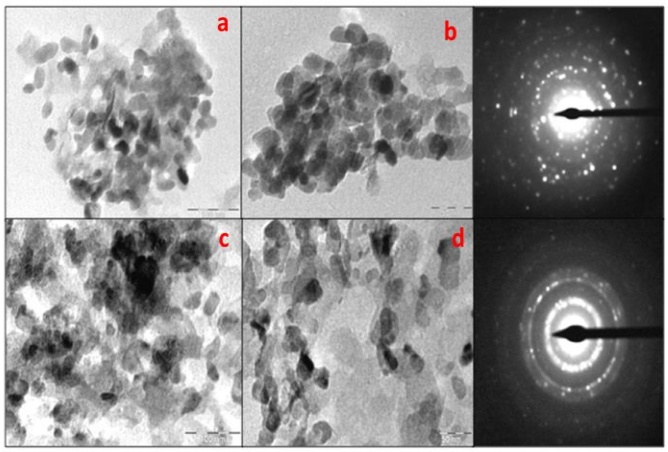

Figure 2b. ZnO particles synthesized with RTILs (a) PAA (b) PAF (c) 3 HPAA (d) 3 HPAF at 0.1 ml

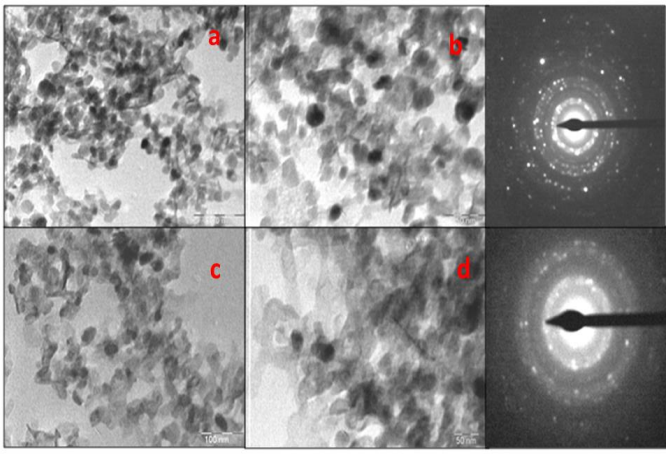

Figure 2c. ZnO particles synthesized with RTILs (a) PAA (b) PAF (c) 3 HPAA (d) 3 HPAF at 0.5 ml

This synthesis method provides control over the surface area. These microscopic results suggest that RTIL's can be used as a template for the fabrication of metal oxide hollow spheres as compared to other alternative methods. The selected-area electron diffraction (SAED) patterns taken from the TEM images for all the samples showed a similar pattern. As can be seen, the observed SAED patterns show distinct spots indexed to (100), (002), (101), (102) and (110) corresponding to wurtzite ZnO structure, which is consistent with the XRD results.

Particle analyzer

Using Nano Particle Analyzer (SZ100) the size of the as-synthesized nanopowders is measured for the RTIL PAA at 0.1ml. The average particle size of the sample is shown in the histogram in Figure 5. As can be seen from the profile, the size of the particles is in good agreement with XRD and TEM observations with an average particle size of 21.6 nm

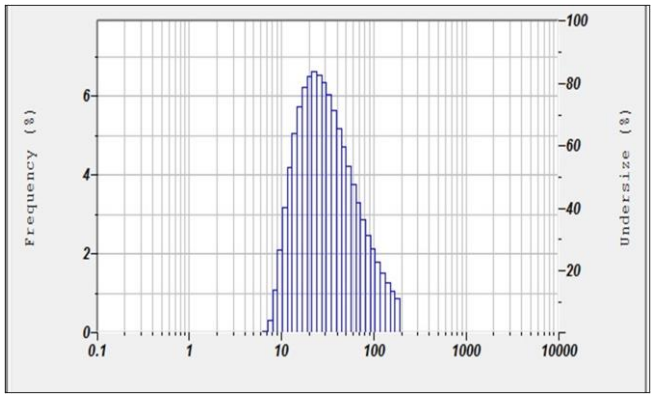

Figure 5. Particle analyzer histograms of ZnO powders.

UV-Vis-DRS spectra

To examine the optical properties, synthesized ZnO nanostructures were examined by ultraviolet-visible-diffused reflectance spectroscopy (UV-Vis-DRS), and results are presented in fig 3. As displayed in figure 3, a strong absorption at about 401, 401, 391, 392, with 0.1 ml and 393, 395, 390, 385 nm with 0.5ml are observed for ZnO nanoparticles. The absorption edge of ZnO nanoparticles shows an obvious blue shift due to the quantum confinement effect. This phenomenon is explained by Burstein–Moss effect.[34-35] The corresponding band gap energies were determined and found to be 3.09, 3.09 3.17, 3.16 with 0.1 ml and 3.15, 3.14, 3.18, 3.22 eV with 0.5 ml (Fig. 3 inset) for synthesized ZnO nanoparticles. The band gap energies are observed slightly lesser than the commercial ZnO (3.37eV). This demonstrates that the synthesized ZnO particles are pure, showing band gap in the range 3.09 eV - 3.22 eV, and has good optical property.

FT-IR spectra

Figure 4 represents the typical FT-IR spectra of as-synthesized ZnO with RTIL's in pressure vial method. The broad peak in the higher energy region, 3100 – 3600 cm^{-1} is due to the stretching vibration of -OH and -NH_2 groups on the surface of ZnO nanoparticles.

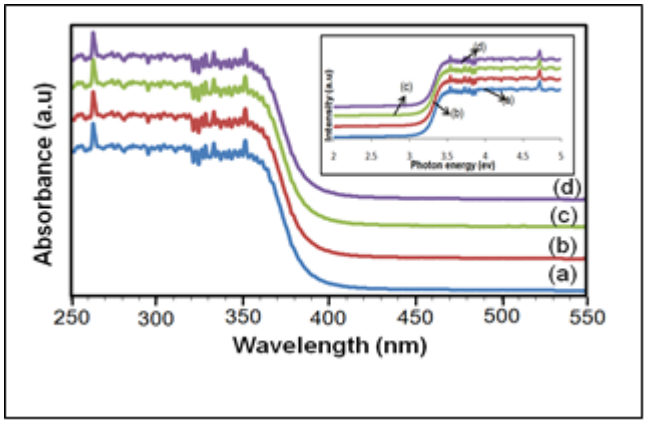

Figure 3. Ultraviolet-visible-diffused reflectance spectroscopy of ZnO nanoparticles synthesised in pressure vial with RTILs (a) PAA (b) PAF (c) 3 HPAA (d) 3 HPAF.

The characteristic absorption peak for the bridging coordination modes of acetate group with Zn appears in the range 1500-1650 cm^{-1} resulting from residual acetate used for the synthesis of ZnO nanoparticles. The peaks at 1000 to 1100 cm^{-1} and 2928 cm^{-1} can be assigned to the symmetric methylene stretching. The stabilization of ZnO nanoparticles by using RTIL caused slight changes in the intensities of the absorption band in the range of 600-400 cm^{-1} that is attributed to the Zn-O stretching (characteristic absorption band). These differences in IR spectra can be explained on the basis of constrained growth of the formed nanoparticles.[36]

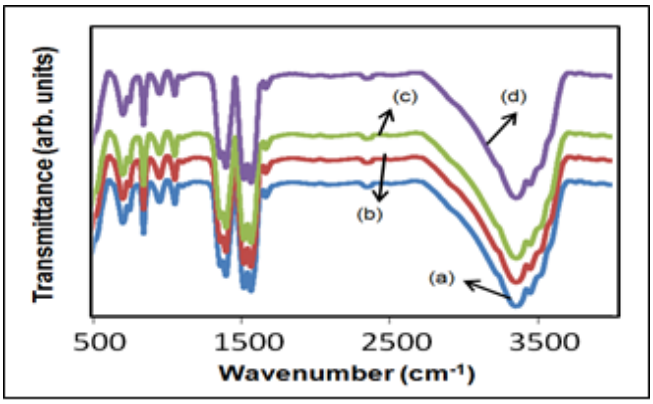

Figure 4. FT-IR spectra of ZnO nanoparticles synthesised in pressure vial with RTIL (a) PAA (b) PAF (c) 3 HPAA (d) 3 HPAF.

Conclusions

In this work, ZnO nanoparticles were synthesized using the direct precipitation method at 80°C by pressure vial reaction. The advantage of this method is that a large quantity of ZnO nanoparticles can be synthesized with high purity and the size of the particles is reduced by applying pressure and also an environmentally friendly route. The role of different concentrations of RTIL's (propylammonium acetate (PAA), propylammonium formate (PAF), 3-hydroxypropylammonium acetate (3-HPAA), 3-hydroxypropylammonium formate(3HPAF) on the particle size was studied. X-ray diffraction results show the formation of a hexagonal wurtzite zinc oxide structure with a high degree of crystallinity. By increasing the concentration ratio of the reactant raw materials from 0.1ml to 0.5ml, the intensity of the reflection peaks increased, and the average size of the as-prepared nanoparticles increased from 10 to 20 nm. Transmission electron microscopy revealed the size distribution of the nanoparticles. The actual average size of nanoparticles obtained by TEM for a concentration ratio of 0.5ml was 20 nm. The ZnO nanoparticles were approximately spherical, confirming the result obtain by TEM. The nanoparticle sizes estimated given XRD and TEM are all in good agreement with each other.

References

[1]Carnes, C. L., Klabunde, K. J., *Langmuir*, **2000**, *16*, 3764, DOI: 10.1021/la991498p

[2]Chen, Y. F., Bagnall, D. M. , Koh, V., Park, K., Hiraga, K., Zhu, Z., Yao, T., *J. Appl. Phys.* **1998**, *84*, 3912–3918, http://doi.org/10.1063/1.368538

[3]Liang, W. Y., Yoffe, A. D., *Phys. Rev. Lett*. **1968**, *20*, 59–62, https://doi.org/10.1103/PhysRevLett.20.59

[4]Jiao, S. J., Zhang, Z. Z., Lu, Y. M., Shen, D. Z., Yao, B., Zhang, J. Y., Li, B. H., Zhao, D. X., Fan, X. W., Tang, Z. K., *Appl. Phys. Lett.* **2006**, *88*, 031911, https://doi.org/10.1063/1.2166686 88.

[5]Kakiuchi, K., Hosono, E., Fujihara,S., *J. Photochem. Photobiol. A* **2006**, *179*, 81, http://dx.doi.org/10.1016/j.jphotochem.2005.07.018

[6]Xiangfeng, C., Dongli, J., Djurisic, A. B., Leung, Y. H., *Chem. Phys. Lett.*, **2005**, *401*, 426.

[7]Gouvea, C. A. K., Wypych, F., Moraes, S. G., Duran, N., Peralta-Zamora, P., *Chemosphere* **2000**, *40*, 427, http://dx.doi.org/10.1016/S0045-6535(99)00312-4

[8]Jo, S. H., Lao, J. Y., Ren, Z. F., Farrer, R. A., Baldacchini, T., Fourkas, J. T., *Appl. Phys. Lett.* **2003**, *83*, 4821, http://dx.doi.org/10.1063/1.1631735.

[9]Kang, H. S., Kang, J. S., Kim, J. W., Lee, S. Y., *Appl. Phys.Lett*, **2004**, *95*, 1246, https://doi.org/10.1063/1.1633343.

[10]Yi, G. C., Wang, C. R., Park, W. I., *Semicond. Sci. Technol.* **2005,** *20*, S22, https://doi.org/10.1088/0268-1242/20/4/003

[11]Daneshvar, N., Aber, S., SeyedDorraji, M. S., Khataee, A. R., Rasoulifard, M. H., *Sep. Purif. Tech*. **2007,** *58*, 91, http://dx.doi.org/10.1016/j.seppur.2007.07.016

[12]Maulenkamp, E. A., *J. Phys. Chem. B* **1998**, *102*, 5566–5572, DOI: 10.1021/jp980730h

[13]Chen, W., Malm, J. O., Zwiller, V., Wallenberg, R., Bovin, J. O., *J. Appl. Phys.* **2001**, *89*, 2671–2675, http://dx.doi.org/10.1063/1.1344582.

[14]Rajalakshmi, M., Arora, A. K., Bendre, B. S., Mahamuni, S., *J. Appl. Phys.* **2000**, *87*, 2445 2448, https://doi.org/10.1063/1.372199 .

[15]Matsumoto, T., Kato, H., Miyamoto, K., Sano, M., Zhukov, E. A., Yao, T., *Appl. Phys. Lett*. **2002**, *81*, 1231–1233, http://dx.doi.org/10.1063/1.1499991.

[16]Wang, J., An, X., Li, Q., Egerton, R. F., *Appl. Phys. Lett*. **2005**, *86*, 201911, https://doi.org/10.1063/1.1927711.

[17]Zhou, H., Wissinger, M., Fallert, J., Hauschild, R., Stelzl, F., Klingshirn, C., Kalt, H., *Appl. Phys. Lett*. **2007**, *91*, 181112, https://doi.org/10.1063/1.2805073.

[18]Kang, B. S., Pearton, S. J., Ren, F., *Appl. Phys. Lett.* **2007**, *90*, 083104, https://doi.org/10.1063/1.2709631.

[19]Hartlieb, K. J., Raston, C. L., Saunders, M., *Chem. Mater*. **2007**, *19*,5453–5459, DOI: 10.1021/cm0715646.

[20]Chung, T. F., Luo, L. B., He, Z. B., Leung, Y. H., Shafiq, I., Yao,Z. Q., Lee, S. T., *Appl. Phys. Lett.*, **2007**, *91*, 233112. https://doi.org/10.1063/1.2811717

[21]Welton, T., *Coord. Chem. Rev.*, **2004,** *248*, 2459, http://dx.doi.org/10.1016/j.ccr.2004.04.015

[22]Parvulescu, V. I., Hardacre, C., *Chem. Rev.*, **2007,** *107*, 2615, DOI: 10.1021/cr050948h

[23]Zhang, Z. C., *Adv. Catal*. **2006**, *49*, 153, http://dx.doi.org/10.1016/S0360-0564(05)49003-3

[24]Jiang, Y., Zhu, Y. J., *J. Phys. Chem. B* 109 (2005) 4361, DOI: 10.1021/jp044350+

[25]Zhai, Y., Gao, Y., Liu, F., Zhang, Q., Gao, G., *Mater. Lett*., **2007**, *61*, 5056, http://dx.doi.org/10.1016/j.matlet.2007.04.002

[26]Yu, N., Gong, L., Song, H., Liu, Y., Yin, D., *J. Solid State Chem.*, **2007**, *180*, 799, http://dx.doi.org/10.1016/j.jssc.2006.11.008

[27]Farag, H. K., Endres, F., *J. Mater. Chem*., **2008**, *18*, 442, DOI 10.1039/B711704C

[28]Mumalo-Djokic, D., Stern, W. B., Taubert, A., *Cryst. Growth Des.* **2008** ,*8*, 330. DOI: 10.1021/cg0701372

[29]Sulochana, M., Satya Vani, Ch., Keerthi Devi, D., Subba Naidu, N. V., B. Sreedhar., *Am. J. Mater. Sci.*, **2013**, *3*, 169-177, DOI: 10.5923/j.materials.20130305.09

[30]Gomez, E., Gonzalez, B., Calvar, N., Tojo, E., Dominguez, A., *J. Chem. Eng. Data*, **2005,** *51*, 2096, DOI: 10.1021/je060228n

[31]Prabhu, Y. T., Rao, K. V., Kumar, V. S. S., Kumari, B. S., *World J. Nanosci. Eng.*, **2014**, *4*, 21-28, DOI.10.4236/wjnse.2014.41004

[32]Bhat D. K., *Nanoscale Res. Lett.*, **2008**, 3(31), DOI: 10.1007/s11671-007-9110-4

[33]Prabhu, Y. T., Venkateswara Rao, K., Sesha Sai, V., Pavani, T., *J. Saudi Chem. Soc.*, **2017,** *21*, 180–185, DOI.10.1016/j.jscs.2015.04.002

[34]Oral, A. Y., Bahsi, Z. B., Aslan, M. H., *Appl. Surf. Sci.* **2007,** *253*, 4593, DOI: 10.1007/s11671-007-9110-4

[35]Prabhu, Y. T., Sesha Sai Kumar, V., Venkateswara Rao, K., *Adv. Sci. Eng. Med.*, **2003,** *5*, 1–8, doi:10.1166/asem.2013.1253

[36]Kaschner, A., Haboeck, U., Strassburg, M., Strassburg, M., Kaczmarczyk, G., Hoffmann, A., Thomsen, C., Zeuner, A., Alves, H. R., Hofmann, D. M., Meyer, B. K., *Appl. Phys. Lett.* **2002,** *80*, 1909 http://dx.doi.org/10.1063/1.1461903

Received: 20.03.2019.
Accepted: 14.04.2017.

SYNTHESIS, CHARACTERIZATION AND BIOLOGICAL ACTIVITIES OF 4-THIAZOLIDINONE AND 2-AZETIDINONE DERIVATIVES

Mahesh B. Swami,[a] Niteshkumar S. Kaminwar,[b] Yogesh W. More,[c] Pintu G. Pathare,[d] László Kótai,[e] Pravin K. Kendrekar[f] and Rajendra P. Pawar[d]*

Keywords: Schiff bases, 4-Thiazolidinone, 2-Azetidinone, Antibacterial activity.

Synthesis of new 1-(4-substituted phenylimino)-1-(4-hydroxyphenyl)propanes has been done successfully. These Schiff bases were converted to 3-ethyl-3(4-hydroxyphenyl)-2-(4-substituted phenyl)isothiazolidin-4-one and 3-chloro-1-(4-substituted phenyl)-4-ethyl-(4-hydroxyphenyl)azetidin-2-one derivatives with thioglycolic acid and chloroacetyl chloride/Et_3N mixture in 1,4-dioxane, respectively. All the synthesized compounds were screened for biological activities.

* Corresponding Authors
E-mail: rppawar@yahoo.com
[a] Department of Chemistry, B. S. College, Basmathnagar. Dist. Hingoli, [M.S], India
[b] Department of Chemistry, L.S.B. College, Dharmabad, Dist. Nanded, [M.S], India
[c] CSIR-Indian Institute of Chemical Technology, Hyderabad 500007, Telangana, India
[d] Department of Chemistry, Deogiri College Aurangabad, [M.S], India
[e] Research Centre for Natural Sciences, Hungarian Academy of Sciences, P. O. Box 17, HU-1525, Budapest, Hungary.
[f] Department of Health Sciences, Central University of Technology, Bloemfontein 9300, Free State, South Africa.

Introduction

Schiff bases are condensation products of primary amines and carbonyl compounds,[1] and they were discovered by the Nobel Prize winner, Hugo Schiff in 1864.[2] Schiff bases (also known as imine or azomethine) are the analogs of the ketones or aldehydes in which the carbonyl group (C=O) has been replaced by azomethine group.[3]

Schiff bases are characterized by the presence of an imine group –N=CH-, in their structure which takes part transamination and racemization reactions in biological system.[1] It exhibits an antibacterial and antifungal effect in their biological properties.[4-5] Metal-imine complexes have been widely investigated due to their antitumor and herbicidal activities. They can work as models for biologically important species.[4]

4-Thiazolidinone and 2-azetidinone derivative constitute an important class of heterocyclic compounds having unique importance due to the broad spectrum of pharmacological activities. They were reported to possess antibacterial and antifungal,[6-8] antitubercular[9] and anti-allergic activity.[10]

4-Thiazolidinones and 2-azetidinones have been synthesized by the condensation of 4,4'-diamino-diphenylsulphone with various aromatic or heterocyclic aldehydes to yield the Schiff's bases,[11] then cyclocondensation of these Schiff's bases with 2-mercaptopropionic acid afforded 4-thiazolidinone derivatives.[12]

In a present study 4-hydroxypropiophenone/3,5-diiodo-4-hydroxypropiophenone treated with primary aromatic amines to form Schiff's bases,[13] then the Schiff's bases on cyclization with thioglycolic acid in 1,4-dioxane gave 4-thiazolidinone derivatives.[14]

Similarly, the reaction of the Schiff bases with chloroacetyl chloride in triethylamine and 1,4 dioxane afforded the corresponding 2-azetidinone derivatives.

All the synthesized compounds were confirmed by IR, ^1H NMR, and mass spectra. The synthesized compounds were screened for antibacterial (*Staphylococcus aureus*, *Escherichia coli*).

Experimental

Melting points were determined in open glass capillaries and were found to be uncorrected. The purity of compounds was checked by TLC. IR spectra were recorded in KBr on a Perkin Elmer spectrometer, 1H NMR spectra were recorded in CD_3OD as solvent and TMS was used as an internal standard. Elemental analysis was carried out on Carlo Erba 1108 analyzer. All reagents were purchased from Aldrich and S.D fine.

Synthesis of Schiff's bases

A mixture of 0.01 mol 4-hydroxypropiophenone and 0.01 mol aromatic amine were dissolved in minimum amount of ethanol and refluxed for 3-4 h. The reaction mixture was cooled and poured onto ice water. The solid was filtered, dried and recrystallized from ethanol.

Synthesis of 4-thiazolidinone derivatives (2a-2f)

Schiff's bases (**1a-1f**) 0.01 mmol and 0.01 mmol thioglycolic acid were dissolved in 15 ml of 1,4-dioxane and refluxed for 9-10 h. The completion of the reaction was checked by TLC. The obtained product was poured onto ice, and the solid was filtered off. The separated solid was washed with sodium bicarbonate solution and dried overnight and weighed.

Synthesis of 2-azitidinone derivatives (3a, 3b)

In a 50 ml beaker were taken 0.1 ml (0.001 mol) chloroacetyl chloride and 15 ml of 1,4-dioxane. In another beaker were taken take 0.3ml (0.003 mol) triethylamine, 15 ml of 1,4-dioxane and 0.01 mol of Schiff's base (**1a** or **1b**). Both the beakers were kept in an ice bath to maintain the temperature about 0 ^{0}C. The chloroacetyl chloride solution was slowly added to the Schiff's base solution with constant stirring between 0 and 5 °C. The reaction mixture was stirred for six hours at room temperature. On completion of reaction (TLC) the excess of dioxane removed by evaporated. The residue was poured onto water. The resulting solid was filtered, washed with water and recrystallized from chloroform.

3-Ethyl-3-(4-hydroxyphenyl)-2-[4-chlorophenyl]iosthiazolidin-4-one (2a)

Light yellow, M.F.$C_{17}H_{16}O_2N_1SCl$, M.W. 333.5, Yield: 62 % , Anal. calcd; C: 61.16, H; 4.79, N; 4.19, S; 9.59, Cl; 10.64. ^{1}H NMR; 7.05(m, CHbenzene), 6.68-6.95 (m, CHbenzene) 4.9-5.0-(s, 1H, aromC-OH), 3.72-(s, 2H, -CH_2), 2.09 (q, 2H, -CH_2), 0.96 (t, 3H,-CH_3), IR KBr cm^{-1} : 1651(C=O), 1605(-CH_2- bend.), 1358(C-N), 993(aromCH=).

3-Ethyl-3-(4-hydroxyphenyl)-2-[pyridine-2yl]-iosthiazolidin-4-one (2b)

White yellow, M.F.$C_{16}H_{16}O_2N_2S$, M.W. 300.0, Yield: 64 %, Anal. calcd; C: 66.89, H; 5.92, N; 4.87, S; 11.14. ^{1}H NMR; 8.07-8.1 (m, CHbenzene), 6.68-6.95 (m, CHbenzene) 4.9-5.0-(s, 1H, aromC-OH), 3.72-(s, 2H,-CH_2), 2.09--(q, 2H, -CH_2), 0.96--(t, 3H,-CH_3), IR KBr cm^{-1}: 1689(C=O), 1605(-CH_2- bend.), 1357 (C-N), 800 (=CHarom).

3-Ethyl-3-(4-hydroxyphenyl)-2-[4-methoxyphenyl]-iosthiazolidin-4-one (2c)

Brown, M.F. $C_{18}H_{19}O_3N_1S$, M.W. 329.0, Yield: 52 % , Anal. calcd; C: 65.65, H; 5.77, N; 4.25, S; 9.72. ^{1}H NMR; 7.12(m, CHbenzene), 6.49-6.77(m, CH benzene), 4.9-5.0(s, 1H, aromC-OH), 3.71(s, 2H,-CH_2), 3.83(s, 3H-CH_3), 2.09(q,2H, -CH_2), 0.96(t, 3H, -CH_3), IR KBr, cm^{-1} : 1648(C=O), 1605(-CH_2- bend.), 1354(C-N), 990(=CHarom).

3-Ethyl-3-(4-hydroxyphenyl)-2-[4-methylphenyl]isothiazo1idin-4-one (2d)

White yellow, M.F.$C_{18}H_{19}O_2N_1S$, M.W. 329.0, Yield: 52 % , Anal. calcd; C: 69.009, H; 6.0702, N; 4.4728, S; 10.2236. ^{1}H NMR; 7.01(m, CHbenzene), 6.49-7.12 (m, CHbenzene) 4.9-5.0(s, 1H, aromC-OH), 3.77(s, 2H, -CH_2), 2.34 (s,3H-CH_3), 2.09(q, 2H, -CH_2), 0.96(t, 3H, -CH_3), IR KBr, cm^{-1}: 1648(C=O), 1605(-CH_2- bend.), 1354-(C-N), 990-(aromCH=).

3-Ethyl-3-(4-hydroxyphenyl)-2-[4-nitrophenyl]isothiazolidin-4-one (2e)

Yellow, M.F.$C_{17}H_{16}O_4N_2S$, M.W. 344.0, Yield: 62.34 %, Anal. calcd; C: 59.30, H; 4.65, N; 8.14, S; 9.30 ^{1}H NMR; 8.04(m, CHbenzene), 6.70-7.12(m, CHbenzene) 4.9-5.0(s, 1H, aromC-OH), 3.77(s, 2H,-CH_2), 2.34 (q, 2H, -CH_2), 0.96 (t, 3H,-CH_3), IR KBr cm^{-1}: 1689(C=O), 1605(-CH_2-, bend.), 1358-(C-N), 993-(=CHarom).

3-Ethyl-3-(3,5-diiodo-4-hydroxyphenyl)-2-[4-methoxyphenyl]-iosthiazolidin-4-one (2f)

Brown, M.F. $C_{17}H_{14}O_2N_1SI_2Cl$, M.W. 543.50, Yield: 49 % , Anal. calcd; C: 65.65, H; 5.77, N; 4.25, S; 9.72. ^{1}H NMR; 7.52(m, CHbenzene), 6.27-6.70(m, CHbenzene) 4.9-5.0(s, 1H, aromC-OH), 3.71(s, 2H, -CH_2), 2.09(q, 2H, CH_2), 0.96(t, 3H, -CH_3), IR KBr cm^{-1}: 1648(C=O), 1605(-CH_2-bend.), 1354-(C-N), 990-(aromCH=).

3-Chloro-1-(4-chlorophenyl)-4-ethyl-(4-hydroxyphenyl)azetidin-2-one (3a)

Brown yellow, M.F.$C_{17}H_{15}O_2NCl_2$, M.W. 336.00, Yield: 51.76 % , Anal. calcd; C: 60.7145, H; 4.642, N; 4.1666, Cl; 21.1309. ^{1}H NMR; 7.04-7.32(m, CHbenzene), 6.65-6.96- (m, CHbenzene), 4.9-5.0(s, 1H, aromC-OH), 5.43(s, 1H, -CH), 1.73(q, 2H, -CH_2), 0.96(t, 3H, -CH_3), IR KBr, cm^{-1}: 1649(C=O), 1605(-CH_2- bend.), 1357-(C-N), 993-(aromCH=).

3-Chloro-4-ethyl-(4-hydroxyphenyl)-1-(pyridine-2-yl)azetidin-2-one (3b)

White yellow, M.F. $C_{17}H_{15}O_2N_2Cl$, M.W. 314.5, Yield: 60.00 %, Anal. calcd; C: 4.86, H; 4.77, N; 8.90, Cl; 11.29. ^{1}H NMR; 8.05-8.1(m, CHbenzene), 6.65-6.96(m, CHbenzene) 4.9-5.0(s, 1H, arom.C-OH), 5.43(s, 1H, -CH), 1.73(q, 2H, -CH_2), 0.96(t, 3H, -CH_3), IR KBr, cm^{-1}: 1689(C=O), 1605(-CH_2- bend.), 1351-(C-N), 800-(aromCH=).

Result and discussion

The Schiff base precursors (**1a-1f**) were prepared in the reaction of 4-hydroxypropiophenone and amine compounds in ethanol under 3-4 h reflux according to the ususal procedure. These Schiff's bases on cyclocondensation reaction in 1,4-dioxane with thioglycolic acid and 1-chloroacetyl chloride afforded 4-thiazolidinone (**2a-2f**) and 2-azitidinone (**3a, 3b**) derivatives, respectively. For example, the compound **1** could be transformed into **2a** and **3a** with thioglycolic acid and chlorocetyl chloride/Et_3N in 1,4-dioxane with 62 and 51 % yield, respectively.

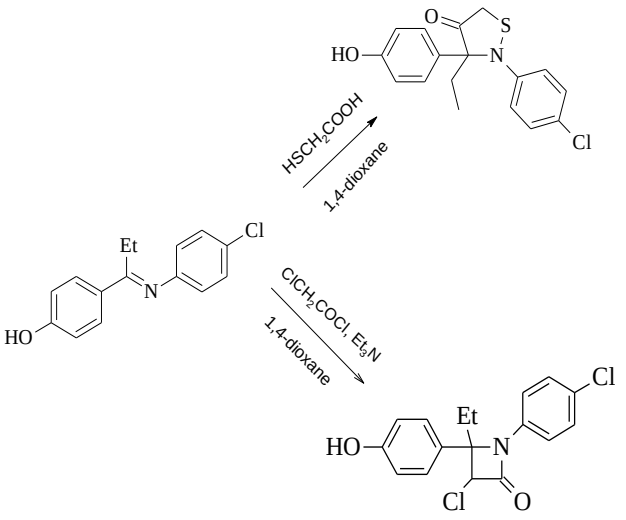

Scheme 1. Synthesis of the isothiazolidinone (**2a-2f**) and azetidinone (**3a** and **3b**) compounds

The structure of the formed compounds (**2a-f** and **3a,3b**) were confirmed by elemental analysis, IR and NMR spectral studies. All of these compound show the band at 1690 cm^{-1} belong to the the cyclic C=O group.

Antibacterial activity of compounds

The synthesized compounds were subjected to antibacterial studies using Staphylococcus aureus and E. Coli bacteria and the results were expressed regarding zones of inhibition.

The antibacterial activity of the series has been carried out against some strain of bacteria. The result shows that the prepared compounds are toxic to bacteria and found to be more active against the above microbes. The comparison of the antibacterial activity of these compounds with penicillin and sulphanylamide shows that these compounds have almost similar activity.

Table 1. Antimicrobial effect of the synthesized compounds (**2a-f** and **3a**, **3b**)

	Zone of inhibition in mm	
Compound	**Staphylococcus aureus**	**E. Coli**
2a	18	16
2b	12	14
2c	18	21
2d	22	24
2e	16	14
2f	17	19
3a	21	18
3b	16	26

Conclusion

The present work describes the synthesis of Schiff's bases, 4-thiazolidinone, and 2-azetidinone derivatives were prepared and reaction completion was confirmed by TLC and synthesized compounds purified by recrystallization. The structure of synthesized compounds assigned by on the basis of the spectral data elemental analysis, IR spectral studies and NMR spectral studies and these compound shows the band at 1690cm^{-1} for the cyclic C=O group. All these compounds show the NMR signal for different kinds of positions at the respective position.

References

[1]Ashraf M. A., Mahmood K., Wajid A.: Synthesis, Characterization and Biological Activity of Schiff Bases. *Int. Conf. Chem. Chem. Process*, IPCBEE, **2011**, *10*, 1–7, IACSIT Press, Singapore.

[2]Kalaivani, S., Priya, N. P., Arunachalam, S., *Int. J. Appl. Biol. Pharm. Technol.*, **2012**, *3*, 219–223.

[3]Ashraf, M., Wajid, A., Mahmood, K., Maah, M., Yusoff, I., *Orient. J. Chem*., **2011**, *27(2)*, 363–372.

[4]Golcu, A., Tumer, M., Demirelli, H., Wheatley, R., *Inorg. Chim. Acta*, **2005**, *358*, 1785–1797. http://dx.doi.org/10.1155/2013/108740

[5]Singh, G. S., Molosti B. J., *Farmaco*., **2005**, *60*, 727-730.

[6]Rahman, V. P., Mkhtar, S., Ansari, W. S., Lemiere G., *Eur. J. Med. Chem.*, **2005**, 40, 173-184. DOI: 10.1016/j.ejmech.2004.10.003

[7]Mehta, D. S. , Shah V. H., *Indian J. Heterocycl. Chem.*, **2001**, *11*, 139-144. DOI: 10.4103/0250-474X.22978

[8]Kucukguzel, S. G., Orul, E. E., Rollas, S., Salin, F., Ozbek A., *Bioorg. Med. Chem*., **2005**, *13*, 6771-6776. http://doi.org/10.1016/j.bmc.2005.07.063

[9]Goel, B., Ram, T., Tyagi, Bansal, R. E., Kumar, A., Mukharjee, D., Sinha J. N., *Eur. J. Med. Chem*., **1999**, *34*, 265-269. http://doi.org/10.1016/S0223-5234(99)80060-9

[10]Soleiman, H. A.; Abdel-Latif, F. M; Khalil, M. A.;Elazab, L. H., Phosphorus, Sulfur and Silicon, **2002**, *177*, 1001. http://dx.doi.org/10.1080/10426500701242848

[11]Elkanzi, N. A. A., Solieman, H. A and Khalafallah, A. K., *Phosphorus, Sulfur, and Silicon*, **2007**, *182*, 1483-1496. http://dx.doi.org/10.1080/10426500701242921

[12]Conli, M., Gulielmetli, R., Metzger, J., *Bull. Soc. Chim. Fr.*, **1967**(8), 2834-2841.

[13]More, S. V., Dongakadekar, D. V., Chavan, R. N., Jadhav, W. N., Bhusare, S. R., Pawar; R. P. *J. Ind. Chem. Soc*., **2002**, *79*, 768-769.

Received: 15.04.2017.
Accepted: 19.03.2017.

SYNTHESIS AND EVALUATION OF BIOLOGICAL ACTIVITIES OF SOME (2-HYDROXY-1-NAPHTHYL)(3-(SUBSTITUTED PHENYL)BICYCLO[2.2.1] HEPTENE-2-YL)METHANONES

G. Thirunarayanan

Keywords: water-mediated Diels-Alder reaction; 2-hydroxy-1-naphthyl chalcones; cyclopentadiene; IR spectra; NMR spectra; antimicrobial activity; antioxidant activity.

Totally twelve ((2-hydroxy-1-naphthyl))(3-(substituted phenyl)bicyclo [2.2.1]hept-5-ene-2-yl)methanones have been synthesized by fly-ash catalyzed water-mediated Diels-Alder [4+2] cycloaddition reaction. The synthesized bicyclic ketones were characterized by their physical constants, analytical and spectroscopic data. The antimicrobial and antioxidant activities of these bicyclic methanones were evaluated using Bauer-Kirby disc diffusion and diphenyl picrylhydrazyl(DPPH) radical scavenging technique. Most of the bicyclic methanones showed good antibacterial and antifungal activities against their microbial strains. The hydroxy- and methoxy- substituted methanones shows significant antioxidant activity.

*Corresponding Authors
Tel.: +914144231215
E-Mail: drgtnarayanan@gmail.com;
thirunarayanan.g.10313@annamalaiuniversity.ac.in
[a] Department of Chemistry, Annamalai University, Annamalainagar-608002, India.

INTRODUCTION

In stereo selective reactions, the Diels-Alder reaction is the most important for of six-membered bicyclic compound synthesis by [4+2] cycloaddition of diene and dienophiles.[1, 2] The retro-Diels-Alder reaction was possible when this reaction is carried out in thermal condition. The mechanistic aspects of reaction conditions, *endo-exo*-product selectivity, and influence of solvents of this Diels-Alder reaction have been reported.[3-7] Currently, greener Diels-Alder reaction is essential for the synthesis of bicyclic compounds with product selectivity. The ease of workup and technical procedure, non-hazardous, shorter reaction time, non-polluted to the environment and good yields are the advantages of this reaction.[1,2,8,9] Rideout and Breslow[10] have studied the cycloaddition reaction of ethylenic ketones and cyclopentadiene in an aqueous medium and they reported the reaction rate is greater than 700 times faster than in non-aqueous media. Many catalysts such as Lewis acids,[5] Bronsted acids,[6,11] asymmetric helical polymers,[12] Cu^{2+} ion-mediated nanotubes[13] and Micellar-DNAs[8,13-18] have been employed for the Diels-Alder [4+2] cycloaddition reaction of cyclopentadiene (diene) and (*E*)-chalcones (dienophiles). The unsaturated compounds, ethylenic ketones, substituted aryl bicyclic ketones possess important biological activities and antibodies.[19-22] Recently, Thirunarayanan has reported the synthesis and biological activities of naphthyl based bicyclo[2.2.1]heptane methanones using greener method.[23] The mono- or di- or tri- or poly –OH (alcohols) and $–OCH_3$ substituted organic compounds possess significant antioxidant activities.[24, 25] Literature survey reveals that the synthesis and the study of pharmacological effects of 2-hydroxy-1-naphthyl based bicyclic methanones are almost absent in the past. Hence, the author has taken efforts to synthesize some 2-hydroxy-1-naphthyl based heptane[2.2.1]methanones by greener method for the evaluation of antimicrobial activity by Bauer-Kirby[26] disc diffusion method and the antioxidant activities by diphenyl picrylhydrazyl (DPPH) radical scavenging[27] activity ability.

MATERIALS AND METHODS

Chemicals used in this investigation were procured from Sigma-Aldrich and E-Merck brands. The source of fly-ash is the Thermal Power Plant-II, Neyveli Lignite Corporation (NLC), Neyveli-607 807, Tamilnadu, India. The Mettler FP51 melting point apparatus was used for determining the melting points of all bicyclo [2.2.1]heptene-2-yl methanones. Thermo Scientific Nicolet iS5, USA made Fourier transform spectrophotometer was used for recording infrared spectra (KBr, 4000-400 cm^{-1}) of all bicyclic ketones. The Bruker AV 400 NMR spectrometer was used for recording nuclear magnetic resonance spectra, operating at 400 MHz for ^1H and 100 MHz for ^{13}C spectra in deuterated chloroform solvent using tetramethylsilane as an internal standard. The mass spectra of methanones were recorded in Shimadzu spectrometer using FAB^+ electron impact and chemical ionization mode.

The bacterial and fungal strains were collected from Faculty of Marine Sciences, Annamalai University, Portonovo Campus, Portonovo-608 502, Tamilnadu, India.

Synthesis of substituted styryl (*E*)-2-hydroxy-1-naphthyl ketones

The substituted styryl (*E*)-2-hydroxy-1-naphthyl ketones were synthesized by literature method.[28]

General procedure for synthesis of (2-hydroxy-1-naphthyl)(3-(substituted phenyl)bicyclo [2.2.1] hept-5-ene-2-yl)methanones

An equimolar quantities of substituted styryl (E)-2-hydroxy-1-naphthyl ketones (2 mmol) in 10 mL of ethanol, cyclopentadiene (2 mmol), and 0.5g of fly-ash in 5 mL of water were stirred for 6 h in 0-4 °C (Scheme 1). The reaction mixture was kept an overnight. Thin layer chromatogram was used for monitoring the completion of the reaction. Separated the organic layer extract by adding 10 mL of dichloromethane, washed with water, brine (10 mL), dried over on anhydrous Na_2SO_4 and concentration gave the solid product. Further, the crude bicyclic methanones were purified by recrystallization with ethanol.

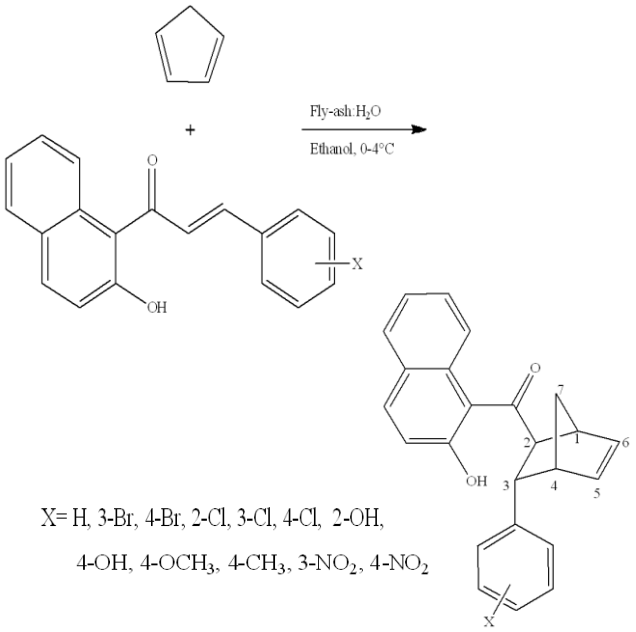

Scheme 1. Synthesis of (2-hydroxy-1-naphthyl)(3-(substituted phenyl)bicyclo[2.2.1]hept-5-en-2-yl)methanones by water-mediated fly-ash catalyzed Diels-Alder reaction of 2-hydroxy-1-naphthyl chalcones and cyclopentadiene.

Antimicrobial activity

The antimicrobial sensitivity assay of prepared bicyclo[2.2.1]heptene-2-yl-methanones were evaluated by means of measuring the diameter of the zone of inhibition in millimeters against their bacterial and fungal strains. There are two gram-positive pathogenic strains (*Staphylococcus aureus, Enterococcus faecalis*) and four gram-negative strains (*Escherichia coli, Klebsiella pneumoniae, Pseudomonas aeruginosa* and *Proteus vulgaris*) were used for evaluation of antimicrobial activities. The Bauer-Kirby[26] disc diffusion technique was employed at the concentration of 250 g mL^{-1} of compounds with ampicillin and streptomycin as standards. The disc diffusion technique was adopted for the evaluation of antifungal activity of all bicyclic ketones against *Candida albicans* strain, and the dilution method was adopted for *Penicillium sp*. and *Aspergillus niger* strains. The dilution concentrations of the prepared bicyclic ketones are 50 g mL^{-1}, and griseofulvin was employed as standard drug.

Measurement of antibacterial sensitivity

The disc diffusion technique was adopted for measurement of antibacterial sensitivity assay of all bicyclic keto compounds. Uniformly spread the prepared bicyclic methanones (0.5mL) over solidified Mueller-Hinton agar. Whatmann No. 1 filter paper discs (5 mm diameters) were made and placed on the medium with potential inhibitor solution. Prevent the collection of water droplets on the medium by kept the discs upside down and incubated at the temperature of 37ºC for 24 h. The discs were examined by measured the diameter in millimeters of the zone of inhibition. The triplicate results were recorded.

Measurement of antifungal sensitivity

The antifungal sensitivity assay of synthesized bicyclic methanones was evaluated using Bauer-Kirby[26] disc diffusion technique. The sterilized potato dextrose agar medium was added to the Petri plates containing 1mL of fungal strains. Uniform spreads of the agar on the plates were performed by means of a clock and anti-clockwise rotation of the discs. The test solution was prepared by dissolving 15 mg of the methanones in 1 mL of dimethylsulfoxide (DMSO) solvent, and it was applied to the discs. This medium was incubated to solidified for 24 or 72 h at 25 or 28 °C. Then these plates were examined for the evaluation of antifungal activity by measurement of the diameter of mm of the zone of inhibition. Triplicate measurement results were recorded.

Measurement of antioxidant activity

The diphenylpicrylhydrazyl (DPPH) radical scavenging activity technique[27] was employed for the measurement of the antioxidant activity of all prepared bicyclic methanones. Sodium acetate buffer solution (20 mL) was prepared by dissolving of sodium acetate (1.64 g) in 15 mL of water, and 150 µL of acetic acid and the final volume was adjusted to 20 mL with water. Diphenyl picrylhydrazyl (DPPH) solution (0.2 mmol, 50 mL) was prepared by dissolving 3.9 g of diphenyl picrylhydrazyl (DPPH) in 50 mL of ethanol. Alpha- tocopherol solution (10 mL) was prepared by dissolving 1mg of alpha-tocopherol in 10mL of ethanol. The buffer solution (1.0 mL) was mixed with 0.5 mL of diphenyl picrylhydrazyl (DPPH) solution in the test tubes and arranged serially. The test solution and α-tocopherol solution were added to the test tubes and kept aside for 30 minutes at room temperature. Measured the absorbance in UV spectrophotometer at 517 nm. The buffer and ethanol were used as the reference. The plot was made with the quantity of bicyclic ketones versus absorption, and the IC_{50} values were determined. The antioxidant activity was expressed by means of IC_{50} values (g mL^{-1}, the concentration required to inhibit DPPH radical formation by 50%). Alpha-Tocopherol was taken as a positive control. The radical scavenging activity (φ) (% of inhibition) was calculated as

$$\varphi = \frac{A_{\text{control}} - A_{\text{sample}}}{A_{\text{control}}}$$

where *A* is the absorbance.

RESULTS AND DISCUSSION

Attempts have been made for the synthesis of (2-hydroxy-1-naphthyl)(3-(substituted phenyl)bicyclo[2.2.1]hept-5-ene-2-yl)methanone derivatives by water-mediated fly-ash catalyzed Diels-Alder reaction with cyclopentadiene as diene and substituted styryl (E)-2-hydroxy-1-naphthyl ketones as dienophiles. Numerous metals and their oxides such as Si, Al, Fe, Ca, C, Mg, K, Na, S, Ti, P, Mn, organic mud and insoluble residues present in the fly-ash.[29] The waste fly-ash was used as a catalyst for organic synthesis. The fly-ash particles are in the silt-sized range of 2-50 microns.30 Glass, mullite-quartz, and magnetic spinel are the three major mineralogical matrices identified in fly ash. The solubility of fly ash has been extensively investigated, and it is largely dependent on factors specific to the extraction methods.

The complete literature study reveals that the long-term leaching studies predicts the fly ash will lose substantial amounts of waste soluble salts, but simulation models predict that the loss of trace elements from fly ash deposits through leaching will be very slow. Traces of radioisotopes are found to be the constituents of fly ash which do not appear to be hazardous. Hence, the author has synthesized (2-hydroxy-1-naphthyl)(3-((un)substituted phenyl)bicyclo-[2.2.1]heptene-2-yl)methanones by water-mediated Diels-Alder reaction of substituted styryl (E)-2-hydroxy-1-naphthyl ketones and cyclopentadiene under cooling condition. During reaction, the chemical species present in the fly-ash was catalyzed the [4+2] cycloaddition reaction. In this water-mediated Diels-Alder reaction the observed yields are more than 60 %. The analytical data, physical constants and mass fragments of synthesized bicyclic methanones are presented in Table 1.

Table 1. The yield, physical constants and mass fragments of (2-hydroxy-1-naphthyl)-3-(substituted phenyl)-bicyclo[2.2.1]hept-5-en-2-yl)methanones

Entry	X	M.F.	M.W.	M.p. °C	Yield,%	Mass (m/z)
1	H	$C_{24}H_{20}O_2$	340	114-115	65	340[M^+], 323, 2623, 197, 171, 169, 143, 126, 120, 77, 17
2	3-Br	$C_{24}H_{19}BrO_2$	419	121-122	63	419[M^+], 421[M^{2+}], 402, 339, 275, 263, 154, 143, 90, 79, 76, 17
3	4-Br	$C_{24}H_{19}BrO_2$	419	116-117	63	419[M^+], 421[M^{2+}], 402, 339, 275, 263, 247, 154, 143, 126, 92, 90, 79, 76, 17
4	2-Cl	$C_{24}H_{19}ClO_2$	375	104-108	60	375[M^+], 377[M^{2+}], 357, 263, 246, 203, 171, 154, 143, 126, 120, 77, 35, 26, 17
5	3-Cl	$C_{24}H_{19}ClO_2$	375	112-113	62	375[M^+], 377[M^{2+}], 357, 263, 246, 231, 171, 143, 126, 120, 111, 77, 35, 17
6	4-Cl	$C_{24}H_{19}ClO_2$	375	132-133	63	375[M^+], 377[M^{2+}], 357, 339, 263, 246, 231, 203, 171, 154, 143, 126, 120, 111, 94, 77, 35, 26, 17
7	2-OH	$C_{24}H_{20}O_3$	356	98-99	62	356[M^+], 339, 263, 196, 171, 143, 120, 92, 77, 66, 34, 17,
8	4-OH	$C_{24}H_{20}O_3$	356	116-117	64	356[M^+], 339, 322, 263, 196, 171, 168, 143, 120, 93, 92, 77, 66, 54, 34, 17,
9	2-OCH_3	$C_{25}H_{22}O_3$	370	111-112	65	370[M^+], 355, 353, 339, 322, 263, 246, 227, 199, 196, 184, 171, 154, 143, 126, 107, 92, 31, 17, 15
10	4-CH_3	$C_{25}H_{22}O_2$	354	126-127	64	354[M^+], 339, 322, 263, 246, 211, 196, 171, 168, 154, 143, 126, 120, 91, 76, 17, 15
11	4-NO_2	$C_{25}H_{19}NO_3$	385	122-123	61	385[M^+], 368, 339, 263, 246, 171, 154, 126, 122, 92, 76, 46
12	4-NO_2	$C_{25}H_{19}NO_3$	385	122-123	61	385[M^+], 368, 339, 263, 246, 242, 214, 171, 154, 143, 126, 122, 92, 76, 46, 28, 17

Table 2. The effect of solvents on the aqueous phase Diels-Alder reaction of styryl-2-hydroxy-1-naphthyl ketone and cyclopentadiene (entry1)

Solvent	Ethanol	Methanol	Dichloromethane	Dioxane	Tetrahydrofuran
Yield	65	63	62	60	62

The effect of the catalyst by means of reusability was studied in this cycloaddition reaction with 2 mmol of styryl (E)-2-hydroxy-1-naphthyl ketone and 2 mmol of cyclopentadiene (entry 1). The first run yield was 65%. The 2nd and 3rd runs gave 60 and 53%. The fourth and fifth runs yield 40% product. The substituted styryl (E)-2-hydroxy-1-naphthyl ketones possess electron-donating substituents (OCH3) gave a higher yield than electron-withdrawing (halogens and nitro) substituents. The catalytic effect of catalyst loading on this cycloaddition reaction was studied by varying the catalyst quantity from 0.1 to 1 g. As the quantity of catalyst increased from 0.1 to 0.4 g, the percentage of yield increased from 60-65%. Further, increase the catalyst quantity beyond 0.4 g, there is no increase in the percentage of yield. The effect of catalyst loading was illustrated in Fig.1.

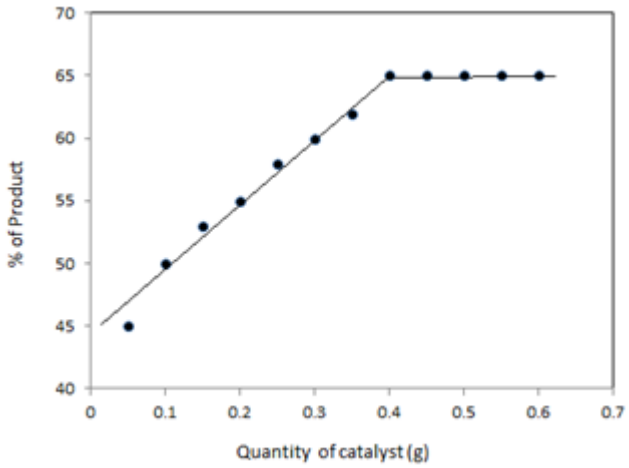

Figure 1. The effect of catalyst loading

The optimum quantity of catalyst loading was in the cycloaddition reaction was found to be 0.4 g. The influence of solvents on this cycloaddition reaction (entry 1) was studied with the same quantity of reactants with solvents such as methanol, dichloromethane, dioxane and tetrahydrofuran and is presented in Table 2. The higher yield was obtained in ethanol with the fly-ash in aqueous medium.The proton and carbon-13 nuclear magnetic resonance spectrum of parent bicyclic methanone are shown in Figs. 2 and 3. The infrared and nuclear magnetic resonance spectral data of bicyclic methanones are summarized as follows.

(2-Hydroxynaphthalen-1-yl)(3-phenylbicyclo[2.2.1]-hept-5-en-2-yl)methanone (1)

IR(KBr) 3468.28, 2989.27, 1675.37, 1548.28, 1431.61, 1024.51, 884.11 cm^{-1}; ^1H NMR (400 MHz, $CDCl_3$): δ = 2.652 (dd, 1H, H_1) *J* = 5.22 and 12.42 Hz, 3.622 (t, 1H, H_2), 3.196(t, 1H, H_3), 2.128(dd, 1H, H_4) *J* = 5.12 and 4.11Hz, 5.478(d, 1H, H_5), 5.939(d, 1H, H_6), 2.078(dd, 1H, H_7) *J* = 9.4 and 16.2Hz, 1.584(dd, 1H, $H_{7'}$) *J* = 6.6 and 12.2 Hz, 7.096-8.435(m, 11H, Ar-H); ^{13}C NMR(100 MHz, $CDCl_3$): δ = 190.53(CO), 40.33(C_1), 54.47(C_2), 46.03(C_3), 50.29(C_4), 135.47($C_{5,6}$), 45.86(C_7), 125.98-141.34(Ar-C).

(3-(3-Bromophenyl)bicyclo[2.2.1]hept-5-en-2-yl)(2-hydroxynaphthalen-1-yl)methanone (2)

IR(KBr) 3438.18, 2968.56, 2822.63, 1678.28, 1558.82, 1462.37, 1131.79, 1088.79, 822.85 cm^{-1}; ^1H NMR(400 MHz, $CDCl_3$): δ 3.076(dd, 1H, H_1), *J* = 7.24 and 9.44 Hz, 3.781(t, 1H, H_2), 3.660(t, 1H, H_3), 2.640(dd, 1H, H_4) *J* = 7.40 and 10.46Hz, 6.621(d, 1H, H_5), 6.618(d, 1H, H_6), 2.041(dd, 1H, H_7)*J* = 5.64 and 7.84 Hz, 1.788(dd, 1H, $H_{7'}$) *J* = 8.66 and 5.94Hz, 7.668-8.881(m, 10H, Ar-H); ^{13}C NMR(100 MHz, $CDCl_3$): δ 190.81(CO), 42.64(C_1), 54.72(C_2), 45.68(C_3), 51.77(C_4), 135.73($C_{5,6}$), 46.23(C_7), 123.52-156.89(Ar-C).

(3-(4-Bromophenyl)bicyclo[2.2.1]hept-5-en-2-yl)(2-hydroxynaphthalen-1-yl)methanone (3)

IR(KBr) 3431.16, 2982.26, 2894.83, 1667.18, 1541.72, 1476.97, 1141.78, 1043.89, 838.78 cm^{-1}; ^1H NMR(400MHz, $CDCl_3$): δ = 2.860(dd, 1H, H_1) *J* = 9.4 and 10.2Hz, 3.768(t, 1H, H_2), 3.573(t, 1H, H_3), 2.816(dd, 1H, H_4) *J*= 7.42and 3.6Hz, 5.3(d, 1H, H_5), 5.958(d, 1H, H_6), 2.158(dd, 1H, H_7) *J* = 12.4 and 6.8 Hz, 1.618(dd, 1H, $H_{7'}$) *J* = 9.5 and 12.4 Hz, 7.638-8.862(m, 10H, Ar-H); ^{13}C NMR(100MHz, $CDCl_3$): δ 189.38(CO), 37.42(C_1), 54.93(C_2), 34.88(C_3), 45.46(C_4), 135.73($C_{5,6}$), 44.54(C_7), 126.78-142.96(Ar-C).

(3-(2-Chlorophenyl)bicyclo[2.2.1]hept-5-en-2-yl)(2-hydroxynaphthalen-1-yl)methanone (4)

IR(KBr) 3432.34, 2996.49, 2889.89, 1683.49, 1595.19, 1463.02, 1224.87, 1068.76, 835.25 cm^{-1}; ^1H NMR(400MHz, $CDCl_3$): δ 3.043(dd, 1H, H_1) *J* = 8.4 and 7.5Hz, 3.432(t, 1H, H_2), 3.238(t, 1H, H_3), 2.220(dd, 1H, H_4) *J* = 6.4 and 8.0Hz, 6.218(d, 1H, H_5), 6.325(d, 1H, H_6), 2.034(dd, 1H, H_7) *J* = 6.72 and 8.92Hz, 1.589(dd, 1H, $H_{7'}$) *J* = 9.81 and 7.5Hz, 7.658-8.741(m, 10H, Ar-H); ^{13}C NMR(100MHz, $CDCl_3$): δ 191.44(CO), 48.28(C_1), 54.68(C_2), 45.73(C_3), 51.41(C_4), 136.48($C_{5,6}$),46.41(C_7), 124.36-152.47(Ar-C).

(3-(3-Chlorophenyl)bicyclo[2.2.1]hept-5-en-2-yl)(2-hydroxynaphthalen-1-yl)methanone (5)

IR(KBr) 3452.13, 2951.09, 2848.09, 1688.59, 1521.89, 1490.02, 1171.28, 1062.27, 861.28 cm^{-1}; ^1H NMR(400MHz, $CDCl_3$): δ 2.738(dd, 1H, H_1) *J* = 4.8 and 10.4Hz, 3.486(t, 1H, H_2), 2.492(t, 1H, H_3), 2.682(dd, 1H, H_4) *J* = 14.8 and 9.2Hz, 5.493(d, 1H, H_5), 6.965(d, 1H, H_6), 2.414(dd, 1H, H_7) *J* = 7.4 and 12.6 Hz, 1.438(dd, 1H, $H_{7'}$) *J*= 9.4 and 8.2 Hz, 7.583-8.776(m, 10H, Ar-H); ^{13}C NMR(100MHz, $CDCl_3$): δ 190.05(CO), 41.20(C_1), 54.81(C_2), 45.19(C_3), 50.37(C_4), 136.26($C_{5,6}$), 46.22(C_7), 125.69-148.80(Ar-C).

(3-(4-Chlorophenyl)bicyclo[2.2.1]hept-5-en-2-yl)(2-hydroxynaphthalen-1-yl)methanone (6)

IR(KBr) 3449.58, 2978.56, 2884.33, 1683.78, 1568.27, 1484.07, 1141.59, 1091.99, 890.85 cm^{-1}; ^1H NMR(400MHz, $CDCl_3$): δ 3.111(dd, 1H, H_1) *J* = 7.4 and 6.2Hz, 3.784(t, 1H, H_2), 3.612(t, 1H, H_3), 2.453(dd, 1H, H_4) *J* = 9.4 and 10.4Hz,

6.017(d, 1H, H_5), 6.102(d, 1H, H_6), 2.036(dd, 1H, H_7) *J* = 11.5 and 8.62Hz, 1.284(dd, 1H, $H_{7'}$) *J* = 8.4 and 6.8Hz, 7.678-8.874(m, 10H, Ar-H); ^{13}C NMR(100MHz, $CDCl_3$): δ 191.48(CO), 41.32(C_1), 54.52(C_2), 46.14(C_3), 51.83(C_4), 136.32($C_{5,6}$), 46.73(C_7), 126.57-153.69(Ar-C).

(3-(2-Hydroxyphenyl)bicyclo[2.2.1]hept-5-en-2-yl)(2-hydroxy-naphthalen-1-ylmethanone (7)

IR(KBr) 3452.93, 2981.57, 2888.59, 1668.34, 1491.51, 1041.89, 893.78 cm^{-1}; ^{1}H NMR(400MHz, $CDCl_3$): δ 3.153(dd, 1H, H_1) *J* = 7.84 and 6.70Hz, 3.563(t, 1H, H_2), 3.792(t, 1H, H_3), 2.618(dd, 1H, H_4) *J* = 11.35 and 7.64Hz, 6.421(d, 1H, H_5), 6.422(d, 1H, H_6), 2.126(dd, 1H, H_7) *J* = 5.18 and 7.42Hz, 1.082(dd, 1H, $H_{7'}$) *J* = 10.24 and 8.63Hz, 7.181-8.579(m, 10H, Ar-H); ^{13}C NMR(100MHz, $CDCl_3$): δ 190.68(CO), 42.81(C_1), 54.72(C_2), 46.62(C_3), 51.79(C_4), 136.23($C_{5,6}$), 47.04(C_7), 125.12-139.92(Ar-C).

(3-(4-Hydroxyphenyl)bicyclo[2.2.1]hept-5-en-2-yl)(2-hydroxy-naphthalen-1-ylmethanone (8)

(IR(KBr) 3478.63, 2991.35, 2888.23, 1689.64, 1468.21, 1048.69, 868.30 cm^{-1}; ^{1}H NMR(400MHz, $CDCl_3$): δ 2.813(dd, 1H, H_1) *J* =16.0 and 6.04Hz, 3.573(t, 1H, H_2), 3.758(t, 1H, H_3), 2.716(dd, 1H, H_4) *J* =11.40 and 8.40Hz, 5.388(d, 1H, H_5), 5.962(d, 1H, H_6), 2.538(dd, 1H, H_7) *J* = 12.2 and 8.2Hz, 1.590(dd, 1H, $H_{7'}$) *J* =10.4 and 11.2Hz, 7.344-8.630(m, 10H, Ar-H); ^{13}C NMR(100MHz, $CDCl_3$): δ 189.88(CO), 43.76(C_1), 52.54(C_2), 44.53(C_3), 50.38(C_4), 135.68($C_{5,6}$), 47.57(C_7), 125.35-153.29(Ar-C).

(3-(4-Methoxyphenyl)bicyclo[2.2.1]hept-5-en-2-yl)(2-hydroxy-naphthalen-1-yl)methanone (9)

IR(KBr) 3538.51, 3022.34, 2993.42, 1663.54, 1561.24, 1458.16, 1255.21, 1088.91, 831.68 cm^{-1}; ^{1}H NMR(400MHz, $CDCl_3$): δ 3.248(dd, 1H, H_1) *J*= 6.4 and 8.4Hz, 3.822(t, 1H, H_2), 3.188(t, 1H, H_3), 2.754(dd, 1H, H_4) *J* = 9.8 and 6.0Hz, 5.582(d, 1H, H_5), 5.638(d, 1H, H_6), 2.215(dd, 1H, H_7) *J* = 12.4 and 7.4Hz, 1.438(dd, 1H, $H_{7'}$) *J* = 10.4 and 11.2Hz, 3.691(s, 3H, OCH_3), 7.688-8.371(m, 10H, Ar-H); ^{13}C NMR(100MHz, $CDCl_3$): δ 190.15(CO), 42.74(C_1), 46.19(C_2), 54.39(C_3), 51.34(C_4), 136.36($C_{5,6}$), 45.88(C_7), 62.80(OCH_3), 125.81-158.94(Ar-C).

(3-(4-Methylphenyl)bicyclo[2.2.1]hept-5-en-2-yl)(2-hydroxynaphthalen-1-yl)methanone (10)

IR(KBr) 3469.13, 3091.00, 2993.87, 1665.34, 1532.65, 1476.34, 1228.31, 1075.34, 873.96 cm^{-1}; ^{1}H NMR(400MHz, $CDCl_3$): δ 2.934(dd, 1H, H_1) *J* = 10.4 and 6.8Hz, 3.694(t, 1H, H_2), 3.190(t, 1H, H_3), 2.688(dd, 1H, H_4) *J* = 9.82 and 7.62Hz, 6.438(d, 1H, H_5), 6.487(d, 1H, H_6), 2.046(dd, 1H, H_7) *J* = 8.64 and 6.60Hz, 1.128(dd, 1H, $H_{7'}$) *J* = 10.34 and 7.62Hz, 3.102(s, 3H, CH_3), 7.322-8.304(m, 10H, Ar-H); ^{13}C NMR(100MHz, $CDCl_3$): δ 189.05(CO), 42.02(C_1), 54.20(C_2), 46.64(C_3), 51.83(C_4), 136.32($C_{5,6}$), 45.56(C_7), 25.87(CH_3), 124.87-154.26(Ar-C).

(3-(3-Nitrophenyl)bicyclo[2.2.1]hept-5-en-2-yl)(2-hydroxy-naphthalen-1-yl)methanone (11)

IR(KBr) 3459.86, 3097.15, 2889.31, 1691.36, 1578.32, 1465.37, 1342.36, 1105.35, 1023.34, 823.51cm^{-1}; ^{1}H NMR(400MHz, $CDCl_3$): δ 3.234(dd, 1H, H_1) *J* = 10.28 and 8.63Hz, 3.668(t, 1H, H_2), 3.551(t, 1H, H_3), 2.679(dd, 1H, H_4) *J* = 9.82 and 10.60Hz, 6.462(d, 1H, H_5), 6.439(d, 1H, H_6), 2.001(dd, 1H, H_7 *J* = 6.82 and 6.68Hz, 1.742(dd, 1H, $H_{7'}$) *J* = 8.84 and 6.62 Hz, 7.766-8.683(m, 10H, Ar-H); ^{13}C NMR(100MHz, $CDCl_3$): δ 191.23(CO), 44.82(C_1), 51.98(C_2), 45.84(C_3), 50.16(C_4), 136.82($C_{5,6}$), 47.37(C_7), 124.95-154.95(Ar-C).

(3-(4-Nitrophenyl)bicyclo[2.2.1]hept-5-en-2-yl)(2-hydroxy-naphthalen-1-yl)methanone (12)

IR(KBr) 3455.98, 3092.34, 1686.76, 1548.22, 1498.13, 1176.16, 998.83, 885.43 cm^{-1}; ^{1}H NMR(400 MHz, $CDCl_3$): δ 3.124(dd, 1H, H_1) *J* = 17.2 and 6.1Hz, 3.743(t, 1H, H_2), 3.527(t, 1H, H_3), 2.758(dd, 1H, H_4) *J*= 12.4 and 4.8Hz, 6.349(d, 1H, H_5), 6.438(d, 1H, H_6), 2.212(dd, 1H, H_7) *J*= 12.4 and 4.4Hz, 1.442(dd, 1H, $H_{7'}$) *J*= 10.4 and 7.4Hz, 7.268-8.558(m, 10H, Ar-H); ^{13}C NMR(100MHz, $CDCl_3$): δ 189.38(CO), 43.74(C_1), 52.46(C_2), 44.55(C_3), 50.38(C_4), 135.76($C_{5,6}$), 46.57(C_7), 125.36-153.29(Ar-C).

Antibacterial activity assay

The disc diffusion technique was followed [24, 27, 30] at a concentration of 250 μg mL-1 ampicillin and streptomycin used as the standard drugs. The measured antibacterial activities regarding zone of inhibition in millimetres of all bicyclic ketones are presented in Table 3.

Compounds **3-6** were shown maximum zone of inhibition against *Escherichia coli*, with greater than 20 mm of the zone of inhibition compared to the methanones **2, 9**, and **12** are moderately active in 13-19 mm of the zone of inhibition. Ketones **8** and **11** are active within 8-12 mm the of zone of inhibition. The bicyclic ketones **4**, **6** and **7** were found to be effective against *S. aureus* greater than 20-24 mm of the zone of inhibition. Compounds **3**, **9** and **10** were moderately active greater than 13-19 mm of the zone of inhibition. The bicyclic methanone **2** and **5** were active within 8-12 mm of the zone of inhibition.

The bicyclic keto derivatives **4** and **6** were more active against *Pseudomonas* showing greater than 20 mm zone of inhibition and the other derivatives **1, 3, 7, 8**, 11 and 12 were showed the zone of inhibitions between 13-19 mm. Compounds **5, 9** and **10** have shown moderately active with the zone of inhibition of 8-12 mm. The bicyclic ketones **2, 5, 6** and **12** are effective against *K. pneumoniae* with 20-24 mm zone of inhibition while the other ketones showed a moderate activity. The methanones **1, 4, 6** and **19** were active when it is screened against *P. vulgaris*, and the other compounds were found to be less effective. The ketones **1, 3** and **5** showed activities against E. faecalis when they are screened with 20-24 mm zone of inhibition.

Table 3. Antibacterial activities of (2-hydroxy-1-naphthyl)(3-(substituted phenyl)bicyclo[2.2.1]hept-5-en-2-yl)methanones.

No	X	*E. coli*	*S. aureus*	*P. aeruginosa*	*K. pneumoniae*	*P.vulgaris*	*E. faecalis*
1	H	---	---	+	---	++	++
2	3-Br	+		---	++	+	---
3	4-Br	++	+	+	---	---	++
4	2-Cl	++	++	++	---	++	+
5	3-Cl	++			++	+	++
6	4-Cl	++	++	++	++	++	---
7	2-OH	---	++	+	---	+	+
8	4-OH	---	---	+	---	---	+
9	4-OCH_3	+	+	---	---	++	---
10	4-CH_3	---	+	---	---	+	---
11	3- NO_2	---	---	+	+	---	+
12	4-NO_2	+	---	+	++	+	---

Disc size:6.35 mm; duration:24-45 h; standard:ampicillin (30-33 mm) and streptomycin (20-25 mm); Control:methanol; ---: No activities; --:active (8-12 mm); +: Moderately active(13-19 mm); ++: active (20-24 mm).

Antifungal activity assay

The observed antifungal activities of all prepared methanones are presented in Table 4. Evaluation of antifungal activities of all methanones against *C. albicans* showed that the three compounds **9**, **11** and **12** are effective with 20 mm as the zone of inhibition in 250 µg mL-1 concentration. The methanones **3, 4, 6** and **7** are active with 13-19 mm zone of inhibition containing one fungal colony, and the compounds **1** and **10** were least active with 8-12 mm zone of inhibition containing two or three fungal colonies. Methanones **2, 5** and **8** were inactive in antifungal activity and they contain heavy fungal colonies.

Table 4. Antifungal activities of (2-hydroxy-1-naphthyl)-3-(substituted phenyl)bicyclo[2.2.1]hept-5-en-2-ylmethanones

No.	X	Disc diffusion technique (250 µg mL^{-1}) *C. albicans*	Drug dilution method (50µg mL^{-1})	
			P. species	*A. niger*
1	H	---	+	+
2	3-Br	---	++	+
3	4-Br	+	---	---
4	2-Cl	+	---	++
5	3-Cl	---	---	---
6	4-Cl	+	---	+
7	2-OH	+	+	++
8	4-OH	---	+	---
9	2-OCH_3	++	++	+
10	4-CH_3		++	+
11	3-NO_2	++	++	++
12	4-NO_2	++	++	++

Standard: Griseofulvin and Gentamycin; Duration: 72 h; Control: Methanol; Medium: Potato dextrose agar; ++: No fungal colony; +: One fungal colony; Two-three fungal colonies; ---: Heavy fungal colony.

Compounds **2, 9** and **10-12** are highly active against *Penicillium species* in 20mm of the zone of inhibitions. Ketones **1, 7** and **8** are active, and they show one fungal colony in13-19 mm of the zone of inhibition. Compounds **5** and **6** produced 2-3 fungal colonies and inactive in 8-12 mm of the zone of inhibition against *Penicillium species*. Heavy fungal colonies were produced by the compounds **3** and **4** leads to inactive against *Penicillium species* fungal strain species. The mm of zone inhibition of ketones against *A. niger* was higher for the compounds **4, 7, 11** and **12** at 20 mm of the zone of inhibition. Compounds **1, 2, 6, 9** and **10** were active in 13-19 mm of the zone of inhibition with one fungal colony. The ketone **13** was least active with 2-3 fungal colonies against *A. niger* fungal strain in 8-12 mm of the zone of inhibition. Bicyclic methanone compounds **5** and **8** are inactive against *A. niger* fungal strain and produced heavy fungal colonies. The presence of bromo-, chloro-, methoxy-, methyl- and nitro- substituents are responsible for the enhancement of antimicrobial activities of methanones.

Anti-oxidant activity

From the statistical results of radical scavenging activity experiments, the observed antioxidant activities of methanones [29,30] were presented in Table 5. From Table 5, all bicyclic methanones are active and shows antioxidant activity referred to standard.

Table 5. Antioxidant activities of (2-hydroxy-1-naphthyl)-3-(substituted phenyl)bicyclo[2.2.1]hept-5-en-2-ylmethanones

Entry	X	Antioxidant activity (DPPH radical scavenging)
1	H	34.78 ± 1.18
2	3-Br	32.89 ± 1.26
3	4-Br	31.59 ± 1.18
4	2-Cl	31.85 ± 1.92
5	3-Cl	32.58 ± 1.19
6	4-Cl	32.95 ± 1.54
7	2-OH	37.01 ± 1.65
8	4-OH	37.16 ± 1.69
9	2-OCH_3	36.90 ± 1.78
10	4-CH_3	34.19 ± 1.25
11	3-NO_2	31.18 ± 1.64
12	4-NO_2	31.94 ± 1.82
	α-Tocoferol	37.34 ± 1.57

The observed percentages of inhibition of diphenyl picrylhydrazyl (DPPH) radical scavenging activities are 31.18–37.16 and the standard have 37.34. Among all methanones, the hydroxy and methoxy-substituted methanones (**7** and **8**) were shown most significant antioxidant activity.

CONCLUSIONS

Some (2-hydroxynaphthalen-1-yl)(3-(substituted phenyl)-bicyclo[2.2.1]hept-5-en-2-yl)methanones have been synthesized by water mediated fly-ash catalyzed Diels-Alder [4+2] cycloaddition of cyclopentadiene and substituted styryl (*E*)-2-hydroxy-1-naphthyl ketones. The yields of these methanones were more than 60 %. This greener method offered pollution free environment, less solvent hazard synthesis, simple operative and handling procedure and obtained the good yields. The purities of the synthesized methanones were examined by their physical constants and spectroscopic data. These data were supported for conformation of formation of bicyclic methanones. The antimicrobial activities of these ketones were evaluated by the Bauer-Kirby method. The halogens, methoxy- and nitro- substituted bicyclic methanones show good antibacterial and antifungal activities against their respective microbial strains. The hydroxy- and methoxy- substituted bicyclic ketones shows significant antioxidant activity.

ACKNOWLEDGMENT

The author gratefully acknowledges the University Grants Commission, New Delhi, India, for financial support Grant no.F.30-23/2011(SA-II), through the UGC-PDF Research Award.

REFERENCES

[1]Hayashi, Y., Samanta, S., Gotoh, H., Ishikawa, H., *Angew. Chem.* **2008**, *47*, 6634. DOI: 10.1002/ange.200801408

[2]Mubofu, E. B., Engberts, J. B. F. N., *J. Phys. Org. Chem*. **2004**, *17*, 180. DOI: 10.1002/poc.711.

[3]Breslow, R., Marita, U., Rideout, D. C., *Tetrahedron Lett*. **1983**, *24*, 1901. DOI: https://doi.org/10.1016/S0040-4039(00)81801-8.

[3]Breslow, R., Marita, U., *Tetrahedron Lett*. **1984**, *25*, 1239. DOI: https://doi.org/10.1016/S0040-4039(01)80122-2

[5]Otto, S., Bertoncin, F., Engberts, J. B. F. N., *J. Am. Chem. Soc*. **1996**, *118*, 7702. DOI:10.1021/ja960318k

[6]Otto, S., Engberts, J. B. F. N., *J. Am. Chem. Soc*. **1999**, *121*, 6798. DOI:10.1021/ja984273u

[7]Fringuelli, F., Piermatti, O., Pizzo, F., Vaccaro, L., *Eur. J. Ora. Chem*. **2001**, 439. DOI: 10.1002/1099-0690(200102)2001:3<439::AID-EJOC439> 3.0.CO;2-B

[8]Boersma, A., Bruin, B., Feringa, B. L., Roelfes, G., *Chem. Commun*. **2012,** 2394. DOI: 10.1039/C2CC17350F

[8]Boersma, A., Feringa, B. L., Roelfes, G., *Org. Lett.* **2007**, *9*, 3647. DOI: 10.1021/ol7015274.

[10]Rideout, D. C., Breslow, R., *J. Am. Chem. Soc*. **1980**, *102*, 7816. DOI:10.1021/ja00546a048

[11]Otto, S., Engberts, J. B. F. N., *Tetrahedron Lett*. **1995**, *36*, 2645. https://doi.org/10.1016/0040-4039(95)00304-U.

[12]Megens, R. P., Roefes, G., *Chem. Eur. J*. **2011**, 17, 8514. DOI:10.1002/chem.201100672

[13]Jin, Q., Zhang, L., Cao, H., Wang, T., Zhu, X., Jiang, J., et al., *Langmuir*, **2011**, *27*, 13847. DOI: 10.1021/la203110z

[14]Kuo, C. H., Niemeyer, C. M., Fruk, L., *Croatia Chem. Acta*. **2011**, *84*, 269. DOI: 10.5562/cca1828

[15]Oltra, N. S., Roelfes, G., *Chem. Commun*. **2008**, 6039. DOI: 10.1039/B814489C

[16]Roelfes, G., Boersma, A. J., Feringa, B. L., *Chem. Commun*. **2006,** 635. DOI:10.1039/B516552K

[17]Otto, S., Engberts, J. B. F. N., Nkwak. J. C. T., *J. Am. Chem. Soc.* **1998,** *120*, 9517. DOI: 10.1021/ja9816537

[18]Boger, D. L., Lerner, R. A., Cravatt, B., *J. Org. Chem*. **1994**, *59*, 5078. DOI: 10.1021/jo00096a064.

[19]Banothu, V., Uma, A., Jayalakshmi, L., *Int. J. Pharm. Pharm. Sci*. **2017**, *9*, 192. DOI: http://dx.doi.org/10.22159/ijpps.2017v9i3.16635

[20]Sukandar, E. Y., Fidrianny, **I.**, Susanto, **E.**, Safitri, **D.,** *Asian J. Pharm. Clin. Res.* **2017,** *10*, 196. DOI: http://dx.doi.org/10.22159/ajpcr.2017.v10i1.14838

[21]Thirunarayanan, G., Mayavel, P., Thirumurthy, K., Dinesh Kumar, S., Sasikala, R., Nisha, P., Nithyaranjani, A., *Eur. Chem. Bull*. **2013**, *2*, 598. DOI:10.17628/ECB.2013.2.598.

[22]Azab, A., *Eur. Chem. Bull*. **2017**, *6*, 59. DOI: 10.17628/ecb.2017.6.59-68.

[23]Thirunarayanan, G., *J. Pharm. Appl. Chem*. **2017**, *3*, 19. DOI: http://dx.doi.org/ 10.18576/jpac/030102

[24]Bhardwaj, A., Modi, K. P., *Int. J. Pharm. Pharm. Sci.* **2017**, *9*, 64. DOI: http://dx.doi.org/10.22159/ijpps.2017v9i3.16362

[25]Banerjee, A., Maji, B., Mukherjee, S., Chaudhuri, K., *Int. J. Curr. Pharm. Res*. **2017**, *9*, 42. DOI: http://dx.doi.org/10.22159/ijcpr.2017v9i2.17379

[26]Bauer, A.W., Kirby, W. M. M., Sherris, J. C., Truck, M., *Am. J. Clin. Pathol*. **1966**, 45, 493. DOI: https://www.ncbi.nlm.nih.gov/pubmed/5325707

[27]Shahidi, F., Zhong, Y., *J. Fun. Food*. **2015**, *18*, 757. DOI: 10.1016/j.jff.2015.01.047

[28]Thirunarayanan, G., Mayavel, P., Thirumurthy, K., *Spectrochim. Acta. Part A.* **2012**, *91*, 18. DOI: 10.1016/j.saa.2012.01.054.

[29]Gopalakrishnan, M., Sureshkumar, P., Kanagarajan, V., Thanusu, J., *Res. Chem. Intermed.* **2007**, *33*, 541. DOI: 10.1163/156856707782565822.

[30]El-Mogazi, D., Lisk, D. J., Weinstein, L. K., *Sci. A Total Environ*. **1988**, *74*, 1. DOI: https://doi.org/10.1016/0048-9697(88)90127-1

Received: 19.03.2017.
Accepted: 16.04.2017.

SYNERGISM OF V_2O_5 AND ZnS IN THE PHOTO-OXIDATIVE CONVERSION OF DIPHENYLAMINE ON CdO SURFACE

C. Karunakaran[a]* and S. Karuthapandian[a]

Keywords: Semiconductor; photocatalysis; sunlight; band gap; interparticle charge transfer.

Diphenylamine (DPA) is photocatalytically oxidized to N-phenyl-p-benzoquinone imine (PBQ) on the surface of CdO in ethanol under UV light as well as natural sunlight. The variation of the rate of PBQ formation on CdO surface with (i) [DPA] and (ii) airflow rate conforms to the Langmuir-Hinshelwood kinetic law. The catalyzed PBQ formation increases with the catalyst loading and light intensity. UV-C light is more effective in catalyzed PBQ formation than UV-A light, and the catalyst is reusable. The reaction mechanism on the illuminated CdO surface is discussed, and the kinetic constants deduced. V_2O_5 and ZnS enhance the photocatalyzed formation of PBQ.

*Corresponding Author
Tel: +919443481590
E-Mail: karunakaranc@rediffmail.com
[a] Department of Chemistry, Annamalai University, Annamalainagar 608002, Tamilnadu, India.

Introduction

Selective chemical transformations brought out by semiconductor photocatalysis attract attention.[1-3] TiO_2 based materials are widely used as photocatalysts for chemical transformation. Alcohols are selectively oxidized to ketones with TiO_2 as a photocatalyst, and functionalized nitroarenes are selectively reduced using N-doped TiO_2 photocatalyst.[2] However, the TiO_2-based photocatalysts require UV light for the organic transformations. A search of a visible light photocatalyst for organic synthesis enables utilization of natural sunlight, and here we report oxidative transformation of diphenylamine (DPA) to N-phenyl-*p*-benzoquinone imine (PBQ) using CdO as a visible light photocatalyst. DPA is widely used in the post-harvest treatment of apple, and pear.[4] Reports on photosensitized oxidation of DPA with UV light are many and cyanoanthracenes[5], and benzophenone[6] are some of the photosensitizers employed. We have reported the photooxidation of DPA to N-phenyl-*p*-benzoquinone imine (PBQ) in the absence of photosensitizer.[7] CdO is a narrow band gap semiconductor, and the aim of the present study is to speed up the oxidative transformation of DPA into PBQ by using CdO as a visible light photocatalyst. Another objective of the present investigation is to establish the kinetic model of the light-induced organic transformation by investigating the reaction with UV light as well as natural sunlight under different experimental conditions. It is also of interest to speed up further the photoinduced reaction on CdO surface through interparticle charge separation process by using particulate CdO-V_2O_5 or CdO-ZnS mixture.

Experimental

CdO, ZnS, and V_2O_5 (Johnson Matthey) were used as supplied and their BET surface areas were determined as 14.45, 7.669 and 16.14 $m^2\ g^{-1}$, respectively. The sizes of the particles suspended in methanol were measured with an Easy particle sizer M1.2 Malvern Instruments (focal length 100 mm, beam length 2.0 mm). Standard procedure was followed to prepare potassium tris(oxalato)ferrate(III), $K_3[Fe(C_2O_4)_3].3H_2O$.[8] DPA, AR (Merck) was used as received. Commercially available ethanol was purified by distillation over calcium oxide.

UV-photocatalysis

The photocatalytic transformation in ethanol with UV-A light was carried out using a multilamp photoreactor with eight 8 W mercury UV lamps (Sankyo Denki, Japan) of wavelength 365 nm, shielded by a highly polished anodized aluminum reflector. Four cooling fans at the bottom of the reactor dissipate the heat produced. A borosilicate glass tube of 15-mm inner diameter was employed as the reaction vessel and was placed at the center of the photoreactor. Air was passed through the DPA solution (5 mM unless otherwise mentioned) which kept the catalyst power (1.0 g unless otherwise stated) under suspension and at constant motion. The airflow rate was measured by soap bubble method which was 7.8 mL s^{-1} unless otherwise given. The photon flux (I) was determined by ferrioxalate actinometry which was 25.2 μeinstein $L^{-1}\ s^{-1}$ unless otherwise stated. The photocatalytic transformation was also carried out in a micro-photoreactor fixed with a 6 W 254 nm low-pressure mercury lamp and a 6 W 365 nm mercury lamp. Quartz and borosilicate glass tubes were employed for 254 and 365 nm lamps, respectively. The volume of the reaction solution was 25 mL in the multilamp photoreactor and 10 mL in the micro-photoreactor. The UV-visible spectra were obtained with a Hitachi U-2001 UV-visible spectrophotometer, after dilution of the solution to retain the absorbance within the Beer-Lambert law limit. The PBQ formed was estimated from its absorbance at 450 nm.

Solar-photocatalysis

The solar photocatalytic transformation was performed in summer (March-July) under the clear sky at 11.30 am - 12.30 pm. The solar irradiance (W m^{-2}) was measured with a Global pyranometer supplied by Industrial Meters, Bombay, India.

The near UV light and visible light of wavelength less than 560 nm are responsible for band gap-excitation of CdO, and the intensity of sunlight (einstein L^{-1} s^{-1}) was also obtained by ferrioxalate actinometry, which covers a wavelength range of 250 – 577 nm; 440 W m^{-2} corresponds to 22 μeinstein L^{-1} s^{-1}. Fresh ethanolic solutions of DPA of required concentration (5 mM unless otherwise stated) were taken in wide cylindrical glass vessels of uniform diameter and the entire bottom of the vessel (11.36 cm^2 unless otherwise mentioned) was covered by CdO powder. Air was bubbled (4.6 mL s^{-1} unless otherwise given) employing a micro pump without disturbing the CdO bed (1.0 g unless otherwise stated). The volume of DPA solution was 25 mL, and the loss of ethanol due to evaporation was compensated periodically. PBQ formed was estimated as stated already.

Results and discussion

Photocatalytic transformation with UV light

The photocatalytic transformation of DPA on CdO surface, in the presence of air in ethanol, was studied using multilamp photoreactor. The UV-visible spectra of the DPA solution at different illumination time presented in Figure 1 display the formation of PBQ (λ_{max}= 450 nm).

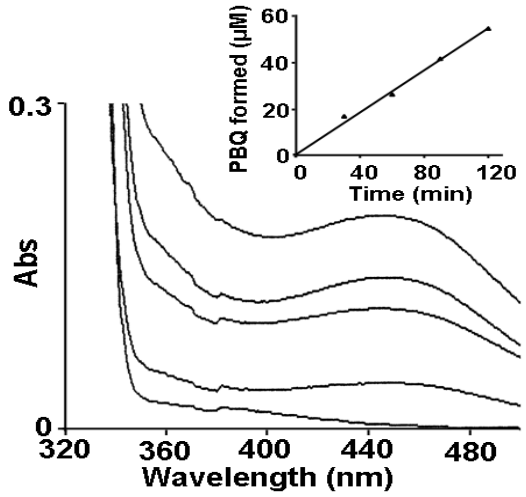

Figure 1. UV-vis spectra of reaction solution (5-times diluted, [DPA] = 20 mM) at 0, 30, 60, 90 and 120 min (↑); inset: linear variation of [PBQ] with illumination time.

The illuminated solution is EPR silent showing the absence of diphenylnitroxide. Besides, thin layer chromatographic analysis using silica gel G coated plate with benzene as eluent shows the formation of a single product; the irradiated DPA solution was evaporated after the recovery of CdO particles and the solid was dissolved in chloroform to develop the chromatogram. The PBQ formed was estimated from the measured absorbance at 450 nm using the reported molar extinction coefficient.[9,10] The linear increase of [PBQ] with irradiation time (Figure 1 inset) affords the initial rate of PBQ formation, and the rates are reproducible to ±6%. As the photoformation of PBQ in the absence of CdO is not negligible [7] the rate of PBQ formation on CdO surface was obtained by measuring the rates of PBQ formation in the presence and absence of CdO. The rate of PBQ formation on CdO increases with [DPA] displaying Langmuir-Hinshelwood kinetics with respect to [DPA]; Figure 2 displays the results.

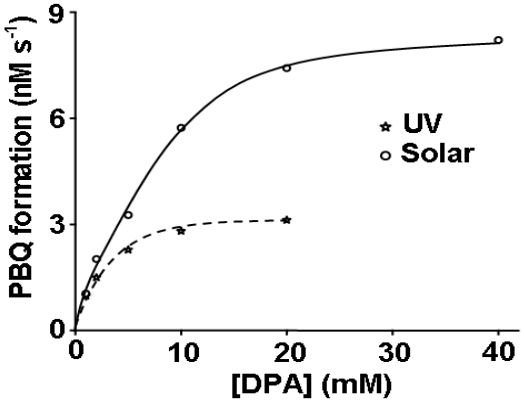

Figure 2. Rate dependence on [DPA].

The increase of the amount of CdO suspended in the DPA solution results in increased PBQ formation on CdO surface, but the rate reaches a limit at high catalyst loading as shown in Figure 3.

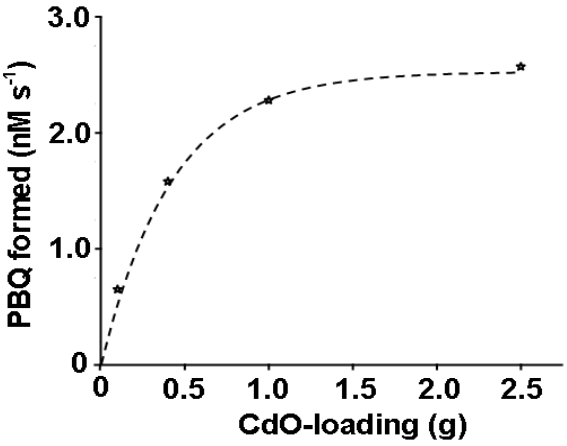

Figure 3. Variation of PBQ-formation rate with catalyst loading.

Determination of the PBQ formation on CdO surface at different airflow rates shows enhancement of the reaction by oxygen and the variation of the reaction rate with the airflow rate conforms to the Langmuir-Hinshelwood kinetics; Figure 4 presents the results. PBQ formation on CdO was also determined without bubbling air, but the solution was not deoxygenated. The dissolved oxygen itself brings in the surface catalyzed reaction, but the PBQ formation is slow. The PBQ formation on CdO was examined at different light intensities. The reaction was carried out with two, four and eight lamps; the angles sustained by the adjacent lamps are 180°, 90° and 45°, respectively. Figure 5 shows the variation of the reaction rate as a function of the photon flux. PBQ is not formed in the absence of irradiation. Study of PBQ formation on CdO surface with a 6 W 365 nm mercury lamp (I = 18.1 μeinstein L^{-1} s^{-1}) and a 6 W 254 nm low-pressure mercury lamp (I = 5.22 μeinstein L^{-1} s^{-1}) separately in the

micro-photoreactor under identical conditions reveals that high energy radiation is more effective in bringing out the surface reaction.

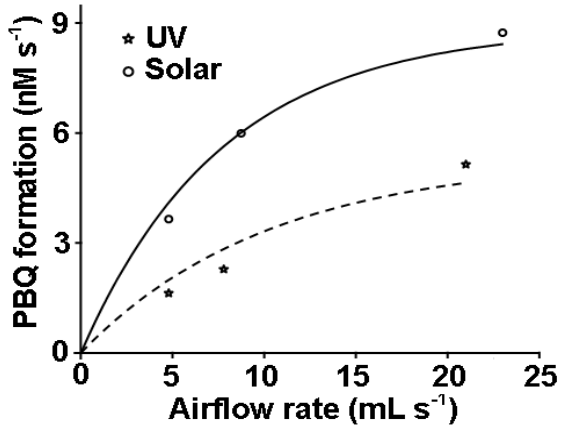

Figure 4. Influence of airflow rate on photocatalytic PBQ-formation.

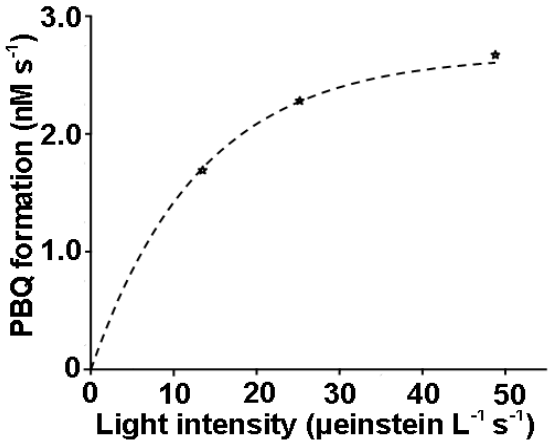

Figure 5. Effect of photon flux on reaction rate.

PBQ formation on CdO with illumination at 365 and 254 nm are 2.2 and 16.5 nM s^{-1}, respectively. The CdO surface does not lose its photocatalytic activity on usage. Reuse of the catalyst reveals sustainable photocatalytic efficiency. Azide ion (5 mM), a singlet oxygen quencher, does not suppress the formation of PBQ indicating the absence of involvement of singlet oxygen in the photocatalysis. This is on the expected line; Fox and Chen[11] ruled out the possibility of singlet oxygen in the TiO_2-photocatalyzed olefin-to-carbonyl oxidative cleavage.

Solar photocatalytic transformation

The photocatalytic transformation of DPA on CdO surface in the presence of air in ethanol under natural sunlight also provides PBQ (*vide infra*). Measurement of solar irradiance (W m^{-2}), even under the clear sky, shows the significant fluctuation of sunlight intensity during the experiment. Hence, the solar experiments at different reaction conditions were carried out in a set so that the quantity of sunlight incident on unit area does not differ. This renders possible the comparison of solar results. A pair of solar experiments carried out simultaneously under identical conditions yield results within ±6%, and this is so on different days. The effect of operational parameters on the surface catalyzed reaction under natural sunlight was investigated by carrying out the given set of experiments simultaneously, and the data in each figure are under identical sunlight intensity. The product formation rates were obtained on illuminating the reaction solutions for 1 h. Figure 2 displays the reaction rate at different [DPA]. The PBQ formation increases with [DPA] and follows Langmuir-Hinshelwood kinetic law. Figure 4 shows the dependence of the rate of surface reaction on the airflow rate. The surface reaction is enhancement by oxygen, and the reaction exhibits Langmuir-Hinshelwood kinetics with respect to oxygen. The PBQ formation on the surface was studied without bubbling air, but the solution was not deoxygenated. The dissolved oxygen itself effects the catalysis. However, the reaction is slow. The PBQ formation on CdO increases linearly with the apparent area of the CdO bed as shown in Figure 6. PBQ is not formed in the absence of illumination. The CdO surface does not lose its catalytic activity on irradiation. Reuse of the CdO powder shows sustainable photocatalytic activity.

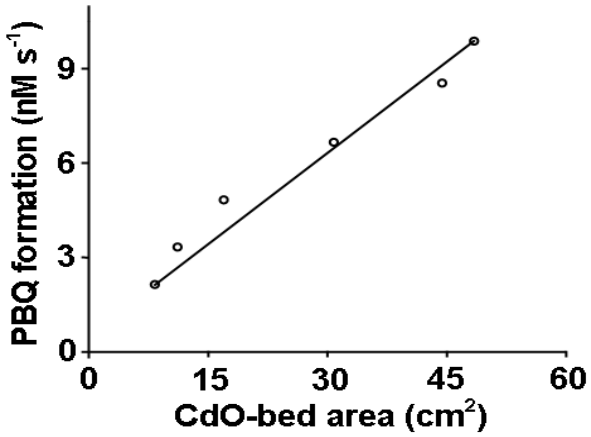

Figure 6. The linear dependence of photocatalytic rate on the apparent surface area.

Mechanism

The determined band gap energy of CdO is 2.2 eV and band gap-illumination results in the creation of electron-hole pairs; electron in the conduction band (CB) and the hole in the valence band (VB). The recombination of the charge carriers in the semiconductor is rapid (occurring in a picosecond time scale) and for an effective photocatalysis, the reactants are to be adsorbed on the surface of CdO.[12] The hole reacts with the adsorbed DPA molecule to form diphenylamine radical-cation ($Ph_2NH^{\bullet+}$). The oxygen molecule adsorbed on the surface of CdO removes the CB electron. The formed superoxide radical-anion is likely to react with diphenylamine radical-cation yielding PBQ (Scheme 1).

$$CdO + h\nu \rightarrow h^+_{(VB)} + e^-_{(CB)}$$

$$Ph_2NH_{(ads)} + h^+_{(VB)} \rightarrow Ph_2NH^{\bullet+}$$

$$O_{2(ads)} + e^-_{(CB)} \rightarrow O_2^{\bullet -}$$

$$Ph_2NH^{\bullet +} + O_2^{\bullet -} \rightarrow$$ 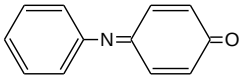 $$+ H_2O$$

Scheme 1. Photocatalytic mechanism

Kinetic law

The kinetic equation corresponding to photoinduced surface reaction taking place in a continuously stirred tank reactor (CSTR)[13] is:

$$\varphi = k\frac{K_1K_2SIC[DPA]\gamma}{(1+K_1[DPA])(1+K_2\gamma)} \quad (1)$$

where

φ is the rate of PBQ photoformation on CdO

K_1 and K_2 are the adsorption coefficients of DPA and O_2 on the illuminated CdO surface,

k is the specific rate of oxidation of DPA,

γ is the airflow rate,

S is the specific surface area of CdO,

C is the amount of CdO suspended per litre, and

I is the intensity of illumination.

The data fit the Langmuir-Hinshelwood curve, drawn using a computer program,[13] confirming the rate law. In addition, linear double reciprocal plots of surface reaction rate versus (i) [DPA] and (ii) airflow rate are in agreement with the kinetic law. The fits provide the adsorption coefficients K_1 and K_2 as 390 L mol^{-1} and 0.031 mL^{-1} s, respectively, and the specific oxidation rate k as 3.4 μmol L m^{-2} $einstein^{-1}$. However, the rate of surface reaction fails to vary linearly with the amount of CdO suspended. This is because of the high catalyst loading. At high CdO loading, the surface area of the catalyst exposed to illumination does not commensurate with the weight of the catalyst. The quantity of CdO employed is beyond the critical amount corresponding to the volume of the reaction solution and reaction vessel; the whole quantity of CdO is not exposed to the light. The photocatalysis lacks linear dependence on illumination intensity; less than first power dependence of surface-photocatalysis rate on light intensity at high photon flux is well known.[14]

Synergism by V_2O_5 and ZnS

Charge transfer across heterojunction in coupled semiconductors enhances the photocatalytic efficiency, and examples for coupled semiconductors are many.[15] In coupled semiconductors, both the semiconductors exist in the same particle, and charge separation occurs within the particle. But what we observe here is enhanced PBQ formation on mixing V_2O_5 or ZnS powder with particulate CdO under UV light. Figure 7 displays the enhanced surface reaction by the CdO-V_2O_5 mixture and CdO-ZnS mixture - the two particulate semiconductors were in suspension and constant motion.

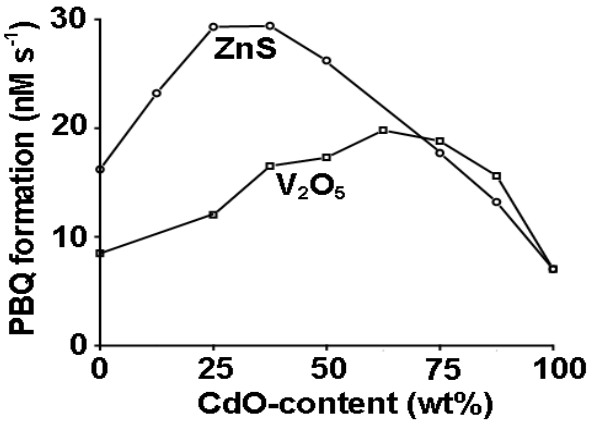

Figure 7. Enhanced PBQ formation on mixing CdO with V_2O_5 or ZnS.

This enhanced photocatalytic transformation is due to interparticle charge transfer. Nanoparticles in suspension aggregate.[16] Figure 8 displays the particle size distributions of CdO, V_2O_5, and ZnS in suspension. They were determined by light scattering technique. But the mean particle sizes (t) of CdO, V_2O_5, and ZnS, obtained by using the relationship $t = 6/\rho S$, where ρ is the material density and S is the specific surface area, are 51, 111, and 190 nm, respectively. Examination of Figure 8 in conjunction with the determined particle sizes shows aggregation of the particles.

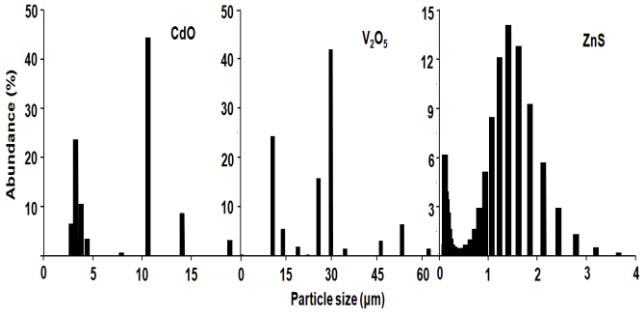

Figure 8. Aggregation of nanoparticles.

As observed in individual semiconductor suspension, aggregation is likely in particulate semiconductor mixtures under suspension, and both the semiconductor particles are likely to be present in the aggregates. Charge transfer between CdO and V_2O_5 or ZnS particles is likely to occur when both the semiconductors are under band gap-illumination and in contact with each other; electron from CB of a semiconductor may move to another if the latter is of low energy, and so is the hole from VB. The CB and VB edge positions of CdO, V_2O_5, and ZnS are presented in Figure 9.[17] The CB, and VB energy levels determine the charge transfer between the particulate semiconductors. The CB electron of CdO is more cathodic than that of V_2O_5. This enables transfer of the electron from the CB of CdO to the

CB of V_2O_5. On the other hand, the CB of CdO is less cathodic than that of ZnS. This favors transfer of CB electron of ZnS to CdO. The VB hole of CdO is less anodic than those of V_2O_5 and ZnS. This renders possible the movement of VB hole of ZnS as well as that of V_2O_5 to CdO. This interparticle charge transfer enhances the photocatalysis. The energy difference between the CB electrons of the two semiconductors is the driving force for the interparticle electron injection, and the free energy change is given by $-\Delta G = e(E_{(CBSC1)} - E_{(CBSC2)}$.[18] In terms of redox chemistry, the CB and VB refer to the reduced and oxidized states in the semiconductor.

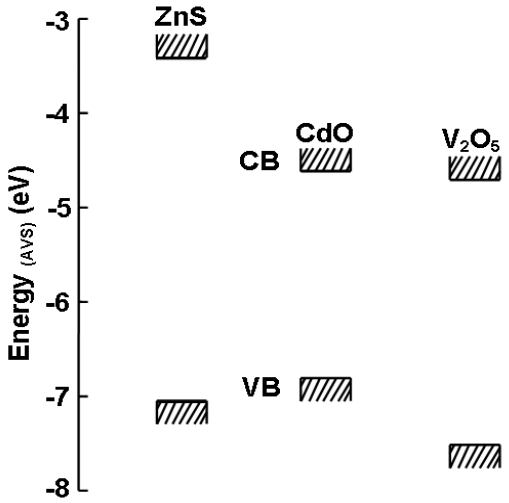

Figure 9. The CB and VB edges.

In CdO, V_2O_5 and ZnS, the CB electrons refer to the reduced forms of Cd^{2+} (*i.e.*, Cd^{+}), V^{5+} (*i.e.*, V^{4+}) and Zn^{2+} (*i.e.*, Zn^{+}), respectively. Similarly, the VB hole refers to the oxidized forms of the corresponding O^{2-} (*i.e.*, O^{-}) or S^{2-} (*i.e.*, S^{-}). The interparticle charge-transfer, the transfer of the electron from the CB of ZnS to that of CdO refers to the electron jump from Zn^{+} to Cd^{2+}. In the case of CB electron movement from CdO to V_2O_5, it is from Cd^{+} to V^{5+}. Similarly, the VB hole-transfer from V_2O_5 and ZnS to CdO corresponds to the hole-jump from O^{-} of V_2O_5 and S^{-} of ZnS to O^{2-} of CdO. The possibility of cross-electron–hole combination, the transfer of the electron from the CB of one semiconductor (SC1) to the VB of the other (SC2) is very remote; the very low population of the excited states makes the electron transfer between two excited states highly improbable. A possible reason for not observing the maximum photocatalytic efficiency at 50% wt. composition for the semiconductor mixtures is the densities and particle sizes of the semiconductors and also the aggregation.

Conclusions

The oxidation of DPA to BPQ on CdO surface is driven by natural sunlight as well as artificial UV light. The BPQ formation enhances with [DPA] and airflow rate and conforms to Langmuir-Hinshelwood kinetic law. The transformation of DPA into PBQ on CdO surface is more under UV-C light than with UV-A light. CdO mixed with either V_2O_5 or ZnS shows the larger formation of PBQ due to interparticle charge separation.

References

[1]Lang, X., Chen, X., Zhao, J., *Chem. Soc. Rev.* **2014,** *43*, 473. https://doi.org/ 10.1039/C3CS60188A

[2]Palmisano, G., Garcia-Lopez, E., Marci, G., Loddo, V., Yurdakal, S., Augugliaro, V., Palmisano, L., *Chem. Commun.*, **2010**, *46*, 7074. https://doi.org/10.1039/C0CC02087G

[3]Shiraishi, Y., Hirai, T., *J. Photochem. Photobiol. C*, **2008**, *9*, 157. https://doi.org/10.1016/j.jphotochemrev.2008.05.001

[4]Zanella, A., *Postharvest Biol. Technol*. **2003**, *27*, 69. https://doi.org/10.1016/S0925-5214(02)00187-4

[5]Chang, Y. C., Chang, P. W., Wang, C. M., *J. Phys. Chem. B*, **2003**, *107*, 1628. https://doi.org/10.1021/jp021852j

[6]Lin, T.S., Retsky, J., *J. Phys. Chem.* **1986**, *90*, 2687. https://doi.org/10.1021/j100403a026

[7]Karunakaran, C., Karuthapandian, S., *Sol. Energy Mater. Sol. Cells*, **2006**, *90*, 1928. https://doi.org/10.1016/j.solmat.2005.12.003

[8]Adams, D. M., Raynor, J. B., *Advanced Practical Inorganic Chemistry*, John Wiley: New York, 1965.

[9]Puri, S., Bansal, W. R., Sidhu, K. S., *Indian J. Chem*. **1973**, *11*, 828.

[10]Bansal, W. R., Ram, N., Sidhu, K. S., *Indian J. Chem. B,* **1976**, *14*, 123.

[11]Fox, M. A., Chen, C. C., *J. Am. Chem. Soc*. **1981**, *103*, 6757. https://doi.org/10.1021/ja00412a044

[12]Xu, H., Ouyang, S., Liu, L., Reunchan, P., Umezawa, N., Ye. J., *J. Mater. Chem. A*, **2014**, *2*, 12642. https://doi.org/10.1039/C4TA00941J

[13]Karunakaran, C., Senthilvalen, S., Karuthapandian, S., *Sol. Energy Mater. Sol. Cells*, **2005**, *89*, 391. https://doi.org/10.1016/j.solmat.2005.01.008

[14]Vincze, L., Kemp, T. J., *J. Photochem. Photobiol. A*, **1995**, *87*, 257. https://doi.org/10.1016/1010-6030(94)03985-4

[15]Karunakaran, C., Sakthiraadha, S., Gomathisankar, P., Vinayagamoorthy, P., *RSC Adv*. **2013**, *3*, 16728. https://doi.org/10.1039/c3ra41872c

[16]Li, M., Noriega-Trevino, M. E., Nino-Martinez, N., Marambio-Jones, C., Wang, J., Damoiseause, R., Ruiz, F., Hock, E. M. V., *Environ. Sci. Technol.* **2011**, *45*, 8989. https://doi.org/10.1021/es201675m

[17]Xu, Y., Schoonen, M. A. A., *Am. Mineral.* **2000**, *85*, 543.

[18]Katoh, R., Furube, A., Yoshihara, T., Hara, K., Fujihashi, G., Takano, S., Murata, S., Arakawa, H., Tachiya, M., *J. Phys. Chem. B*, **2004**, *108*, 4818. https://doi.org/10.1021/jp031260g

Received: 20.03.2017.
Accepted: 23.04.2017.

Cu(II) ION REMOVAL FROM AQUEOUS SOLUTION BY AN *in situ* SYNTHESIZED *Phragmites australis*/EMERALDINE BASE BIOCOMPOSITE

Silviya Lavrova,[a]* Filipa Velichkova-Teneva[a] and Bogdana Koumanova[a]

Keywords: *In situ* polymerization, polyaniline, *Phragmites australis*, copper ions adsorption.

The influence of *in situ* synthesized biocomposite consisted of *Phragmites australis* (Pha) - common reed and emeraldine base (Emb) on the removal of copper ion from aqueous media is discussed. The biocomposites were prepared with two different ratios of common reed/aniline (samples Pha/Emb1 and Pha/Emb2, respectively. Physicochemical parameters such as initial copper ion concentration, composite dosage and contact time between the composites and Cu(II) ions in aqueous solution were studied. An assessment of the equilibrium and the kinetics of sorption of copper ions has been made. Removal efficiency of 99.6 % was achieved with Pha/Emb1 and 91.9 % with Pha/Emb2, respectively. The experimental results were fitted to the isotherms of Langmuir, Freundlich, Temkin and Dubinin-Radushkevich. It was established that the Langmuir isotherm is more suitable for the case of emeraldine base and for composite Pha/Emb1, while the Dubinin-Radushkevich isotherm is more suitable for the case of Pha/Emb2 (with higher content of common reed). The influence of the plant quantity in the biocomposite is important for the mechanism of Cu^{2+} removal. Physical adsorption and ion exchange are dominant in the case of Pha/Emb1, and Emb, while in the case of Pha/Emb2 the chemical interaction is predominant. The kinetics of Cu(II) adsorption onto biocomposites followed pseudo-second-order model.

* Corresponding Authors
Telephone: +359 2 8163 303
E-Mail: *engeco2001@uctm.edu**, *fvelichk@uctm.edu*, *bkk@uctm.edu*
[a] University of Chemical Technology and Metallurgy, Postal address: 8 Kliment Ohridski Blvd., Sofia 1756, Bulgaria

Introduction

The industrial wastewaters in most cases contain metal ions which can be removed by chemical or physicochemical processes. Because of their hazard impact on the environment and the high cost of the used methods, it needs to develop new, cost-effective and efficient methods for industrial wastewater treatment. The most widely used methods for metal ions removal from aqueous medium is precipitation, adsorption and ion exchange, because of their effectiveness, low cost and possibility of metal recovery.

Increasing attention to the biosorbents such as rice hulls, raw pomegranate peel, peanut shells, sphagnum moss peat, tree fern, as well as dried activated sludge, is paid because they are widely spread, not expensive raw materials.[1-6] Also, there are various polymeric substances which can capture various ions, as a result of the complexation reactions. Such materials are chitosan,[7,8] polythioamide,[9] polypyrrole,[10] polyaniline,[11] etc. These polymers can be used either separately or as composites - the combination of different polymers[12,13,15] or combination of the polymer with some adsorbents.[14-16]

One of the widely used polymeric substance is polyaniline, which conductive properties and complexing ability are well-known. The polyaniline can be found in one of three idealized oxidation states – leucoemeraldine, emeraldine, and (per)nigraniline. The emeraldine form of polyaniline exists as emeraldine salt and emeraldine base. The deprotonated nonconducting emeraldine base has more free electron pairs in its structure in comparison with protonated conducting emeraldine salt, which contribute to its better complexation ability.[17-19] The combination of these polymeric compounds with different sorbents leads to increasing of the wastewater treatment efficiency, which is due to the enlarged surface area and the greater electron donor capacity.[20,21] Recently the scientists are focused their attention on the synthesis of biocomposites, which are consisted of residual vegetation and polymeric substances.[22-24] It is known that for the treatment of different kinds of wastewaters constructed wetland systems are used. In them different macrophytes are growing - *Phragmites australis*, *Typha latifolia*, etc., which have the ability to extract and accumulate a variety of contaminants from the treated water.[25,26] These plants are widely spread in nature, which makes their residuals a readily available and inexpensive raw material which can be used further as a sorption material.

The aim of this study was to examine the possibility of the copper ions removal from an aqueous solution by a biocomposite of *Phragmites australis* and emeraldine base. The influence of the initial Cu(II) concentration, the biocomposite dose and the contact time of the removal process were studied. An assessment of the equilibrium and the kinetics of sorption of copper ions has been made.

Material and Methods

Aniline ($C_6H_5NH_2$), hydrochloric acid (HCl), ammonium persulfate ($(NH_4)_2S_2O_8$), sodium hydroxide (NaOH), copper sulfate pentahydrate ($CuSO_4.5H_2O$), sodium acetate

($C_2H_3NaO_2$) and acetic acid (CH_3COOH) pure for analysis were used in the experiments. Distilled water was also used. Leaves of *Phragmites australis* (common reed) from a comparatively clean area in this study were used. After collection, they were washed using tap water then followed with distilled water to remove the dust particles. The washed crops were dried for 2 h at 60 °C. The dried material was rinsed with acetone and then with 0.3 M NaOH and was again dried at the same temperature to constant mass. After its pre-treatment, the dried material was finely ground.

Preparation of the biocomposites

The preparation of the biocomposites was carried out at standard conditions. For the preparation of the biocomposites, two different *Phragmites australis*/aniline ratios were used. In the first case the ratio was 1:15 (Pha/Emb1) and in the second case it was 1:4 (Pha/Emb2). The preliminary weighed amounts of common reed (leaves) were mixed with 1938.6 mL of 1 M HCl under continuous stirring at 800 rpm for 24 h. After that 61.4 mL of aniline was added to the reaction mixture and the suspension was stirred for 24 h at room temperature. The solution of the oxidant, which was necessary for the preparation of polyaniline from aniline monomer, was prepared by dilution of ammonium persulfate ($(NH_4)_2S_2O_8$) with distilled water to a volume of 800 mL. This solution was added to the reaction mixture, and the resulting suspension was stirred continuously for another 24 hours. The suspension was filtered and washed with distilled water. In order to remove the impurities and possible residual monomers, the suspension was washed several times with a mixture of water and methanol at a ratio of 80:20. At the end of the process, the polymerized aniline monomer in the biocomposites composition was under protonated form - emeraldine salt.

It is known that emeraldine salt is not particularly efficient for the removal of ions from an aqueous media and it has to be converted to more effective form - emeraldine base. The conversion of emeraldine salt into emeraldine base was carried out via washing the resulting precipitate with 1 M NaOH to pH 10.0-11.0. Thus deprotonation was achieved, consisting in the release of electron pairs at the nitrogen atoms in the amine groups of the emeraldine base polymer chain. These free electron pairs are the places where the metal ions, contained in the aqueous media, can be trapped. The washed precipitate was dried at 60 °C to a constant mass. Well-dried biocomposite was ground to a homogeneous powder.

Preparation of standard solutions of copper ions

Standard solutions with copper ions concentrations of 1.0, 2.0, 4.0, 6.0, 8.0, 10.0, 30.0, and 50.0 mg L^{-1} were prepared, using $CuSO_4.5H_2O$ and distilled water.

Adsorption equilibrium study

The adsorption equilibrium for the removal of copper ion was studied, using 50 mL of aqueous solutions containing Cu(II) concentrations between 1 and 50 mg L^{-1} contacting with 0.1 g of the two types of biocomposites and pure emeraldine base for comparison, respectively. Shaking was carried out until equilibrium achievement.

The amount of adsorption at equilibrium[27] in (mg g^{-1}) was computed as follows:

$$q_e = \frac{(C_0 - C_e)V}{m} \quad (1)$$

where

C_0 and C_e are the initial and equilibrium copper ions concentrations (mg L^{-1}), respectively,

V is the volume of the solution (L), and

m (g) is the mass of the biocomposite.

Adsorption kinetic studies

In order to establish the influence of the contact time and the composite dosage on the adsorption of copper ions by *Phragmites australis*/emeraldine base biocomposites, kinetic studies were performed. For this purpose individual samples with initial copper ions concentration of 50.0 mg L^{-1} (C_0) were prepared. The volume of each sample was 50 mL, and the certain amount of the biocomposites (0.1, 0.5, 1.0 and 1.5 g) were added to each of them. The samples were poured in iodine flasks and were shaken in a plate shaker for 1, 3, 5, 7, 10, 15, 30, 60 and 360 min, respectively.

Inductively Coupled Plasma - Optical Emission Spectroscopy ("Prodigy" High dispersion ICP-OES, Telledyne Leeman Labs) was used for determination of the copper ions concentration. All experiments were conducted at 20 °C and in order to avoid Cu(II) precipitation, the pH of the aqueous solutions was adjusted to 5. [28]

The Cu(II) removal efficiency was determined according to the formula:

$$RE(\%) = \frac{(C_0 - C_t)}{C_0} 100 \quad (2)$$

where

C_0 is the initial copper ions concentration and

C_t is their concentration at time t in mg L^{-1}.

In this study the obtained results were fitted into the isotherms of Langmuir,[29] Freundlich,[30] Temkin[31] and Dubinin-Raduskevich[32,33] and the kinetic experimental data were analyzed by comparative estimation of the applicability of the pseudo-first-order model,[34] pseudo-second-order model,[35] Elovich kinetic model[36] and the intraparticle diffusion model[37] (Table 1).

Table 1. Isotherm and kinetic models used to interpret the experimental results.

Model	Linear form	Plot
Two-parameter isotherm models		
Langmuir[29]	$\frac{C_e}{q_e} = \frac{1}{q_m b} + \frac{C_e}{q_m}$	$\frac{C_e}{q_e}$ *vs* C_e
Freundlich[30]	$\log q_e = \log K_f + \frac{1}{n}\log C_e$	$\frac{1}{q_e}$ *vs* $\frac{1}{C_e}$
Temkin[31]	$q_e = \frac{RT}{b_T}\ln(A_T C_e)$	q_e *vs* $\ln C_e$
Dubinin-Radushkevich[32,33]	$q_e = q_D C_e(\exp -\beta\varepsilon^2)$	q_e *vs* ε^2
Kinetic models		
Pseudo-first-order model[34]	$\log(q_e - q_t) = \log q_e - \frac{k_1}{2.303}t$	$\log(q_e - q_t)$ *vs* t
Pseudo-second-order model[35]	$\frac{t}{q_t} = \frac{1}{k_2 q_e^2} + \frac{1}{q_e}t$	$\frac{t}{q_t}$ *vs* t
Elovich model[36]	$q_t = \frac{1}{b}\ln(ab) + \frac{1}{t}\ln t$	q_t *vs* $\ln t$
Intraparticle diffusion model[37]	$q_t = K_{id}t^{1/2} + \theta$	q_t *vs* $t^{1/2}$

Results and Discussion

Adsorption equilibrium

The experimental equilibrium data of copper ions adsorption on Emb, Pha/Emb1, and Pha/Emb2 were described by the Langmuir, Freundlich, Temkin and Dubinin–Radushkevich isotherm models (Figure 1). The calculated model parameters and regression coefficients (R^2) are presented in Table 2.

The R_L values obtained from Langmuir isotherm model for all adsorbents indicate that for all cases, the adsorption is favourable. This model describes well the experimental data for Emb and Pha/Emb1, confirmed by the high correlation coefficient. The 1/*n* values obtained for the adsorption process according to the Freundlich isotherm model for all solids corresponds to a beneficial adsorption. Concerning the adequacy of this model to the experimental data, the correlation coefficient is lower, compared to Langmuir model.

The Temkin isotherm model describes the data for Emb and Pha/Emb1 inconveniently, compared to the other two parameter models, as low correlation coefficient observed. On the other hand, the correlation coefficient for Pha/Emb2 is the highest, compared to the two previous models. The calculated values of *E* from the Dubinin–Radushkevich isotherm model were 2.5 and 5 KJ mol^{-1} for Emb and Pha/Emb1, respectively.

Table 2. Isotherm constants of two-parameter models for Cu(II) adsorption.

Model	Parameter	Adsorbents		
		Emb	Pha/Emb1	Pha/Emb2
Langmuir	q_m	8.0775	12.469	9.8135
	b	0.2363	5.2079	0.1454
	R_L	0.0780	0.0038	0.1209
	R^2	0.9766	0.9998	0.7322
Freundlich	K_F	1.5185	5.9865	1.3663
	$1/n$	0.4851	0.4350	0.6563
	R^2	0.9693	0.7727	0.6483
Tempkin	A_T	2.1328	4.6268	1.8462
	b_T	1161.7	535.48	1344.6
	R^2	0.9187	0.9682	0.9874
Dubinin-Radushkevich	q_D	3.4445	10.726	8.2016
	β	8.10^{-8}	2.10^{-8}	$4.9.10^{-7}$
	E	2.5	5.0	10.1
	R^2	0.7400	0.9034	0.9444

According to the literature, the value of E in the range of 1 - 8 KJ mol^{-1} indicates physical adsorption process.[38] For the second biocomposite, Pha/Emb2, the numerical value of E is equal to 10.1 KJ mol^{-1}, which is the indicator for ion exchange adsorption. This different behaviour is also observed when taking into account the correlation coefficient, higher for Pha/Emb2 than Emb and Pha/Emb1. As it can be seen in Figure 1, this model isotherm fits very well the experimental isotherm for Pha/Emb2 compared to the other models.

In order to estimate the effect of the initial copper ions concentration on the removal efficiency, 0.1 g of the biocomposites was used, and the initial copper ions concentration was varied from 1 and 50 mg L^{-1}. The results are presented in Figure 2.

From the obtained results it was observed that with increasing of the initial copper ions concentration, the removal efficiency of 0.1 g biocomposites and pure emeraldine base was reduced. The higher removal efficiency of copper ions at lower concentrations can be explained by the existence of enough free nitrogen atoms in the polymer chain, which have a higher electron density namely those involved in the complexing with copper ions. With increasing of the metal ions concentration, the possibility of their binding to the polymer structure reduces. The results show that the presence of *Phragmites australis* has a certain impact on the treatment efficiency, but the usage of the larger amount of it does not lead to a higher removal of copper ions.

The results show that the Pha/Emb1 is more effective in comparison with Pha/Emb2 and Emb. The copper ions removal efficiency increases up to an optimal dose above which the removal efficiency does not significantly change. It might be observed because, at fixed initial adsorbate concentration, the increasing biocomposite doses provide greater surface area, more adsorption sites and more available free electron pairs in the polymeric structure of the emeraldine base.

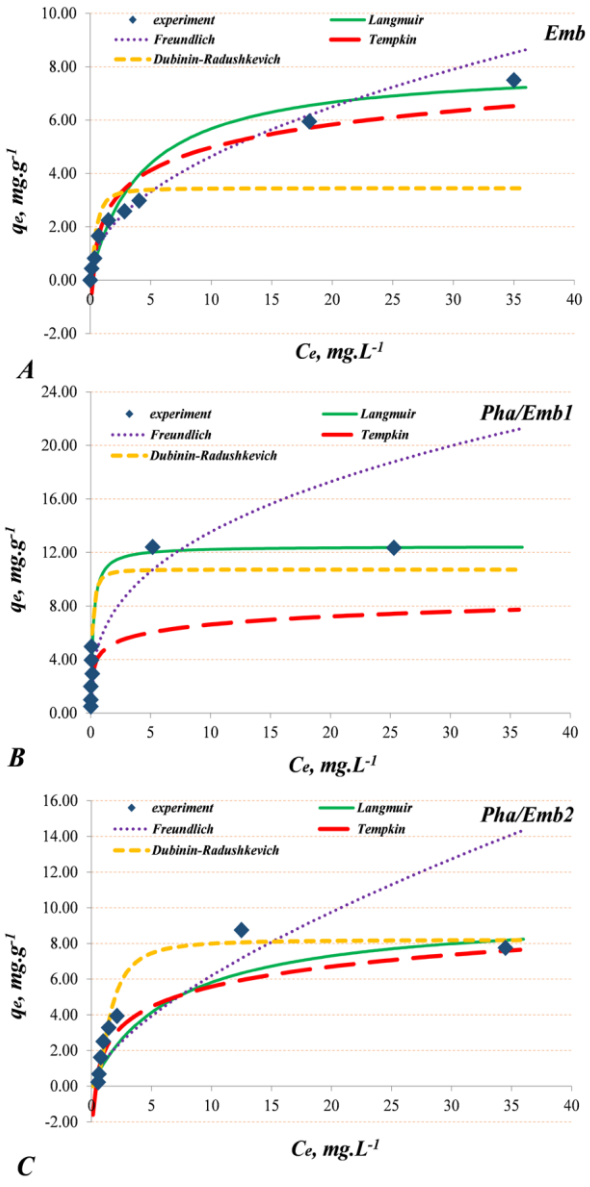

Figure 1. Experimental and model adsorption isotherms for Emb (A), Pha/Emb1 (B) and Pha/Emb2 (C).

The removal efficiencies obtained for 6 hours using Pha/Emb1 and Pha/Emb2 compared with the removal efficiencies obtained at the same time using pure emeraldine base are presented in Figure 3.

Adsorption kinetics

The examination of adsorption kinetics in wastewater treatment is of importance because it provides information for the mechanism of the considered process. The effect of the contact time and biocomposite dosage on the adsorption kinetics of Cu(II) was examined. The mechanism of the process studied was analysed by comparative estimation of the applicability of the pseudo-first-order, pseudo-second order, Elovich kinetic model, and the Intraparticle diffusion model.

Table 3. Adsorption kinetic model rate constants for Cu(II) adsorption onto Pha/Emb1 and Pha/Emb2.

Adsorbent	Pseudo-first-order				Pseudo-second-order			Elovich's equation		
	q_{exp}, mg g^{-1}	k_1, min^{-1}	$q_{e,calc}$, mg g^{-1}	R^2	k_2, min^{-1}	$q_{e,calc}$, mg g^{-1}	R^2	A, mg g^{-1} min^{-1}	1/b, mg g^{-1}	R^2
Pha/Emb1	13.67	0.02902	1.7998	0.6867	0.03807	13.74	0.9999	500,7	8.1086	0.8156
Pha/Emb2	8.89	0.02671	1.7463	0.5576	0.03083	8.96	0.9998	9.413	3.3791	0.7871

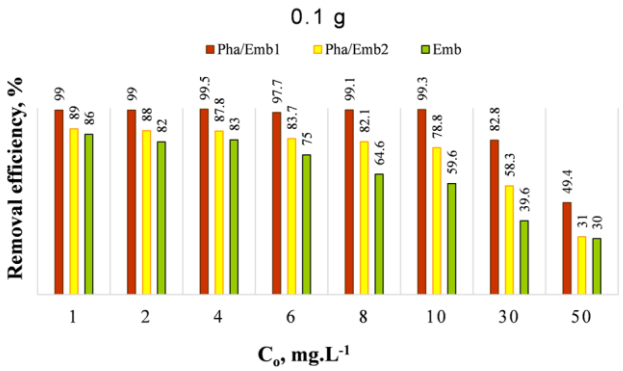

Figure 2. Effect of the initial copper ions concentration on the removal efficiency using Emb, Pha/Emb1, and Pha/Emb2.

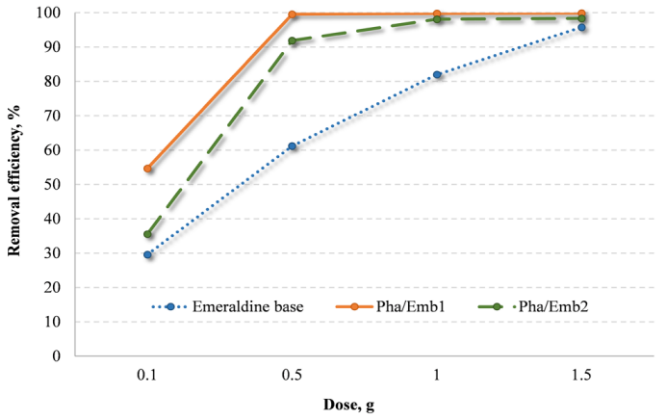

Figure 3. Removal efficiencies obtained at 360 min, using Emeraldine base, Pha/Emb1, and Pha/Emb2.

The experimental kinetic curves for Cu(II) sorption on the Pha/Emb1 and Pha/Emb2 are presented in Figures 4 and 5, respectively. The values of the calculated model's parameters and regression coefficients are presented in Table 3.

The constants k_1 and q_e were calculated using the slope and intercept of plots of $log(q_e-q_t)$ versus t (Table 3). The application of Pseudo-first-order model is inappropriate as experimental observations are nonlinear. This result also in a very low correlation coefficient and subsequently a significant difference in the experimental and calculated adsorption capacities. This result suggests that the adsorption of Cu(II) onto Pha/Emb1 and Pha/Emb2 did not follow pseudo-first-order kinetics.

The constants k_2 and q_e were calculated using the slope and intercept of plots of t/q_t versus t (Figure 4, Table 3). Fitted equilibrium adsorption capacities are in close agreement with those observed experimentally.

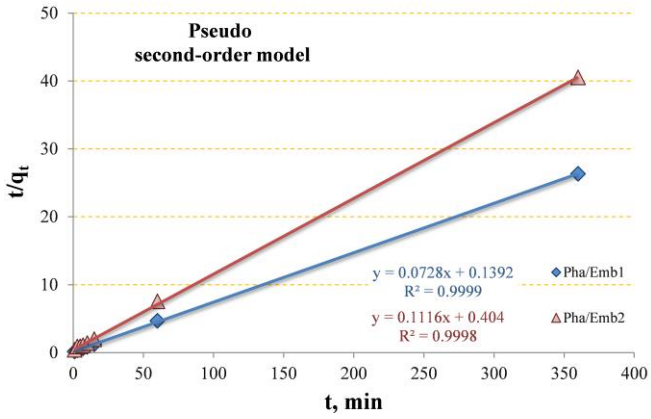

Figure 4. Application of the pseudo-second-order model. Operating conditions: C_0 = 50 mg.L^{-1}, $m_{ads.}$ = 0.1 g, pH = 5, T = 20 °C.

Furthermore, the correlation coefficients (R^2) for the pseudo-second-order kinetic model are much higher than the correlation coefficients derived from pseudo-first-order model fits. The good agreement between model fit and experimentally observed equilibrium adsorption capacity in addition to the large correlation coefficient suggests that Cu(II) adsorption followed pseudo-second-order kinetics and Cu(II) ions were adsorbed onto the Pha/Emb1 and Pha/Emb2 surfaces via mechanism including chemical interaction.

If Elovich model applies, it should lead to a straight line by plotting q_t as a function of ln*(t)* (Figure 5, Table 3).

The intraparticle diffusion rate constant k_i was calculated from the slope of the second linear section (Figure 6, Table 4). The value of the intercept C in this second section provides information related to the thickness of the boundary layer.[39] Larger intercepts suggest that the surface diffusion has a greater role as the rate-limiting step.

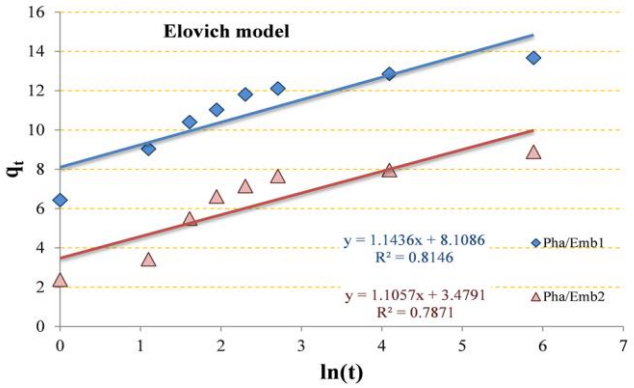

Figure 5. Application of the Elovich model. Operating conditions: C_0 = 50 mg.L^{-1}, $m_{ads.}$ = 0.1 g, pH = 5, T = 20 °C.

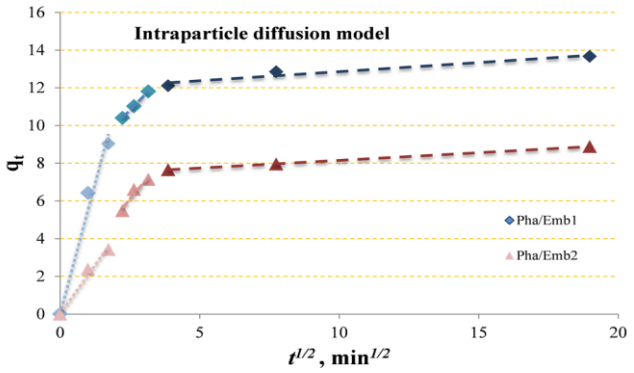

Figure 6. Kinetics of Cu(II) adsorption according to the intraparticle diffusion model. Operating conditions: C_0 = 50 mg.L^{-1}, $m_{ads.}$ = 0.1 g, pH = 5, T = 20 °C.

Table 4. Intraparticle diffusion coefficients and intercept values for Cu(II) adsorption.

Composite	k_i, mg g^{-1} h$^{-0.5}$	Intercept values, C	R^2
Pha/Emb1	1.5171	7.0122	1.0000
Pha/Emb2	1.7544	1.7126	0.9283

The main removal of the Cu(II) becomes immediately after mixing of the biocomposites with the model solutions (Figure 7). The concentration of copper ions was decreasing up to 1 min, then only a slight change of the concentrations could be observed.

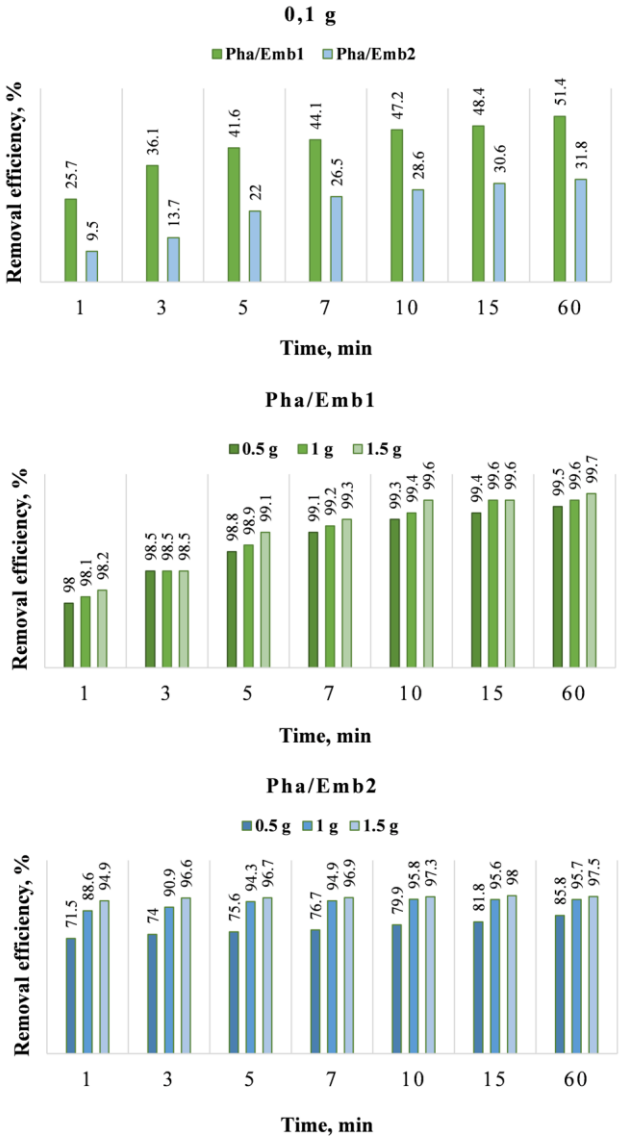

Figure 7. Influence of the contact time on the copper ions removal efficiency.

Conclusions

The possibility of the copper ions removal from aqueous solution by *in situ* synthesized biocomposite of *Phragmites australis* and emeraldine base as well the adsorption mechanism have been studied. The results indicate that the biocomposite Pha/Emb1 has a considerable potential for copper ions removal and that it is more effective in comparison with Pha/Emb2.

The results show that the presence of *Phragmites australis* has an impact on the treatment efficiency, but the usage of the greater amount of it does not lead to a greater removal of copper ions. The calculated values of E from the Dubinin–Radushkevich isotherm model were 2.5 and 5 KJ mol^{-1} for Emb and Pha/Emb1, respectively which indicate physical adsorption process. For the second biocomposite, Pha/Emb2, the numerical value of E is equal to 10.1 KJ mol^{-1}, which is the indicator for ion exchange adsorption. The experimental data were better described by the pseudo-second-order model.

References

[1]Jeon, Ch., *J. Ind. Eng. Chem.*, **2011**, *17*, 517. http://dx.doi.org/10.1016/j.jiec.2010.10.020.

[2]Ben-Ali, S., Jaouali, I., Souissi-Najar, S., Ouederni, A., *J. Clean. Prod.*, **2017**, *142*, 3809. http://dx.doi.org/10.1016/j.jclepro.2016.10.081

[3]Witek-Krowiak, A., Szafran, R., Modelski, S., *Desalination*, **2011**, *265*, 126. http://dx.doi.org/10.1016/j.desal.2010.07.042

[4]Ho, Y., McKay, G., *Wat. Res.*, **2000**, *34(3)*, 735. http://dx.doi.org/10.1016/S0043-1354(99)00232-8

[5]Ho, Y., *Biores. Technol.*, **2005**, *96*, 1292. http://dx.doi.org/10.1016/j.biortech.2004.10.011

[6]Zare, H., Heydarzade, H., Rahimnejad, M., Tardast, A., Seyfi, M., Peyghambarzadeh, S., *Arab. J. Chem.*, **2015**, *8*, 858. http://dx.doi.org/10.1016/j.arabjc.2012.11.019

[7]Mende, M., Schwarz, D., Steinbach, Ch., Boldt, R., Schwarz, S., *Colloids Surf., A*, **2016**, *510*, 275. http://dx.doi.org/10.1016/j.colsurfa.2016.08.033

[8]Shariful, M., Sharif, S., Lee, J., Habiba, U., Ang, B., Amalina, M., *Carbohydr. Polym.*, **2017**, *157*, 57. http://dx.doi.org/10.1016/j.carbpol.2016.09.063

[9]Kagaya, S., Miyazaki, H., Ito, M., Tohda, K., Kanbara, T., *J. Hazard. Mater.*, **2010**, *175*, 1113. http://dx.doi.org/10.1016/j.jhazmat.2009.10.099

[10]Abdi, S., Nasiri, M., Mesbahi, A., Khani, M., *J. Hazard. Mater.*, **2017**, *332*, 132. http://dx.doi.org/10.1016/j.jhazmat.2017.01.013

[11]Wang, J., Zhang, K., Zhao, L., *Chem. Eng. J.*, **2014**, *239*, 123. http://dx.doi.org/10.1016/j.cej.2013.11.006

[12]Kumar, R., Oves, M., Almeelbi, T., Al-Makishah, N., Barakat, M., *J. Colloid Interface Sci.*, **2017**, *490*, 488. http://dx.doi.org/10.1016/j.jcis.2016.11.082

[13]Li, X., Zhou, H., Wu, W., Wei, S., Xu, Y., Kuang, Y., *J. Colloid Interface Sci.*, **2015**, *448*, 389. http://dx.doi.org/10.1016/j.jcis.2015.02.039

[14]Mthombeni, N., Mbakop, S., Ochieng, A., Onyango, M., *J. Taiwan Inst. Chem. Eng.*, **2016**, *66*, 172. http://dx.doi.org/10.1016/j.jtice.2016.06.016

[15]Chen, L., Feng, S., Zhao, D., Chen, S., Li, F., Chen, C., *J. Colloid Interface Sci.*, **2017**, *490*, 197. http://dx.doi.org/10.1016/j.jcis.2016.11.050

[16]Ansari, R., Dezhampanah, H., Eur. Chem. Bull., **2013**, 2(4), 220. doi: 10.17628/ECB.2013.2.220

[17]Stejskal, J., Gilbert, R., *Pure Appl. Chem.*, **2002**, *74(5)*, 857.

[18]Mahato, N., Parveen, N., Cho, M., *Mater. Lett.*, **2015**, *161*, 372. http://dx.doi.org/10.1016/j.matlet.2015.08.138

[19]Borah, R., Baerjee, S., Kumar, A., *Synth. Met.*, **2014**, *197*, 225. http://dx.doi.org/10.1016/j.synthmet.2014.08.018

[20]Shyaa, A., Hasan, A., Abbas, M., *J. Saudi Chem. Soc.*, **2015**, *19*, 101. http://dx.doi.org/10.1016/j.jscs.2012.01.001

[21]Kaur, B., Srivastava, R., *Sens. Actuator B-Chem.*, **2015**, *211*, 476. http://dx.doi.org/10.1016/j.snb.2015.01.081

[22]Phan, T., Do, N., Mai, T., *Adv. Nat. Sci-Nanosci.*, **2010**, *1*, 1. doi:10.1088/2043-6262/1/3/035006

[23]Kumar, P., Chakaborty, S., Ray, M., *Chem. Eng. J.*, **2008**, *141*, 130. http://dx.doi.org/10.1016/j.cej.2007.11.004

[24]Ghorbani, M., Eisazadeh, H., Ghoreyshi, A., *IJEE.*, **2012**, *3(1)*, 66-71. doi: 10.5829/idosi.ijee.2012.03.01.3343

[25]Vymazal, J., Březinová, T., *Chem. Eng. J.*, **2016**, *290*, 232. http://dx.doi.org/10.1016/j.cej.2015.12.108

[26]Kumari, M., Tripathi, B., *Ecotoxicol. Environ. Saf.*, **2015**, *112*, 80. http://dx.doi.org/10.1016/j.ecoenv.2014.10.034

[27]Vanderborght, M., Van Grieken, E., *Anal. Chem.*, **1977**, *49(2)*, 311. doi: 10.1021/ac50010a032

[28]Srithongkham, S., Vivitchanont, L, Krongtaew, C., *J. Mater. Sci. Eng. B.*, **2012**, *2(4)*, 213.

[29]Langmuir, I., *J. Am. Chem. Soc.*, **1918**, *40*, 1361. doi: 10.1021/ja02242a004

[30]Freundlich, H., *Phys. Chem. Soc.*, **1906**, *40*, 1361.

[31]Aharoni, C., Ungarish, M., *J. Chem. Soc. Faraday Trans.*, **1977**, *73*, 456. doi:10.1039/F19777300456

[32]Dabrowski, A., *Adv. Colloid Interface Sci.*, **2001**, *93*, 135-224.

[33]Hutson, N., Yang, R., *Adsorption*, **1997**, *3*, 189. http://dx.doi.org/10.1007/BF01650130

[34]Lagergren, S., *Ksver. Veterskapsakad. Handl.*, **1898**, *24*, 1.

[35]Farooq U., Khan M. A., Athar W., Kozinski J. A., *Chem. Eng. J.*, **2011**, *171*, 400. http://dx.doi.org/10.1016/j.cej.2011.03.094

[36]Zeldowitsch, J., *Acta Physicochim. URSS*, **1934**, *1*, 364.

[37]Crank G., The mathematics of diffusion. London, New York: Clarendon Press, **1933**.

[38]Helfferich, F., *Ion Exchange*, McGraw-Hill, New York, USA, **1962**.

[39]Kavitha, D., Namasivayam, C., *Bioresour. Technol.*, **2007**, *98*, 14. http://dx.doi.org/10.1016/j.biortech.2005.12.008

Received:03.04.2017.
Accepted:26.04.2017.

ENHANCING PHOTOCATALYTIC ACTIVITY OF BISMUTH FERRITE BY DOPING WITH COBALT AND ITS USE FOR DEGRADATION OF EVANS BLUE

Arpita Paliwal,[a]* Rakshit Ameta,[b] and Suresh C. Ameta[b]

Keywords: Evans blue, Bismuth ferrite, Co-doped bismuth ferrite, Heterogeneous, Photocatalytic degradation.

An attempt has been made to enhance the photocatalytic activity of bismuth ferrite by doping it with cobalt, to prepare a catalyst to use in wide pH range for the photodegradation of Evans blue dye. The progress of the reaction has been monitored spectrophotometrically by measuring the absorbance of the reaction mixture at definite time intervals. Different parameters such as pH, the concentration of dye, amount of semiconductor and light intensity were varied to achieve the optimum rate of photodegradation. The results show that doping of bismuth ferrite by cobalt increases the rate of photocatalytic degradation due to narrowing of the band gap. Undoped bismuth ferrite has the highest catalytic activity in basic while the Co-doped catalyst in acidic medium. A tentative mechanism for the reaction has been proposed.

* Corresponding Authors
E-Mail: paliwalarpita7@gmail.com
[a] Photochemistry Laboratory, Department of Chemistry, M. L. Sukhadia University, Udaipur – 313001 (Raj.) INDIA
[b] Department of Chemistry, PAHER University, Udaipur-13003 (Raj.) INDIA

Introduction

Natural water resources are becoming polluted as a result of human activities, including industries causing water pollution. Polluted water may have adverse effects on animals, plant life and humans. One of the sources of polluted water is textile industries, where waste water is colored due to dye components. Azo dyes are the largest and most important class of synthetic organic dyes. It has been observed that azo dyes are used more than 50 % of all dyes because of their chemical stability and versatility.[1] Azo dyes are not biodegradable by aerobic treatment processes,[2] and under anaerobic condition, they give potentially carcinogenic aromatic amines, which cause long-term health concerns.[3] Evans Blue or T-1824 is an azo dye, which has a very high affinity for serum albumin.

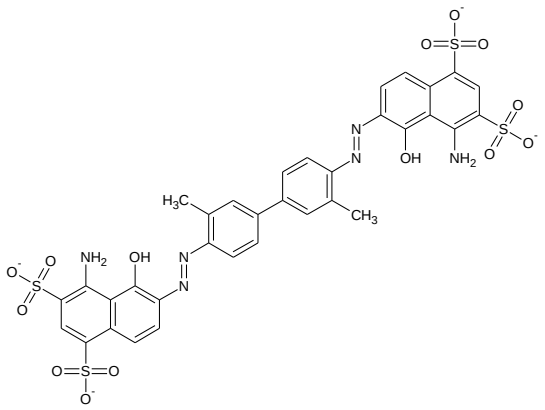

Figure 1. Structure of Evans blue

The synthetic dyes used in a wide-range of technologies,[4] but their toxic nature generate demand for removal of dyes from wastewater. The most common methods used for the treatment of effluents from dyeing industries are membrane filtration, coagulation-flocculation, biological treatment, catalytic oxidation, sorption process, ion exchange, etc. These treatment methods for the removal of dyes from the waste water suffer from some or other drawbacks.

To develop an efficient method for converting such dyestuffs into harmless products, advanced oxidation processes (AOPs) have been widely studied in recent years. AOPs are promising methods for the treatment of wastewaters containing organic pollutants and involve two stages– first is the formation of strong oxidants and second is the reaction of these oxidants with organic contaminants in water. The efficiency of the AOP is maximized by the use of an appropriate catalyst and/or ultraviolet light.[5-7] Photocatalytic degradation has been found to be a very efficient process for mineralization of organic pollutants. The photocatalyst is a substance, which is activated by absorbing a photon and is capable of accelerating a reaction without being consumed.[8]

Bismuth ferrite ($BiFeO_3$), is the most attractive and promising photocatalyst given photo-oxidation potential and chemical stability. Degradation of a non-biodegradable Evans blue has been carried out by the heterogeneous photo-Fenton-like processes using copper pyrovanadate ($Cu_3V_2(OH)_2O_7 \cdot 2H_2O$) as a photocatalyst.[9] They also observed photocatalytic degradation of Evans blue by heterogeneous photo-Fenton-like catalysts $Cu_2V_2O_7$ and $Cr_2V_4O_{13}$.[10] Electrochemical processes for the degradation of Evans Blue based on Fenton's reaction chemistry. [11] The effect of Ag deposition on TiO_2 for the degradation of Evans blue. [12]

Bismuth ferrite (BFO) with different particle sizes and morphologies has been synthesized by various preparation methods such as sol-gel, hydrothermal and microwave hydrothermal and studied the effects of particle size and

presence of dopants on the photocatalytic activity,[13] e.g. in photocatalytic degradation of tetracycline[14] and methylene blue,[15,16] malachite green,[17] or methyl orange.[18,19] The effect of various synthetic techniques and the presence of chelating agents on the properties $BiFeO_3$ in degradation of various organic contaminants such as Bisphenol A or Rhodamin B have also been studied.[20-24] Now, we have studied the effect of Co-doping on the photocatalytic activity of $BiFeO_3$ in the degradation of Evans Blue dye.

Experimental

Synthesis of undoped and Co-doped bismuth ferrite

Undoped and Co-doped bismuth ferrite were synthesized by hydrothermal, and polyol methods, respectively and these were characterized by SEM-EDS techniques.[25] To a solution of $Bi(NO_3)_3.5H_2O$ in ethylene glycol, a stoichiometric amount of $Fe(NO_3)_3.9H_2O$ in distilled water was slowly added under vigorous stirring for 30 min. Aqueous ammonia (approx. 60 mL) was slowly dropped into the homogeneous solution to adjust pH > 10 by constant stirring to give brown colored precipitates. Then it was filtered, washed with water and dried at 80°C. The resulting solid was calcined for 3 hours at 200 °C.

Co-doped bismuth ferrite was synthesized from $Bi(NO_3)_3.5H_2O$ (4.85 g), $Fe(NO_3)_3.9H_2O$ (4.04 g), and $Co(NO_3)_2.6H_2O$ (0.24 g) taken in a beaker contains 36 mL of ethylene glycol. The solution was heated up to 200°C for 90 min to remove the ethylene glycol.

Photocatalytic procedure

The photocatalytic activity of the catalyst was evaluated by measuring the rate of degradation of Evans blue. A stock solution of dye (1.0 x 10^{-3} M) was prepared by dissolving (0.0960 g) of dye in 100 mL of doubly distilled water. pH of the dye solution was measured by a digital pH meter (Systronics Model 335), and the desired pH of the solution was adjusted by the addition of standard 0.1 *N* sulphuric acid and 0.1 *N* sodium hydroxide solutions. The reaction mixture containing 0.10 g photocatalyst was exposed to a 200 W tungsten lamp, and about 3 mL aliquot was taken out every 10 min. Absorbance (*A*) was measured at λ_{max}=620 nm. A water filter was used to cut off thermal radiations. The intensity of light was varied by changing the distance between the light source and reaction mixture, and it was measured by Suryamapi (CEL Model SM 201). The absorbance of the solution at various time intervals was measured with the help of spectrophotometer (Systronics Model 106).

It was observed that the absorbance of the solution decreases with increasing the time of exposure, which indicates that the concentration of Evans blue dye decreases with increasing time. The calculation of degradation efficiency (φ) was made by the relation:

$$\varphi = 100\,\frac{A - A_0}{A_0} \qquad (1)$$

Here A_0 is initial absorbance, and A is absorbance after degradation of dye at time t. A plot of 1 + log A versus time was linear following pseudo-first order kinetics. Typical runs are given in Table 1 and graphically presented in Figure 2.

The rate constant was calculated by using the expression:

$$k = 2.303 \times \text{slope} \qquad (2)$$

Table 1. Typical runs for photocatalytic degradation of Evans blue.

Time, min	Undoped $BiFeO_3$		Co-doped $BiFeO_3$	
	A	**1 + log*A***	***A***	**1 + log*A***
0.0	0.337	0.5276	0.339	0.5302
5.0	-	-	0.324	0.5105
10.0	0.317	0.5010	0.305	0.4843
15.0	-	-	0.294	0.4683
20.0	0.303	0.4814	0.279	0.4456
25.0	-	-	0.265	0.4232
30.0	0.288	0.4594	0.255	0.4065
35.0	-	-	0.239	0.3784
40.0	0.270	0.4314	0.231	0.3636
45.0	-	-	0.220	0.3424
50.0	0.258	0.4116	0.206	0.3139
60.0	0.245	0.3892	-	-
70.0	0.230	0.3617	-	-
80.0	0.220	0.3424	-	-
k, s^{-1}	8.95×10^{-5}		16.12×10^{-5}	
φ, %	34.71		39.23	

Undoped $BiFeO_3$: pH=7.7, [Evans blue]=1.50×10^{-5} M, Semiconductor=0.10 g, Light intensity=70.0 mWcm^{-2}. **Co-doped $BiFeO_3$:** pH =3.5, [Evans blue]=2.00×10^{-5} M, Semiconductor=0.10 g, Light intensity=60.0 mWcm^{-2}

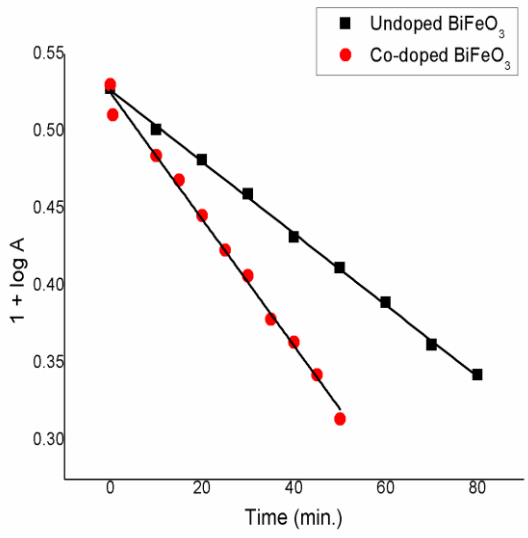

Figure 2. Typical run for on photocatalytic degradation of Evans Blue

Results and discussion

Effect of parameters

The rate of degradation has been investigated in pH range 3.0–7.5 and 1.5-3.5 for undoped and Co-doped $BiFeO_3$, respectively. All other parameters were kept to be identical. The results are summarized in Table 2 and Figure 3. It was observed that with an increase in pH, the rate of reaction increases. After attaining the maximum value at pH 7.0 and pH 2.5 for undoped and Co-doped $BiFeO_3$, respectively, the rate decreases with a further increase in pH. In this case, the presence of scavenger i.e. 2-propanol does not affect the rate of reaction adversely and hence, it may be concluded that $^{\bullet}OH$ radical does not participate in the degradation. It was interesting to observe that undoped $BiFeO_3$ was active in basic range (3.0–7.5) while Co-doped $BiFeO_3$ was active in acidic range (1.5-3.5).

Table 2. Effect of pH on photocatalytic degradation of Evans Blue

pH	Rate constant, $k \times 10^5$ s^{-1}	
	$BiFeO_3$	Co-doped $BiFeO_3$
1.5	-	9.64
1.8	-	12.97
2.2	-	15.04
2.5	-	16.12
2.7	-	14.46
3.0	1.51	12.13
3.2	1.86	10.08
3.5	2.32	8.02
4.0	3.80	-
4.5	4.41	-
5.0	5.02	-
5.5	5.72	-
6.0	6.46	-
6.5	7.18	-
7.0	8.95	-
7.5	7.24	-
8.0	6.09	-

Undoped $BiFeO_3$: [Evans blue]=1.50×10^{-5} M, semiconductor=0.10 g, Light intensity=70.0 $mWcm^{-2}$. Co-doped $BiFeO_3$: [Evans blue]=2.00×10^{-5} M, semiconductor=0.10 g, Light intensity=60.0 $mWcm^{-2}$

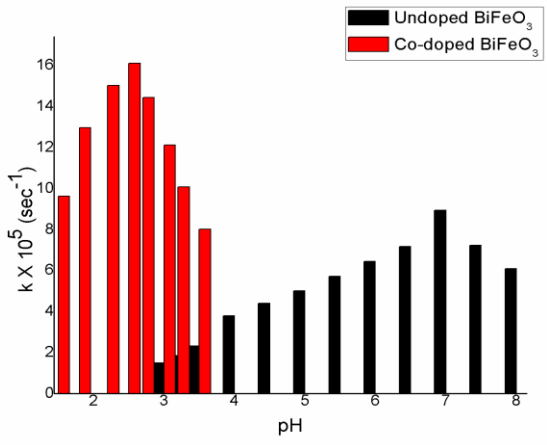

Figure 3. Effect of pH on photocatalytic degradation of Evan's Blue

The effect of variation of concentration of Evans blue on its degradation rate has been observed in the range from 0.4×10^{-5} to 1.6×10^{-5} M for both undoped and Co-doped $BiFeO_3$ keeping all other parameters to be the same. The results are given in Table 3 and Figure 4. It has been observed that the rate of degradation increases with increasing concentration of dye up to 0.6×10^{-5} M for both, undoped and Co-doped $BiFeO_3$. Further increase in concentration beyond this limit results in a decrease in degradation rate. This may be explained on the basis that on increasing the concentration of dye, the reaction rate increases as more molecules of dyes were available but a further increase in concentration results appearing an internal filter effect which does not permit sufficient amount of light to reach the surface of the photocatalyst thus, decreasing the rate of photocatalytic degradation of Evans blue occurs.

Table 3. Effect of dye concentration on photocatalytic degradation of Evans Blue

[Evans blue] $\times 10^5$ M	Rate constant, $k \times 10^5$, s^{-1}	
	$BiFeO_3$	Co-doped $BiFeO_3$
0.4	5.26	10.16
0.5	6.71	13.70
0.6	8.95	16.12
0.8	8.02	15.41
1.0	6.43	13.18
1.2	5.10	10.26
1.4	4.07	8.49
1.6	3.24	7.00

Undoped $BiFeO_3$: pH=7.7, semiconductor=0.10 g, light intensity=70.0 $mWcm^{-2}$. Co-doped $BiFeO_3$: pH=3.5, semiconductor=0.10 g, light intensity=60.0 $mWcm^{-2}$

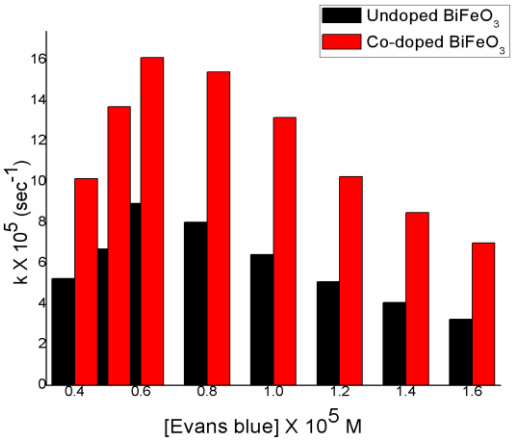

Figure 4. Effect of dye concentration on photocatalytic degradation of Evan's Blue

The effect of variation of the amount of catalyst on the rate of dye degradation has been studied in the range from 0.02 to 0.14 g in 50 mL and the results are reported in Table 4 and Figure 5. It has been observed that with an increase in the amount of catalyst, the rate of degradation increases to a certain amount of catalyst i.e. 0.10 g, for both; undoped and Co-doped $BiFeO_3$. Beyond this point, the rate of reaction becomes virtually constant.

This behavior may be explained by the fact that with an increase in the amount of catalyst, the exposed surface area of catalyst will increase. Hence, the rise in the rate of reaction has been observed, but with further increase in the amount of catalyst beyond a limit, the only thickness of the layer (and not the exposed surface area) will increase at the bottom of the reaction vessel, which was completely covered by the catalyst.

Table 4. Effect of amount of catalyst on photocatalytic degradation of Evans Blue

Photocatalyst g in 50 mL	**Rate constant. $k \times 10^5$ s^{-1}**	
	$BiFeO_3$	**Co-doped $BiFeO_3$**
0.02	3.43	5.02
0.04	5.50	7.04
0.06	6.19	8.42
0.08	7.57	13.09
0.10	8.95	16.12
0.12	8.90	16.09
0.14	8.96	16.13

Undoped $BiFeO_3$: pH = 7.7, [Evans blue] = 1.50×10^{-5} M, Light intensity = 70.0 $mWcm^{-2}$. Co-doped $BiFeO_3$: pH = 3.5, [Evans blue] = 2.00×10^{-5} M, Light intensity = 60.0 $mWcm^{-2}$

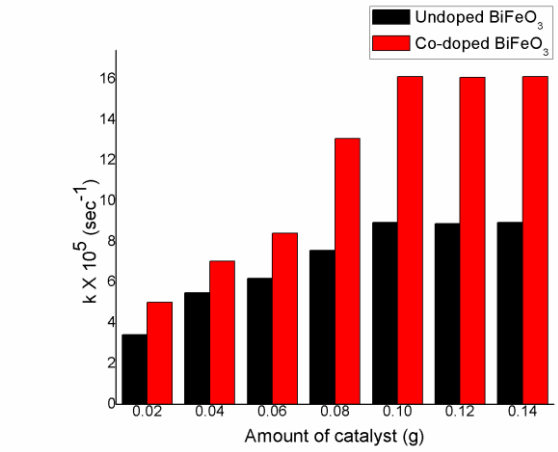

Figure 5. Effect of amount of catalyst on photocatalytic degradation of Evans Blue

The effect of light intensity on the rate of dye degradation was also studied by varying the intensity of light from 20.0 to 70.0 $mWcm^{-2}$. The observations are presented in Table 5 and Figure 6. The data indicate that with increasing light intensity, the rate of reaction increases and maximum rates were found at 70.0 and 60.0 mW cm^{-2} for undoped and Co-doped $BiFeO_3$, respectively. It may be explained on the basis that as the light intensity was increased, the number of photons striking per unit area also increases, resulting in higher rate of degradation for both. Further increase in the light intensity may start some thermal side reactions.

Mechanism

On the basis of the experimental observations, a tentative mechanism has been proposed for the degradation of Evans blue in the presence of bismuth ferrite (undoped and Co-doped).

Table 5. Effect of light intensity on photocatalytic degradation of Evans Blue

Light intensity, mW cm^{-2}	**Rate constant, $k \times 10^5$ s^{-1}**	
	$BiFeO_3$	Co-doped $BiFeO_3$
20.0	3.83	10.74
30.0	4.02	11.51
40.0	4.47	13.81
50.0	5.16	14.58
60.0	5.75	16.12
70.0	8.95	15.35

Undoped $BiFeO_3$: pH = 7.7, [Evans blue] = 1.50×10^{-5} M, Semiconductor = 0.10 g. **Co-doped $BiFeO_3$:** pH = 3.5, [Evans blue] = 2.00×10^{-5} M, Semiconductor = 0.10 g

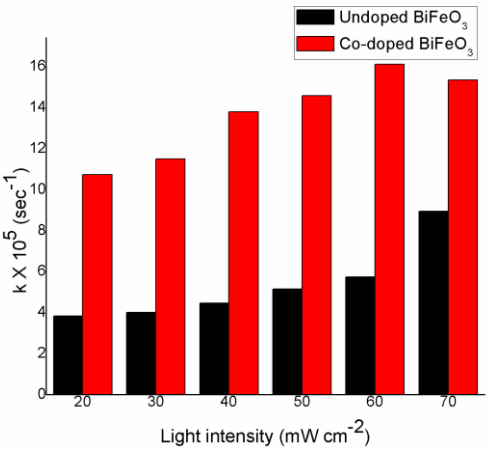

Figure 6. Effect of light intensity on photocatalytic degradation of Evans Blue

Evans blue absorbs radiations of suitable wavelength and transforms to singlet then triplet excited state (intersystem crossing, ISC). The semiconductor also absorbs light to excite an electron from its valence band (VB) to its conduction band (CB), which will be abstracted by dissolved oxygen to generate $O_2^{\bullet-}$ (in basic media, undoped $BiFeO_3$) or $HO_2^{\bullet}$ radicals (in acidic medium, Co-doped $BiFeO_3$). These radicals can oxidize the dye to its leuco form ultimately degrading to products

$$^1EB_0 \longrightarrow {}^1EB_1 \quad (3)$$

$$^1EB_1 \longrightarrow {}^3EB_1 \quad (4)$$

$$BiFeO_3 \longrightarrow BiFeO_3\,(h^+(VB)+e^-(CB)) \quad (5)$$

$$O_2(\text{dissolved oxygen}) + e^-(CB) \longrightarrow O_2^{\bullet-} \quad (6)$$

In acidic medium-

$$O_2^{\bullet-} + H^+ \longrightarrow HO_2^{\bullet} \quad (7)$$

$$^3EB_1 + HO_2^{\bullet} \longrightarrow \text{Leuco EB} \quad (8)$$

$$\text{Leuco EB} \longrightarrow \text{Products} \quad (9)$$

In basic medium-

$^3EB_1 + O_2^{\bullet-} \longrightarrow$ Leuco EB (10)

Leuco EB $\longrightarrow$ Products (11)

Carrying out the reaction in the presence of $^{\bullet}OH$ radical scavenger, 2-propanol, the reaction rates were unaffected. This unambiguously shows that there was no involvement of $^{\bullet}OH$ radicals in the reactions as an active oxidizing species.

Conclusion

At optimal conditions, the rate of degradation of Evans blue for undoped and the Co-doped $BiFeO_3$ system was obtained as $8.95 \times 10^{-5}$and 16.12×10^{-5} sec^{-1}, respectively. Thus, the doping of $BiFeO_3$ by cobalt ions enhances the rate of photodegradation of Evans blue almost 1.8 times (80% increase).

Acknowledgements

One of the authors Arpita Paliwal is thankful to Department of Chemistry, M. L. Sukhadia University, Udaipur for providing laboratory facilities.

References

[1]Neamtu, M., Siminiceanu, I., Yediler, A. and Kettrup, A., *Dyes and Pigments*, **2002**, *53(2)*, 93-99. http://doi.org/10.1016/S0143-7208(02)00012-8

[2]Pagga, U., and Drown, D., *Chemosphere*, 1986, 15(4), 479-491. https://doi.org/10.1016/0045-6535(86)90542-4

[3]Brown, D. and Hamberger, B., *Chemosphere*, 1987, 16(7), 1539-1553. https://doi.org/10.1016/0045-6535(87)90094-4

[4]Whitaker, C. M., and Willock, C. C., *Dyeing with Coal Tar Dyestuffs*, **1949**, 5, 1-7, Tindall & Cox Baillière,

[5]Legrini, O., Oliveros, E., and Braun, A. M., *Chem. Rev*., **1993**, *93(2)*, 671-698. https://doi.org/10.1021/cr00018a003

[6]von Sonntag, C., *Water Sci. Technol.*, **2008**, *58(5)*, 1015-1021. https://doi.org/10.2166/wst.2008.467

[7]Matilainen, A. and Sillanpää, M., *Chemosphere*, **2010**, *80(4)*, 351-365. http://doi.org/10.1016/j.chemosphere.2010.04.067

[8]Fox, M., *Photocatalytic oxidation of organic substances*. In: Kluwer (Ed.) *Photocatalysis and Environment: Trends and Applications.* New York Acad Pub, **1988**, 445–467.

[9]Kalal, S., Pandey, A., Ameta, C., Ameta, R. and Punjabi, P. B., *Eur. Chem. Bull*., **2015**, *4(4)*, 218-223. https://doi.org/10.17628/ECB.2015.4.218

[10]Kalal, S., Pandey, S., Ameta, R. and Punjabi, P. B., *Cogent Chemistry*, **2016**, *2*, 1143344, p.12. http://dx.doi.org/10.1080/23312009.2016.1143344.

[11]Antonin, V. S., Garcia-Segura, S., Santos, M. C. and Brillas, E., *J. Electroanal. Chem.*, **2015**, *747*, 1–11. http://doi.org/10.1016/j.jelechem.2015.03.032

[12]Shintre, S. and Thakur, P., *Indian J. Chem. Tech*., **2016,** *23*, 232-236.

[13]Gao, T., Chen, Z., Huang, Q., Niu, F., Huang, X., Qin, L. and Huang, Y., *Rev. Adv. Mater. Sci*., **2015**, *40*, 97-109.

[14]Xue, Z., Wang, T., Chen, B., Malkoske, T., Yu, S. and Tang, Y., *Materials*, **2015**, *8(9)*, 6360-6378. https://doi.org/10.3390/ma8095310

[15]Soltani, T. and Entezari, M.H., *J. Mol. Catal. A: Chem*., **2013**, *377*, 197–203. http://doi.org/10.1016/j.molcata.2013.05.004

[16]Mohan, S., Subramanian, B. and Sarveswaran, G., *J. Mater. Chem. C*, **2014,** *2(33)*, 6835-6842. https://doi.org/10.1039/C4TC01038H

[17]Jain, S., Krishna, R. H., Shivakumara, C., Motappa, M. G. and Nagabhushana, B. M., *Int. J. Curr. Biotechnol*., **2015**, *3(11)*, 1-7.

[18]Xie, H., Wang, K., Jiang, Y., Zhao, Y. and Wang, Y., *Met. Org. Nano. Met. Chem*., **2014**, *44(9)*, 1363-1367. http://dx.doi.org/10.1080/15533174.2013.801859

[19]Liu, Z., Qi, Y. and Lu, C., *J. Mater. Sci: Mater. Electron*., **2010**, *21(4)*, 380-384. http://doi.org/10.1007/s10854-009-9928-x

[20]Wei, J., Zhang, C. and Xu, Z., *Mater. Res. Bull*, **2012**, *47(11)*, 3513–3517. http://doi.org/10.1016/j.materresbull.2012.06.068

[21]Wang, N., Zhu, L., Lei, M., She, Y., Cao, M. and Tang, H., *ACS Catal*, **2011**, *1(10)*, 1193–1202. http://doi.org/10.1021/cs2002862

[22]Kaur, M., Yadav, K.L. and Uniyal, P., Adv. Mater. Lett., 2015, 6(10), 895-901. http://doi.org/10.5185/amlett.2015.5861

[23]Li, S., Lin, Y.H., Zhang, B.P., Nan, C.W. and Wang, Y., *J. Appl. Phys.*, **2009**, *105(5)*, 056105. http://doi.org/10.1063/1.3091286

[24]Wang, X., Lin, Y., Ding, X. and Jiang, J., *J. Alloys. Compd.*, **2011** *509(23)*, 6585–6588. http://doi.org/10.1016/j.jallcom.2011.03.074

[25]Paliwal, A., Ameta, R., Punjabi, P. B., and Ameta, S. C., *Indian J. Chem. A*, **2017** (communicated).

Received: 10.04.2017.
Accepted: 29.04.2017.

INFLUENCE OF SUPPORT PHASES ON THE NICKEL CATALYSED SELECTIVE HYDROGENATION OF CINNAMALDEHYDE

M. G. Prakash,[a,b] R. Mahalakshmy,[b] K. R. Krishnamurthy[a] and B. Viswanathan[a]*

Keywords: Cinnamaldehyde; hydrogenation; role of supports; polymorphs of titania; nickel at interface

Ni (15% w/w) supported on alumina, silica, and titania (P-25, anatase and rutile phases) have been investigated for the liquid phase hydrogenation of cinnamaldehyde. XRD, TPR and XPS data (binding energy shifts for Ni_{2p}) indicate metal-support interactions in all supported catalysts. Weaker binding of H_2 on Ni/TiO_2 (H_2-TPD) improves activity. Ni/TiO_2 phases display higher cinnamaldehyde conversion and selectivity to cinnamyl alcohol compared to the catalysts supported on alumina and silica. Amongst the three polymorphs of titania, the maximum activity, and selectivity displayed by Ni/ TiO_2-P-25, is attributed to the active Ni crystallites located at the interface between anatase and rutile phases in titania P-25 matrix (HRTEM). Though Ni crystallites on alumina and silica are relatively smaller (compared to those on the three TiO_2 phases) in size, their activity vis-à-vis for those supported on titania phases is less, implying that factors other than crystallite size influence the performance.

*Corresponding authors
Dr. B. Viswanathan
E-mail: bvnathan@iitm.ac.in
[a] National Centre for Catalysis Research (NCCR), Indian Institute of Technology, Madras, Chennai-600036, India.
[b] Department of Chemistry, Thiagarajar College, Madurai Kamaraj University, Madurai-625009, India.

INTRODUCTION

Selective hydrogenation of cinnamaldehyde (CAL) to cinnamyl alcohol (COL) and hydrocinnamaldehyde (HCAL) is a key step in the synthesis of fine chemicals for pharmaceutical and fragrance applications.[1] Formation of COL by a preferential hydrogenation of the C=O group is not favoured, because the hydrogenation of C=C double bond, leading to the formation of HCAL, is thermodynamically favoured by 35 kJ mol^{-1} and the kinetics of hydrogenation also favours this route.[2] Conventionally, hydrogenation of C=O bond in CAL is achieved by reduction with various hydride donors, such as $LiAlH_4$ and $NaBH_4$.[3-5] Development of non-noble metal catalysts with high activity and selectivity towards COL remains a challenge.[6,7] Supported noble metal (Pt, Pd, & Ir) catalysts have been studied extensively for this reaction. Selectivity towards COL is significantly influenced by several factors such as metal particle size,[8-11] nature of support,[12] promoters[13] and solvents.[14]

A number of supports like titania, zirconia, silica, and alumina have been explored for the selective hydrogenation of CAL. Reducible supports like TiO_2, Nb_2O_5 are known to promote SMSI effect, which helps in achieving higher selectivity to COL.[15-16] Graphene oxide supported Pt catalysts display high selectivity for COL (85.3%).[17] Graphene increases electron density around Pt, which does not favor adsorption of CAL via C=C bond and hence the improvement in COL selectivity. Xiaonian Li et al.[18] have reported COL selectivity of 83.8% on Au/TiO_2 and 55.6% on Ir/TiO_2. While Co supported on TiO_2 exhibits COL selectivity of 58.8%, the selectivity increases to 74-83 % when ZSM-5 is used as support.[19,20] Marchi et al.[21] have studied liquid phase hydrogenation of cinnamaldehyde over Cu/SiO_2, Cu-Al, Cu-Zn-Al, Cu-Ni-Zn-Al and Cu-Co-Zn-Al oxide catalysts and observed selectivity of 10-52.9% for COL.

TiO_2 supported catalysts significantly enhance the rate of C=O hydrogenation over Pt, Ni, Co metals, although the hydrogenation of C=C double bonds or aromatic rings have not been observed.[22-24] Reducibility of TiO_2 results in the formation of oxygen deficient TiO_{2-x} phase containing Ti^{3+} ions, which tend to polarize C=O, leading to higher selectivity towards COL.[25]

Phase composition and polymorph character of the supports, which define the location/environment of active phases/metals play crucial role in controlling activity and selectivity.[26] In order to investigate these specific aspects, a systematic study has been carried out on Ni-based catalysts supported on different supports like, alumina, silica, different polymorphs of titania, namely, anatase, rutile and mixed phase containing anatase & rutile (titania P-25) towards selective hydrogenation of CAL. To the best of our knowledge, there are no reports on the influence of such supports on Ni-based catalysts for hydrogenation of CAL.

EXPERIMENTAL

TiO_2-P-25 (Evonik), TiO_2 anatase (Hombikat), Pural (Sasol), SiO_2 (Evonik) were commercial samples and used as such. TiO_2-Rutile sample from Aldrich was used as such. $Ni(CH_3COO)_2.4H_2O$ (CDH), NaOH (SRL), D-glucose (Merck), methanol, liquor ammonia (Qualigens) and cinnamaldehyde (Aldrich) were used as such. Pural (pseudo-boehmite) was calcined at 450°C in air for 4 h to get gamma alumina support.

Preparation of supported nickel catalysts

All catalysts were prepared by chemical reduction of nickel acetate, using D-glucose as reducing as well as capping agent.[27] Nickel nanoparticles, stabilized in alkaline medium, were anchored onto different supports. Typically, 0.74 g of Nickel acetate and 40 ml of D-glucose solution (0.15 M) were mixed and stirred for 30 min at room temperature. 10 ml of liquor ammonia was added drop-wise to the mixture. Refluxing the mixture for 5 h at 80ºC turned its color to black indicating the reduction of Ni^{2+} ions to Ni. Then, 1 g of support (alumina/silica/TiO_2(P-25 type)/TiO_2-anatase/TiO_2-rutile) was added to the solution containing Ni nanoparticles and stirred for 2 h. The mixture was cooled to ambient temperature, centrifuged, washed with anhydrous ethanol and dried at 60 ºC for 24 h. All catalysts were pre-reduced in hydrogen gas flow at 300 °C for 2 h. All characterization and hydrogenation experiments were carried out with pre-reduced catalysts after appropriate pre-treatment procedures.

Characterization of catalysts

XRD measurements were carried out on a Rigaku Miniflex II powder X-ray diffractometer with a Ni-filtered CuKα radiation source (λ = 1.5406 Aº) operating at 30 kV and 15 mA. High angle (10 – 90°) diffraction patterns were obtained with a scanning rate of 3° min^{-1}. The crystallite size was calculated by X-ray line broadening method[28] using Debye-Scherrer equation (1).

$$d = K\frac{\lambda}{\beta\cos\theta} \qquad (1)$$

where

d is the crystallite size in *nm*,

K is the numerical (crystallite shape) constant (K = 0.89 in this case),

λ is the wavelength of radiation used (λ= 1.5405 Å),

β is full width at half maximum (FWHM) in radians

θ is the Bragg diffraction angle in degrees, at the peak maximum.

The surface morphology and composition of the support and deposited material were studied using a QUANTA 200-FEI instrument equipped with an METEK energy dispersive X-ray analysis (EDX) system. The sample in powdered form was spread on the carbon tape (adhesive tape, normally used in SEM measurements for conduction purpose) and mounted on the SEM sample holder and imaged.

Transmission electron micrographs were recorded on a Philips CM20 model (120 kV) and JEOL 3010 model (200KV). Few milligrams of the samples (1-2 mg) were dispersed in few mL (4-5 mL) of ethanol by ultrasonication for 30 minutes, and the sample was kept aside for 10 min. A drop of the top layer was placed on a carbon-coated copper grid and allowed to dry in air at room temperature. Image J software was used to calculate the crystallite sizes. Based on the mean crystallite size measured from TEM data, Ni metal dispersion (φ) was calculated using the formula (2)

$$\varphi = \frac{600M_{\mathrm{Ni}}}{\rho d_{\mathrm{nm}} a_{\mathrm{Ni}} N_{\mathrm{A}}} \qquad (2)$$

where

M is the molecular weight of metal in case,

a is the atomic surface area (3.8×10^{-20} m^2/atom for Ni),

ρ is the metal density (8.9 g/cm^3 of Ni),

N_a is Avogadro's number, and

d_{nm} is the average particle diameter estimated from TEM in nanometers.

TPR patterns for the catalysts were recorded in Micromeritics-Auto Chem II 2920 unit using argon (95 %) + hydrogen (5 %) mixture as the carrier gas. The hydrogen consumption was recorded with TCD cell. For TPR measurements, the catalysts (50 mg) were pretreated at 300 ºC in air (25 cm^3 min^{-1}) for 1 hour and then cooled to room temperature. Gas flow was changed to 5%H_2/Ar (25 cm^3 min^{-1}) at room temperature. After stabilization of the baseline, TPR was started from RT to 700 ºC @ 10 ºC min^{-1}.

Ni metal surface area measurements were performed by H_2 pulse chemisorption in the same unit. 50 mg of catalysts were pre-treated at 300 ºC in high purity Ar gas (25 cm^3 min^{-1}) for 1 h and then cooled to room temperature under Ar flow. The catalysts were reduced at 300 °C for 2 h under 10 % H_2/Ar flow, cooled down to RT under Ar. H_2 pulses were injected with Ar as a carrier gas until the eluted peak area of consecutive pulses was constant.

For H_2 TPD measurements, 50 mg of catalyst was reduced in hydrogen flow (25 cm^3 min^{-1}) at 300 °C for 4 h and cooled to ambient temperature. Ar flow (30 cm^3 min^{-1}) was then introduced, and the catalyst was purged for 30 min. After the stabilization of the baseline, TPD of H_2 was recorded up to 700 ^{0}C at a temperature ramp of 10 ^{0}C min^{-1}.

The metal content of the supported catalyst was estimated by ICP-OES (Perkin Elmer Optima Model 5300 DV) after calibration with a standard solution containing known metal content. The metal was extracted from the catalyst by boiling in aqua-regia.

Nitrogen adsorption-desorption isotherm measurements were carried out at 77 K using a Micrometrics ASAP 2020 surface area analyzer. Before adsorption, the samples were evacuated at 523 K for 12 h. The specific surface area of the samples was estimated using the Brunauer-Emmett-Teller (BET) method, and the pore size was calculated by Barrett-Joyner-Halenda (BJH) method. The pore volume was determined from the amount of nitrogen adsorbed at P/P_0= 0.95

The X-ray photoelectron spectroscopic studies were carried out using Omicron Nanotechnology instrument with MgK_α radiation. The base pressure of the analysis chamber during the scan was $2\cdot10^{-10}$ millibar. The pass energies for individual scan and survey are 20 and 100 eV, respectively. The spectra were recorded with the step width of 0.05 eV.

Performance evaluation of catalysts

Hydrogenation reactions were performed in liquid phase, in a 100 ml Parr reactor (Model-4848). The autoclave was charged with 150 mg of pre-reduced catalyst, 1.2 g of cinnamaldehyde and 16 ml of methanol. After purging first with nitrogen (three times) and then with hydrogen (three times) the autoclave was pressurized with hydrogen to the desired value of 20 kg/cm^2. The reactions were carried out for different catalysts at 120°C, for 1 h, with stirring rate of 600 rpm. No increase in conversion was observed at stirring rates higher than 600 rpm indicating that at this rate mass transfer limitations could be ruled out. The reaction products were separated by filtration and analyzed on Perkin Elmer Clarus-500 GC with ZB-1 capillary column and FID.

The experimental/process conditions mentioned above have been arrived at after carrying out a set of experiments aimed at optimization of reaction conditions. All the experiments for optimization were carried out with 15 % w/w Ni/TiO_2-P-25 catalyst.

RESULTS AND DISCUSSION

Ni contents in the final catalysts were checked by ICP-OES analysis and found to be 14.5-15.2 % w/w as per expectations.

X-ray diffraction

XRD patterns for nickel catalysts on three titania phases (Hombikat, Rutile, and P-25) in reduced form are shown in Fig. 1. Strong diffraction peaks at 2θ values 25.3º, 37º, 37.8º, 38.6º, 48.2º (anatase) and 27.5º, 36.2º, 39.4º, 41.3º, 44.1º (rutile) ascribed to the support TiO_2 and Ni crystallites with fcc structure at 2θ values 44.7º, 51.8º and 76.3º are observed. While the d-lines for P-25 & rutile phases are sharp, due to crystalline character, the d-lines for Hombikat are somewhat diffused and broad, indicating amorphous nature.

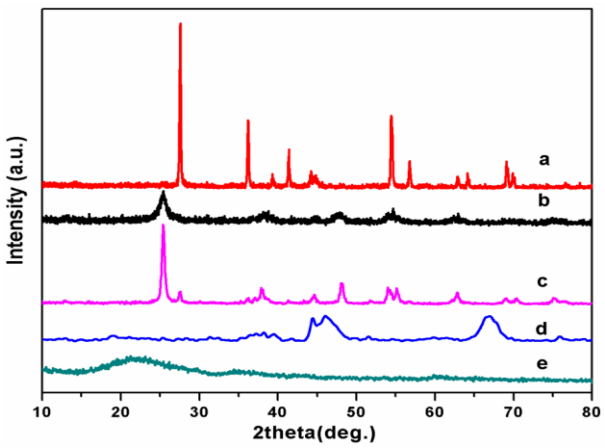

Figure 1. XRD Patterns for a) Ni/ TiO_2 Rutile b) Ni/ TiO_2 Hombikat c) Ni/ TiO_2 P-25 d) Ni/Al_2O_3 e) Ni/SiO_2.

Nickel was predominantly dispersed as Ni^0 on all the three supports. On the other hand, the XRD pattern for Ni/SiO_2 catalyst displays broad silica peak around 2θ = 23° indicating the amorphous character of silica. No d-lines due to Ni^0 could be observed, suggesting, that the nickel was finely dispersed on the surface of the silica support. XRD pattern of Ni/Al_2O_3 catalyst shows that the main diffraction peaks due to Al_2O_3 are shifted to lower angles, possibly due to the formation of $NiAl_2O_4$ with spinel structure.[29] It is clear that nickel particles are highly dispersed on the supports.

Temperature programmed reduction (TPR)

Both Ni/TiO_2 (rutile), and Ni/TiO_2 (P-25) catalysts (curves a and c in Fig. 2) exhibited similar reduction patterns, with a major reduction peak at 343°C, along with a shoulder at 225 °C. While the shoulder at lower temperature indicates the presence of small amount of free NiO, the peak at 343 °C corresponds to the reduction of dispersed NiO. Ni/TiO_2 (Hombikat, curve b) shows only one reduction maximum at 340 °C, due to dispersed NiO, followed by a negative peak, possibly due to the desorption of split over hydrogen from the support.

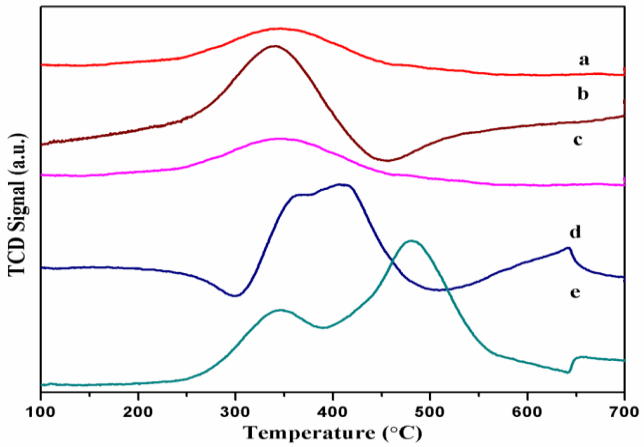

Figure 2. TPR profiles for a) Ni/Rutile b) Ni/Hombikat c) Ni/P-25 d) Ni/Al_2O_3 e) Ni/SiO_2.

High surface area and the presence of surface hydroxyl groups in Hombikat may have been responsible for the spill over. For Ni/Al_2O_3 catalysts (curve d), three reduction maxima are observed. The first peak at 362 °C is assigned to dispersed nickel oxide with weak interaction with support. The second peak around at 411 °C can be assigned to the typical reduction peak of Ni^{2+} that has interacted with the support alumina, possibly forming aluminate. The third peak around at 641 °C can be attributed to the reduction of nickel aluminate species. In the case of Ni/SiO_2 (curve e), besides a low temperature reduction peak at 343 °C which is attributed to the reduction of dispersed and weakly bound NiO particles, two more reduction peaks at higher temperatures at 482 and 655 °C are observed, which could be ascribed to the reduction of strongly bound Ni^{2+} in contact with the oxide support and possible nickel silicate like phase.[30] To summarize, TPR studies clearly show that the nature of the supports governs the reduction pattern and metal-support interactions in the case of nickel supported on different carriers.

Temperature programmed desorption of H_2 (H_2TPD)

In order to study the nature of adsorbed hydrogen, on Ni H_2-TPD studies were carried out. Fig. 3 shows the H_2-TPD patterns for the Ni catalysts on different carriers.

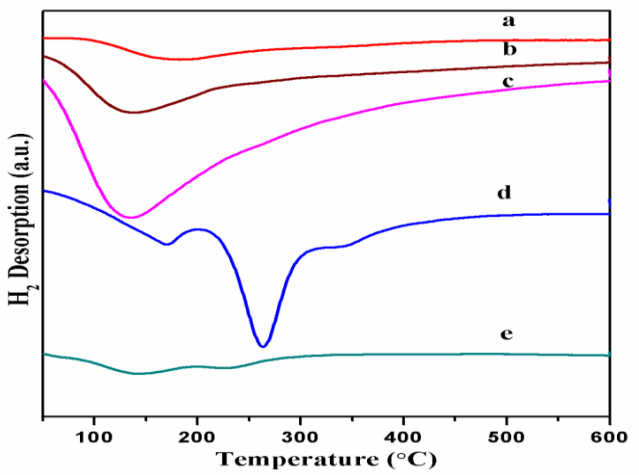

Figure 3. H_2-TPDprofiles for- a) Ni/Rutile b) Ni/Hombikat c) Ni/P-25 d) Ni/Al_2O_3 e) Ni/SiO_2

For all catalysts, a low-temperature desorption peak appears at 110- 160°C in the TPD profiles, which is usually attributed to the H_2 adsorbed on the Ni metal. Low-temperature desorption peak areas decrease in the following order: Ni/P25 > Ni/Hombikat > Ni/Rutile >Ni/SiO_2 > Ni/Al_2O_3 indicating that titania supported catalysts contain a larger fraction of reactive hydrogen. It is suggested that on Ni/TiO_2 (Hombikat, Rutile, and P25), bonding of hydrogen on Ni is weak and hence in the reactive state.[31] Low-intensity high temperatures desorption peaks around 210-270°C, possibly due to strongly chemisorbed hydrogen or the spillover of hydrogen atoms from metal to the support are also observed on Ni/SiO_2 and Ni/Al_2O_3 catalysts.[32] Additionally, Ni/Al_2O_3 displays one high temperature weak and broad desorption peak at 345°C. These higher temperature desorption peaks may be ascribed to the split over of hydrogen atoms from the Ni metal to the support, which recombine and desorb. The observed variations in H_2-TPD and TPR profiles indicate that the activation and spillover of hydrogen on the Ni catalyst surface are strongly affected by the properties of supports.

Scanning electron microscopy (SEM)

The morphology of reduced nickel catalysts on different supports was studied by SEM technique (Fig.4). Spherical shaped nano size nickel particles are observed for titania (Hombikat, P25, and Rutile) supported catalysts. In the case of Al_2O_3 and SiO_2 supported catalysts, no specific morphology is seen, but the certain degree of agglomeration of nano-sized particles is observed.

Transmission electron microscopy (TEM)

Representative TEM images of Ni/TiO_2 (Hombikat, Rutile, and P-25), Ni/Al_2O_3 and Ni/SiO_2 catalysts are shown in Fig.5. Ni/ TiO_2 P-25 catalyst shows a narrow particle size distribution, within a range of 7-10 nm. In the case of Ni/Hombikat and Ni/Rutile catalysts, particles with sizes ranging from 11-12 nm are observed. Smaller Ni crystallites, 7-9 nm, are observed in alumina and silica supported catalysts. Crystallite size of all catalysts are in the order: Ni/SiO_2 < Ni/Al_2O_3, < Ni/Hombikat < Ni/Rutile < Ni P-25, in agreement with the crystallite size values calculated by Scherrer formula based on the X-ray line broadening analysis. Ni metal dispersion and crystallite size values obtained by hydrogen chemisorption data are listed Table.1.

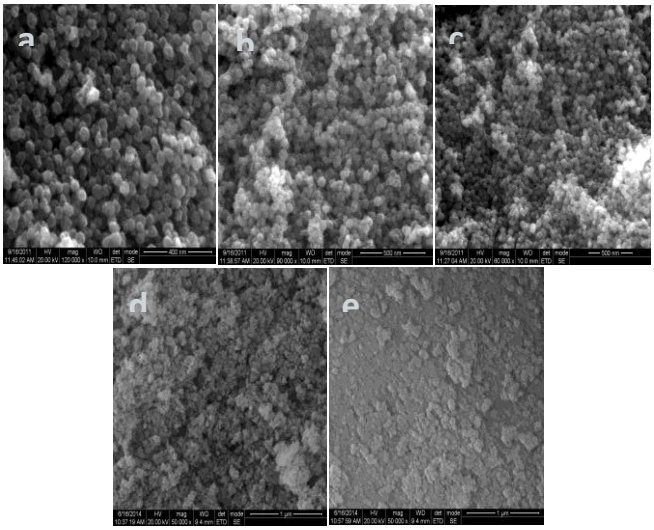

Figure 4. SEM images for a) Ni/Rutile b) Ni/Hombikat c) Ni/P-25 d) Ni/Al_2O_3 e) Ni/SiO_2

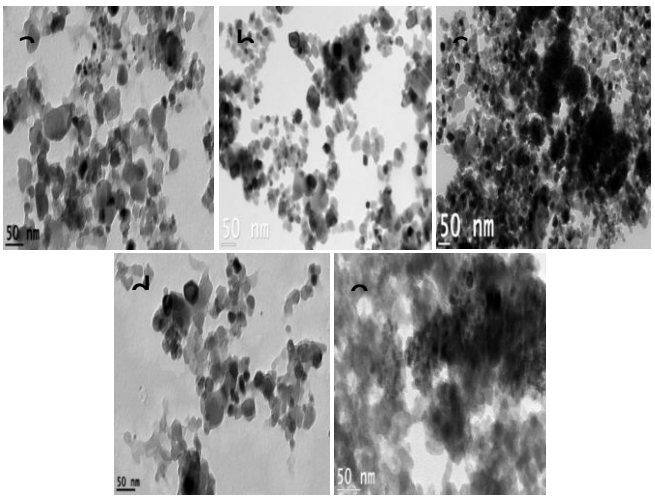

Figure 5. TEM images for a) Ni/Rutile b) Ni/Hombikat c) Ni/P-25 d) Ni/Al_2O_3 e) Ni/SiO_2

HRTEM image for Ni/TiO_2-P-25 is presented in Fig.6 wherein the prominent lattice fringes corresponding to (101) plane of anatase (0.35nm), (110) plane of rutile (0.32nm) phases in TiO_2-P-25 are observed along with those for (111) plane for fcc Ni crystallite (0.20nm). The micrograph clearly shows the presence of Ni crystallites in the interface between anatase and rutile phases of titania.

Table 1. Textural properties of nickel based catalysts

Catalyst	S_{BET}, $m^2 g^{-1}$	Pore volume, cm^3 g	Pore size, nm	Ni dispersion, %[a]	Ni crystallite size, nm		
					XRD	H_2	TEM
Ni/P25	50	0.20	16.1	9.5	10	10	9.8
Ni/Hombikat	311	0.33	5.0	8.9	8.8	12	11.7
Ni/Rutile	9.2	0.05	22.0	8.7	9.1	13	12.2
Ni/SiO_2	73	0.93	7.4	13.8	6.8	7.3	7.7
Ni/Al_2O_3	60	0.61	9.0	10.7	8.5	9.1	8.9

[a]-from H_2 chemisorption, XRD-XLBA, TEM

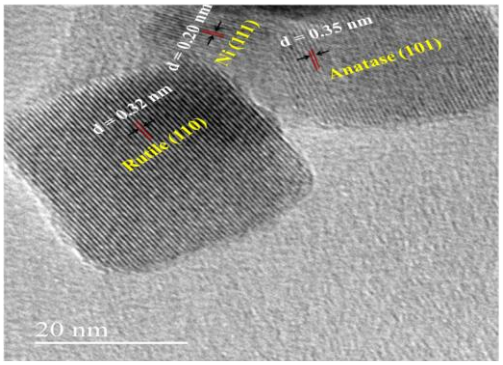

Figure 6. Lattice fringe image for anatase, rutile and Ni crystallites in Ni/TiO_2 P-25 catalyst

X-ray photoelectron spectroscopy (XPS)

On Ni catalysts supported on titania (P-25, Hombikat and Rutile) binding energy values for Ni $2p_{3/2}$ peaks were observed at 852.6 eV and 853.5 eV, which could be attributed to Ni^0 (metallic state) and residual Ni^{2+}species respectively[33] (Fig.7). In the case of Ni/SiO_2 $Ni2p_{3/2}$ peak for metallic Ni appears at 852.8 eV, with a slight shift with respect to the BE of metallic Ni. This may be due to the covalent interactions between Ni and Si catalysts.[34] The shift in the binding energy of Ni $2p_{3/2}$ peak observed for Ni/Al_2O_3 is consistent with the reported Ni $2p_{3/2}$ binding energy shift for $NiAl_2O_4$[35], which is in agreement with the XRD data.

N_2-Physisorption and H_2 pulse chemisorption

Textural properties, nickel dispersion and Ni particle size of supported Ni catalysts are listed in Table.1. The addition of 15 wt.% Ni metal to the corresponding support causes a slight change in the BET surface area, pore volume and average pore size. According to the H_2 pulse chemisorption results, the Ni/TiO_2 (Hombikat, Rutile and P25) catalysts have lower nickel dispersion than Ni/Al_2O_3 and Ni/SiO_2 catalysts.[36] TEM results on the catalysts corroborate this aspect.

Selective hydrogenation of cinnamaldehyde

The results on the selective hydrogenation of cinnamaldehyde (CAL) on Ni catalysts with different supports are given in Table 2. Ni/TiO_2 P25) displayed the highest CAL conversion (91%) with a maximum selectivity of 61% to COL. Hombikat and rutile titania supported Ni catalysts showed the moderate conversion of 57 % and 51 %, respectively but the selectivity towards COL was nearly half of the value (30.3 % and 24.4% respectively) displayed by the P-25 supported catalyst. Ni/SiO_2 and Ni/Al_2O_3 catalysts show still lower CAL conversion and COL selectivity. It is clear that the nature of the support and its morphology/polymorph character influences the activity and selectivity.

Table 2. Conversion and selectivity data for hydrogenation of cinnamaldehyde at 120 °C

Catalyst	CAL conv., %	Selectivity, %			
		HCAL	COL	HCOL	Others
Ni/P25	91	31	61	6.9	1.1
Ni/Hombikat	57	66	30.3	1.2	2.5
Ni/Rutile	51	72	24.4	1.0	2.6
Ni/SiO_2	38	79	18	0.8	2.2
Ni/Al_2O_3	18	78.8	17.2	0.6	3.4

Catalyst wt. -150 mg; COL-1.2 g, methanol-16 mL, pressure – 20 kg cm^{-2}, Reaction time – 1 h.

Among the three different types of supports, titania, alumina and silica, all the three titania supports display higher activity and selectivity vis-à-vis the other two types of supports. Reducibility of TiO_2 results in the formation of oxygen deficient TiO_{2-x} phase containing Ti^{3+} ions, which tend to decorate Ni crystallites and polarize C=O, leading to higher activity and selectivity towards COL. Small amounts of unreduced NiO present in the catalyst acts as Lewis acid sites, which also activates the C=O.[15] Superior performance of Co/TiO_2 compared to Co supported on alumina and silica supports[25] lends credence to this phenomenon. Though Ni crystallite size of alumina and silica are small, activity for CAL conversion and selectivity for COL are lower, compared to those on titania supports, implying that the crystallite size alone is not the key factor in determining the performance. Besides, some part Ni, present as nickel aluminate/silicate in alumina/silica supports, may not be available for the reaction.

Amongst the three polymorphs of titania, maximum activity and selectivity displayed by Ni-P-25 (Table 2) could be attributed to the active Ni crystallites located at the interface between anatase and rutile phases in titania P-25 matrix, as revealed by the HRTEM studies (Fig.6). The superior performance of active metals, located preferentially at the interface between two polymorphs in a support matrix, has been reported earlier.

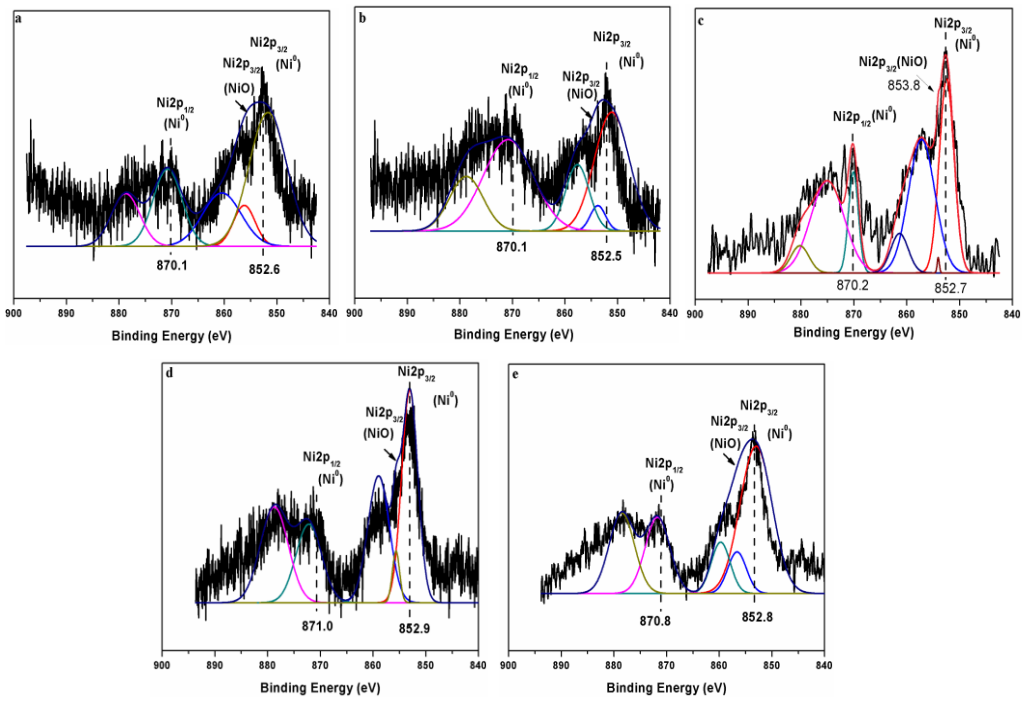

Figure 7. XPS spectrum for- a) Ni/Rutile b) Ni/Hombikat c) Ni/P-25 d) Ni/Al_2O_3 e) Ni/SiO_2.

Bin Wang et.al[37] have observed that Cu crystallites located at the interface between anatase and rutile phases in TiO_2 P-25 display high activity and selectivity for the hydrogenation of dimethyl oxalate to ethylene glycol. Wang et al. also observed that on pure anatase and rutile phases, in the absence of interfaces, Cu underwent agglomeration. Thus the presence of interfaces in P-25 helps in the activation as well as the dispersion of Cu. High activity of Au crystallites preferentially located at the interfaces in TiO_2 P-25 has been observed for the production of H_2 from ethanol-water mixtures.[38] Corresponding anatase, and rutile titania supported Au nanocrystals displayed lower activity. Synergistic electron transfer between the two polymorphs of titania and Au nanocrystals is proposed to be the reason for the high activity. Tsukomoto et al.[39] have reported that Au nanoparticles of size < 5 nm, located preferentially at the anatase –rutile interface in P-25, are highly active for the photocatalytic oxidation of alcohol. It is proposed that the catalyst architecture consisting of anatase-Au-rutile function as a joint active site, facilitating smooth electron transfer from Au to titania. In the present case, such preferential location of Ni nanoparticles in the interfaces (between anatase and rutile) within titania P-25 phase (Fig.6) could be responsible for the higher CAL conversion, and selectivity for COL observed with Ni/TiO_2P-25.

Conclusions

Nickel catalysts supported on alumina, silica and three different phases of titania (anatase, rutile & P-25) display distinct physicochemical characteristics that profoundly influence their activity and selectivity for hydrogenation of cinnamaldehyde. XRD and TPR data reveal that metal-support interactions are prominent in all supported catalysts. Morphology of titania supports influences the reduction behavior of the respective NiO phases. XPS studies indicate the presence of small amounts of unreduced NiO in all the five catalysts. Shifts in the XPS binding energy for Ni2p lines are indicative of metal-support interactions. H_2 TPD studies show that the bonding of hydrogen on titania supported catalysts is weaker and hence more reactive than that on alumina and silica supported catalysts. Nickel crystallite sizes measured by TEM and H_2 chemisorption studies fall in the narrow range of 7-12 nm. Catalysts supported on titania display higher CAL conversion and selectivity to COL in comparison with those supported on alumina and silica. Reducibility of TiO_2 leads to the formation of oxygen deficient TiO_{2-x} phase containing Ti^{3+} ions, which tend to decorate Ni crystallites and polarize C=O, leading to higher activity and selectivity towards COL. Small amounts of unreduced NiO acts as Lewis acid sites, which also activate the C=O. Amongst the three polymorphs of titania, maximum activity and selectivity displayed by Ni-P-25 titania could be attributed to the active Ni crystallites located at the interface between anatase and rutile phases in titania P-25 matrix.

Acknowledgements

The authors would like to express their gratefulness to the Dept. of Science & Technology, Govt. of India for establishing research facilities at NCCR. MGP is thankful to CSIR for the award of SRF scholarship. Authors acknowledge the supply of Hombikat TiO_2 (Anatase) by M/s Sachtleben Chemie, Germany and M/s.Evonik Industries, Germany for TiO_2-P-25

References

[1]Gallezot, P., Richard, D., *Catal. Rev. Sci. Eng*., **1998**, *40*, 81. http://dx.doi.org/10.1080/01614949808007106

[2] Mohr, C., Hofmeister, H., Radnik, J., Claus, P., *J. Am. Chem. Soc*., **2003**, *125*, 1905. http://dx.doi.org/10.1021/ja027321q CC

[3] Daimon, A., Kamitanaka, T., Kishida, N., Matsuda, T., Harada, T., *J. Supercritical Fluids*, **2006**, *37*, 215. http://doi.org/10.1016/j.supflu.2005.09.001

[4]Kluson, P., Cerveny, L., *Appl. Catal. A Gen*.,**1995**, 128, 13. https://doi.org/10.1016/0926-860X (95)00046-1

[5]Ponec, V., *Appl. Catal. A Gen*., **1997**, *149*, 27. https://doi.org/10.1016/S0926-860X (96)00250-5

[6]Singh, U. K, Vannice, M. A., *Appl. Catal. A Gen*., **2001**, *213*, 1. http://doi.org/10.1016/S0926-860X (00)00885-1

[7]Cerveny, L., Ruzicka, V., *Catal. Rev. Sci. Eng*., **1982**, *24*, 503. http://dx.doi.org/10.1080/03602458208079662

[8]Milone, C., Crisafaulli, R., Ingoglia, S. L., Galvagno, S., *Catal. Today*, **2007**, *122*, 341. http://doi.org/10.1016/j.cattod.2007.01.011

[9]Kartusch, C., Van Bokhoven, J. A., *Gold Bull*., **2009**, *42*, 343. http://dx.doi.org /10.1007/BF03214957

[10]Merlo, A. B., Machado, B. F., Vetere, V., Faria, J. L., Casella, M. L., *Appl. Catal. A. Gen*., **2010**, *383*, 43. http://doi.org/10.1016/j.apcata.2010.05.020

[11]Plomp, A. J., Vuori, H. A., Krause, O. I., de Jong, K. P., Bitter, J. H., *Appl. Catal. A Gen*., **2008**, *351*, 9. http://doi.org/10.1016/j.apcata.2008.08.018

[12]Jurvilliers, X., Schneider, R., Fort, Y., Ghanbaja, J., *Appl. Org. Metal. Chem.* **2003**, *17*, 161. http://dx.doi.org /10.1002/aoc.398

[13]Mahata, N., Concalves, F., Fernando, M., Pereira, R., Figueiredo, J. L., *Appl. Catal. A Gen*., **2008**, *339*, 159. http://doi.org/10.1016/j.apcata.2008.01.023

[14]Zhang, L., Winterbottom, J. M., Boyes, A. P., Raymahasay, S., *J. Chem. Technol. Biotechnol.*, **1998**, *72*, 264. http://dx.doi.org /10.1002/(SICI)1097-4660

[15]Prakash, M. G., Mahalakshmy, R., Krishnamurthy, K. R., Viswanathan, B., *Catal. Sci. Technol*., **2015**, *5*, 3313. http://dx.doi.org //10.1039/C4CY01379D

[16]Reyes, P., Rojas, H., Pecchi, G., Fierro, J. L. G., *J. Mol. Catal. A. Chem.*, **2002**, *179*, 293. http://doi.org/10.1016/S1381-1169(01)00409-5

[17]Shi, J., Nie, R., Chen, P., Hou, Z., *Catal. Commun*., **2013**, *41*, 101. http://doi.org/10.1016/j.catcom.2013.07.012

[18]Zhao, J., Ni, J., Xu, J., Xu, X., Li, X., *Catal. Commun*., **2014**, *54*, 72. http://doi.org/10.1016/j.catcom.2014.05.012

[19]Wu, Z., Zhao, J., Zhang, M., Li, W., Tao, K., *Catal. Commun*., **2010**, *11*, 973. http://doi.org/10.1016/j.catcom.2010.04.018

[20]Zhang, B., Zhang, X. B., Xu, L. Y., Zhang, Y. J., Qin, Y .H., Liang, C. F., *React. Kinet. Mech. Cat*., **2013**, *110*, 207. http://dx.doi.org /10.1007/s11144-013-0589-7.

[21]Marchi, A. J., Gordo, D. A., Trasarti, A. F., Aspesteguia, C. R., *Appl. Catal. A. Gen*., **2003**, *249*, 53. http://doi.org/10.1016/S0926-860X (03)00199-6

[22]Englisch, M., Jentys, A., Lercher, J. A., *J. Catal.*, **1997**, *166*, 25. https://doi.org/10.1006/jcat.1997.1494

[23]Bhogeswararao, S., Kumar, V. P., Chary, K. V. R., Srinivas, D., *Catal. Lett*., **2013**, *143*, 1266. doi:10.1007/s10562-013-1064-9

[24]Rudolf, C., Dragoi, B., Ungureanu, A., Chirieac, A., Royer, Nastro, S. A., Dumitriu, E., *Catal. Sci. Technol*., **2014**, *4*, 179. http://dx.doi.org /10.1039/C3CY00611E

[25]Raj, K. J. A., Prakash, M. G., Elangovan, T., Viswanathan, B., *Catal. Lett*., **2012**, *142*, 87. doi:10.1007/s10562-011-0693-0

[26]Ruppert, A. M., Grams, J., Je˛drzejczyk, M., Matras-Michalska, J., Keller, N., Ostojska, K., Sautet, P., *ChemSusChem*., **2015**, *8*, 1538. http://dx 10.1002/cssc.201403332

[27]Vasseem, M., Tripathy, N,, Khang, G., Halm, Y., *RSC. Adv*., **2013**, *3*, 9698. http://dx.doi.org /10.1039/C3RA40462E.

[28]Als-Nielsen, J., McMorrow, D., *Elements of Modern X-ray Physics*, John Wiley & Sons, Ltd., **2001**.

[29]Schefer, B., Heijeinga, J. J., Moulijn, J. A., *J. Phys. Chem*., **1987**, *91*, 4752., http://dx.doi.org /10.1021/j100302a023

[30]Liu, Y., Chen, J., Zhang, J., *Chin. J. Chem. Eng*., **2007**, *15*, 63. https://doi.org/10.1016/S1004-9541(07) 60034-2

[31]Amorima, C., Wang, X., Keane, M. A., *Chin. J. Catal*., **2011**, *32*, 746. http://dx.doi.org/10.1016/S1872-2067(10) 60228-8

[32]Braos-García, P., García-Sancho, C., Infantes-Molina, A., Rodríguez-Castellón, E., Jiménez-López, A., *Appl. Catal. A Gen.*, **2010**, *381*, 132. http://doi.org/10.1016/j.apcata.2010.03.061

[33]Grosvenor, A. P., Biesinger, M. C., Smart, R. St. C., McIntyre, N. S., *Surf. Sci*., **2006**, *600*, 1771. http://doi.org/10.1016/j.susc.2006.01.041

[34]Chen, X., Li, M., Xinkui, J., Williams, C. T., Liang, C., *Ind. Eng. Chem. Res*., **2012**, *51*, 3604. http://dx.doi.org /10.1021/ie202227j

[35]Heracleous, E., Lee, A. F., Wilson, K., Lemonidou, A. A., *J. Catal.*, **2005**, *231*, 159. http//doi.org/10.1016/j.jcat.2005.01.015

[36]Liu, N. Y., Feng, J. T., He, Y. F., Sun, J. H., Li, D. Q., *Catal. Sci. Technol*., **2015**, *5*, 1231. http://dx.doi.org /10.1039/C4CY01160K

[37]Wang, B., Wen, C., Cui, Y., Chen, X., Dong, Y., Dai, W. L, *RSC Adv.*, **2015**, *5*, 29040. http://dx.doi.org /10.1039/C5RA00053J

[38]Jovic, V., Chen, W. T., Sun-Waterhouse, D., Blackford, M. G., Idriss, H., Waterhouse, G. I. N., *J. Catal*., **2013**, *305*, 307. http://doi.org/10.1016/j.jcat.2013.05.031

[39]Tsukamoto, D., Shiraishi, Y. A., Sugano, S., Tanaka, S., Hirai, T., *J. Am. Chem. Soc*., **2012**, *134*, 6309. http://dx.doi.org/10.1021/ja2120647

Received: 19.03.2017.
Accepted: 30.04.2017.